The Role of Vav Family Guanine-Nucleotide Exchange Factors and their Substrates in B Cell Antigen Receptor Signaling

Dissertation

for the award of the degree

"*doctor rerum naturalium*"

of the Georg-August-Universität Göttingen

within the doctoral program Molecular Medicine

of the Georg-August University School of Science (GAUSS)

submitted by Jens Erik Löber

from Gießen, Germany

Göttingen 2020

This thesis entitled “The Role of Vav Family Guanine-Nucleotide Exchange Factors and their Substrates in B Cell Antigen Receptor Signaling” was conducted from November 2016 until April 2020 in the Institute of Cellular and Molecular Immunology at the Medical Faculty of the Georg-August University Göttingen under the supervision of Dr. Niklas Engels. Several data sets generated and presented in this thesis were included in the manuscript “Vav family members constitute disparate branching points for distinct BCR signaling pathways” which is currently under revision at the European Journal of Immunology. In detail, the manuscript contains data from figures 3.1, 3.2, 4.3, 4.4, 4.5, 4.7, 4.8, 4.9, 4.11, 4.12, 4.14, 4.15, 4.30, 4.32, 4.33, 4.34, 4.35, 4.36 and 4.40.

Thesis Committee

Prof. Dr. Jürgen Wienands, Institute of Cellular and Molecular Immunology, University of Göttingen, Medical Faculty (UMG)

Prof. Dr. Michael Uwe Martin, Professorship for Immunology, University of Gießen, Faculty 08: Biology and Chemistry

Univ.-Prof. Dr. Björn Chapuy, Hematology and Oncology, University of Göttingen, Medical Faculty (UMG)

Members of the Examination Board

Referee: Prof. Dr. Jürgen Wienands, Institute of Cellular and Molecular Immunology, University of Göttingen, Medical Faculty (UMG)

2nd Referee: Univ.-Prof. Dr. Björn Chapuy, Hematology and Oncology, University of Göttingen, Medical Faculty (UMG)

Further members of the Examination Board

Prof. Dr. Michael Uwe Martin, Professorship for Immunology, University of Gießen, Faculty 08: Biology and Chemistry

Prof. Dr. Lutz Walter, Department of Primate Genetics, German Primate Center, Göttingen

Prof. Dr. Matthias Dobbelstein, Institute of Molecular Oncology, University of Göttingen, Medical Faculty (UMG)

Prof. Dr. Dieter Kube, Hematology and Oncology, University of Göttingen, Medical Faculty (UMG)

Affidavit

I hereby declare that the submitted thesis “The role of Vav family guanine-nucleotide exchange factors and their substrates in B Cell Antigen Receptor Signaling” is my own work. All sources and aids are acknowledged as references.

_____ Göttingen, April 30th, 2020

Jens Löber

Acknowledgements

First, I want to express my gratitude to Prof. Wienands for giving me the chance to conduct my Ph.D. thesis in his lab. Thanks for mentoring me and being part of my thesis committee. In this context, I also want to thank Prof. Martin and Prof. Chapuy! Not only for being members of my thesis committee with exciting discussion and helpful advice during the meetings, but also for being part of my education. I learned a lot from you and would not be at this point of my scientific career without you!

Niklas, I'm sincerely thankful for your supervision and guidance throughout my whole Ph.D. project. It always was a pleasure to work with you and I learned a lot from your knowledge and experiences. Thanks for the lively scientific discussions but also the conversations aside from science about soccer, football and vacations. Very big thank-you for your support and advise for any kind of presentation for various scientific meetings and especially for proof-reading my dissertation. I really appreciated the time together on both, personal and professional levels and hope that this teamwork won't end with this thesis.

In addition, I want to thank all current and former members of the department for being lovely colleagues and great times in the past three and a half years! Special thanks to Christoffer, who introduced me to my project and helped me a lot in the first month of my thesis. Thank you, Ines, for excellent technical assistance. Anika, thanks a lot for your help regarding organizational issues. Stela, Christina, Vanessa, Alina, Kanika, Arshiya, Matthias, Michael Saed, Florian and Jan, thank you for fun mensa times and great activities beyond the lab. I also want to thank my lab rotation and thesis students Ritu, Marcel, Niloofar and Chantal.

Next, I want to thank the Deutsche Forschungsgemeinschaft (DFG) for the funding of my project. In addition, I want to thank the Transregio 130 and the related integrated research training group "B cells and beyond" for additional financial support and all the contacts I could establish during several scientific meetings. Thanks to the graduate program "Molecular Medicine" within the GGNB for excellent coordination.

Last, but most importantly, I want to thank my family and my friends for your perpetual support. Very special thanks to my parents and my brother for unconditional support in any situation. I'm more than thankful for my long-term best friends Viviana and Dominik - I can count on you in every situation of my life. Furthermore, I want to thank Sarah, Caroline, Lara, Sofía, Marie, Julia, Louisa, Raúl, Alexandar, Jan, David, André, Eugen, Florian, Kingsly, Patrick and Wai-Hon for all the fun apart from work! All of you guys helped me a lot to maintain a healthy work-life balance! I really appreciate and enjoy every single second with all of you. Caroline, thanks a ton for proof-reading my thesis.

Table of Contents

1. Abstract

Stimulation of the B cell antigen receptor (BCR) triggers an intracellular signaling cascade through its integral signaling components Igα and Igβ. This signaling cascade involves several protein classes like kinases, lipases and adaptor molecules and ultimately leads to nuclear translocation of transcription factors such as NF-κB and NFAT, promotes proliferation and metabolism via the PI3K/Akt kinase pathway, induces actin remodeling and activates MAPK like JNK, Erk and p38. The signaling cascade downstream of the BCR plays a crucial role in the life of B cells, starting from maturation of the cells in the bone marrow to activation and differentiation in peripheral lymphoid organs. Any dysregulation of this pathway can cause severe diseases such as immunodeficiencies, autoimmune diseases or malignancies. Hence, it is important to understand the biochemical mechanisms by which this signaling pathway is controlled. However, the exact function of some of the involved players, such as the Vav family of guanine nucleotide exchange factors, still remains only partially understood. Using a cellular model system based on a Vav1-deficient subline of a human B cell line, our group revealed a critical role of Vav family members for BCR-proximal signaling reactions including mobilization of the second messenger Ca^{2+}. This work unraveled several other signaling axes within the BCR signaling cascade, such as induction of actin remodeling, activation of MAPK p38 and Erk and phosphorylation of Akt, that depend on the expression of Vav family members. Strikingly, all of those signaling axes were significantly impeded upon loss of the catalytic guanine-nucleotide exchange factor (GEF) activity of Vav family members. Interestingly, Vav2 was able to mediate BCR-induced actin remodeling and phosphorylation of Akt even though it does not support BCR-induced Ca^{2+}-mobilization. *In vitro* GEF-activity assays revealed Vav family isoform-specific activation of the Rho family. Whereas Vav1 mediated activation of Rac1 and RhoA, Vav2 selectively activated Rac1 and Vav3 showed GEF activity only towards RhoA. Thus, activation of RhoA appears to be required for BCR-induced Ca^{2+}-mobilization while GEF-activity towards Rac1 supports actin remodeling and phosphorylation of Akt upon stimulation of the BCR. Consequently, a new class of catalytic activity, i.e. the GEF-activity of Vav family proteins towards different Rho family small G proteins, was identified to be required for BCR-induced signaling. Moreover, it was shown, that the BCR-induced activation of Akt, actin cytoskeleton remodeling and Ca^{2+}-influx were independent from each other. This work suggests that Vav family members do not just act as adaptor proteins in the BCR signaling cascade but represent central enzymatic coordinators of distinct signaling pathways downstream of the BCR.

2. Introduction

2.1. The human immune system

The essential function of the immune system in humans is to protect the organism against pathogenic microbes that infiltrate through physical barriers such as the skin or mucous membranes[1]. Therefore, the immune system developed various mechanisms to cope with these pathogens, some of which are directed against evolutionary constant and indispensable structures of these pathogens whereas others were adopted to new, previously unknown patterns[2,3]. The different parts of the immune system that respond to either class of pathogen-derived molecules are termed innate immunity and adaptive immunity, respectively. In fact, the human immune system is a highly developed “disseminated organ” that is able to discriminate between “self” and “foreign”, but also between “harmless” and “harmful” structures[4]. In contrast to most other organs of the human body, the immune system is not a solid organ but is distributed across the whole body as primary and secondary lymphoid tissues[5]. In addition, immune cells patrol through the body via blood and lymph stream and reside in various tissues[1].

The innate immune system constitutes the first line of defense and consists of several cell types like granulocytes, macrophages and dendritic cells that are activated by binding of pathogen-derived ligands to specific germ line-encoded so-called pattern recognition receptors (PRRs)[6,7]. This first line of defense is primarily characterized by phagocytosis of pathogens or their destruction through release of reactive oxygen species[1]. Antigenic peptides of extracellularly phagocytosed pathogens are furthermore presented on major histocompatibility complex class II (MHC II) molecules on the surface of the cells to activate the adaptive immune system[4]. Both processes are supported by defensins and circulating proteins of the complement system that are constantly produced by immune cells[8,9]. Binding of complement system factors to a pathogen enhances phagocytosis, a phenomenon known as opsonization[8]. In addition, proteins of the complement system can form a membrane attack complex in the plasma membrane of pathogens that ultimately leads to perforation and destruction of the pathogen[1,8].

Natural killer cells belong to innate lymphocytes and essentially contribute to the elimination of virally infected cells or tumor cells. In addition to the antigen presenting cells of the innate immune system, almost every somatic cell type constantly presents peptides derived from intracellular proteins bound to MHC I on their surface. During viral infection or upon malignant transformation, this presentation of intracellular peptides on MHC I is frequently downregulated or blocked to evade immune recognition. However, loss of MHC I on the surface of cells is

recognized by natural killer cells which then mediate cytotoxic functions by induction of apoptosis through perforin and granzyme B[10].

Adaptive immunity is mediated by B and T lymphocytes and in contrast to innate immune mechanisms elicits highly specific immune responses to defined pathogenic molecules (antigens). Adaptive immunity furthermore establishes an immunological memory upon first encounter with a pathogen, causing a much more robust response on pathogen re-encounter[4]. Despite the differences, innate immunity and adaptive immunity are connected in several ways, e.g. through antigen-presenting dendritic cells and the complement system[8,11]. Lymphocyte precursor cells derive from hematopoietic stem cells in the bone marrow and undergo subsequent maturation steps in distinct primary lymphoid tissues. Whereas B cells remain in the bone marrow for the most part of their development, T precursor cells migrate to the thymus for this process[4]. T cells are responsible for the cell-mediated adaptive immune response, that includes clearance of intracellular pathogens after recognition of peptides presented on MHC I, which they detect with their clonotypic antigen-specific T cell receptors (TCRs). B cells on the other hand mediate the humoral adaptive immune response, predominantly by the production of antigen-specific antibodies that have a variety of functions. Antibodies can neutralize pathogens, stimulate their phagocytosis via opsonization, and activate the complement system[3,12,13]. Both, B and T cells acquire their antigen specificity via a process called somatic recombination of antigen receptor gene segments that takes place during cellular maturation. The result of this unique DNA recombination process is a vast number of clonotypic T and B lymphocytes, each of which expresses an antigen receptor (TCR or BCR, respectively) with a unique specificity[14]. This random process is necessary since the limited number of approximately (approx.) 20,000 to 25,000 genes of the human genome would not allow to generate the enormous numbers of adaptive antigen receptor specificities[3,15]. However, since somatic recombination is a random process at the DNA level, B and T cells have to pass several checkpoints during their maturation to ensure that the newly arranged receptors are functional yet do not detect self-antigens[16,17].

2.2. B cells - origin, maturation, differentiation, effects

B cells differentiate from hematopoietic stem cells in the bone marrow into precursors of naïve B cells followed by further maturation in the same compartment[18]. To become a functional naïve B cell, precursor B cells rearrange gene segments called variable- (V_H), diversifying- (D_H) and joining (J_H) segments of the immunoglobulin (Ig) heavy chain locus. Subsequently, the V_L- and J_L-regions of the Ig light chain are rearranged to generate a functional BCR with unique specificity[14]. Besides the membrane-anchored mature immunoglobulin, the BCR contains two additional molecules referred to as Igα and Igβ (CD79A and CD79B) that are covalently linked to each other via disulfide bonds. After antigen recognition via the membrane-

anchored immunoglobulin, the intracellular signals are triggered through this heterodimeric, integral signaling unit of Igα and Igβ[19]. In consequence, this multi protein complex has to fulfill two functions: antigen recognition in the extracellular milieu followed transmission of signals into the cytosol after ligand binding and antigen internalization for processing and subsequent presentation of the antigen in MHC II[20,21]. During somatic recombination of the heavy and light chain gene loci, a repertoire of up to 5 x 10^{13} specificities are generated, which is accompanied by apoptosis of a large number of cells having dysfunctional receptors[14]. At first, in pro-B cells, the Ig heavy chain is rearranged and functionality is tested using a surrogate light chain, forming the so-called pre-B-cell receptor. Functional rearrangement of the Ig heavy chain allows progression to the pre-B cell state in which the light chain regions are rearranged[22,23]. Upon successful generation of fully functional BCRs, B cells are still immature and migrate from the bone marrow to the spleen, where they further mature into naïve follicular or marginal zone B cells (Figure 2.1)[14]. Most of the naïve B cells reside in secondary lymphoid organs, although recirculation to the blood is possible by attraction through sphingosine-1-phosphate (S1P), a lipid present in high concentrations in the blood[24].

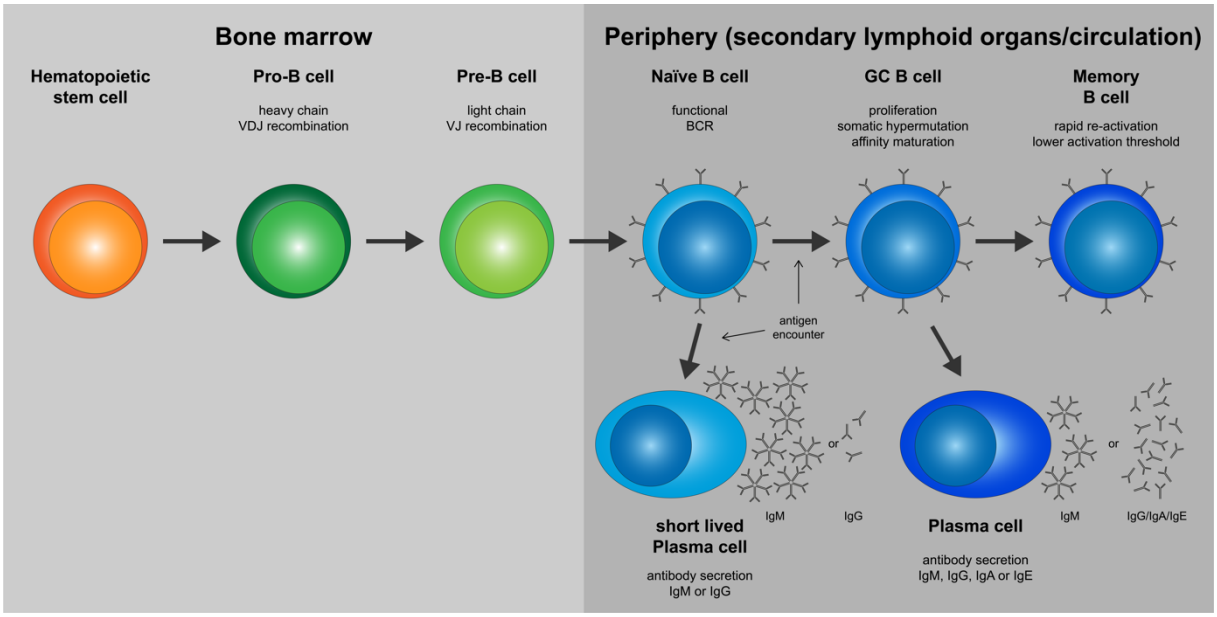

Figure 2.1 Schematic overview of B cell maturation. B cells originate from hematopoietic stem cells. When a functional BCR is rearranged they ultimately differentiate into plasma cells or memory B cells. Bone marrow compartment is shaded in light grey and the periphery consisting of secondary lymphoid organs and circulating cells is shaded in dark grey. GC = germinal center.

Naïve B cells are activated by encounter with their cognate antigen resulting in stimulation of the BCR. Activation of a B cell ultimately leads to production and secretion of antibodies. Importantly, the specificity of the secreted antibody corresponds to the specificity of the membrane-bound immunoglobulin[4,21]. While marginal zone B cells require additional signals from PRRs, such as Toll-like receptors for full activation, follicular B cells, in contrast, need costimulatory factors provided by T helper cells for proper activation[25]. The BCR specificities of marginal zone B cells are often directed against polysaccharides and glycolipids, whereas

the BCRs of follicular B cells recognize protein-based antigens[26]. Activation of B cells induces proliferation (clonal expansion) and the daughter cells undergo two fates: either they further differentiate into short-lived plasma cells that secrete low affinity IgM antibodies, or they seed in lymphoid follicles to form germinal centers (GCs)[27]. GCs contain two regions, the dark and the light zone. In the dark zone, activated B cells strongly proliferate, allowing somatic hypermutation. In this process mutations are introduced into the antigen binding sites (rearranged VDJ and VJ regions of the Ig heavy and light chains, respectively) to improve binding to their cognate antigen[28]. In the light zone of GCs, B cells are selected according to their affinity of the previously mutated BCR and B cells can undergo class switch recombination[28]. In contrast, a recent report suggests that class switch recombination occurs infrequently in GCs, which is supported by the presence of short-lived plasma cells that secrete antibodies of IgG isotype[29]. Ultimately, B cells leaving GCs express BCRs with improved affinity and often with a different isotype. Most of these cells further differentiate into antibody secreting plasma cells, while some of them differentiate into long-lived memory B cells[28]. An important characteristic of memory B cells is a rapid re-activation upon re-infection with the same pathogen, leading to a fast, more robust and thus more effective secondary humoral immune response[30].

Soluble antibodies and the membrane-anchored immunoglobulin consist of two equal heavy chain and two equal light chain (either κ or λ type) molecules that are linked by disulfide bridges. The N-terminal regions of Ig heavy chains with the rearranged VDJ segments in combination with rearranged VJ segments of the light chains determine the specificity. The C-terminal region (Fc-region) of the Ig heavy chains however determines the isotype. To date, five different isotypes of antibodies are described, IgM, IgD, IgG, IgA and IgE, each of which has unique characteristics[26]. While antibodies of the IgM isotype are mainly produced after the first encounter with an antigen, a high number of activated B cells switch to IgG isotypes during the GC reaction[27,31]. These antibodies, dependent on their IgG subtype, have outstanding qualities in opsonization, neutralization and activation of the complement system and constitute 75% of all antibodies of the serum. 10% of antibodies in serum are IgM and 15% IgA, which mainly act in mucous membranes[31]. Barely any detectable amounts of both IgD (< 0.5%) and IgE (< 0.1%) are present in the serum, even though IgE antibodies are widely known for their role in protection against helminths and as mediators of allergies[31]. Furthermore, vaccinations trigger the production and secretion of antibodies by B cells and antibodies are widely used in research and diagnostic, as well as for treatment of autoimmune and cancer diseases[32–34].

2.3. B cell antigen receptor signaling

From development of hematopoietic stem cells to the activation of matured B cells, the BCR-mediated signaling plays an indispensable role for B cells. Currently, two different models of BCR activation are discussed. In the crosslinking model it is suggested that individual BCRs are distributed all over the surface of B cells, preventing any interactions in the absence of antigens. After binding of an antigen, multiple receptors are crosslinked and thereby, due to close proximity, the intracellular signal transduction is induced[35]. On the other hand, the association-dissociation model proposes that the BCRs are grouped in islands in the resting state and antigen binding triggers dissociation of that complex leading to intracellular signal transduction[36,37].

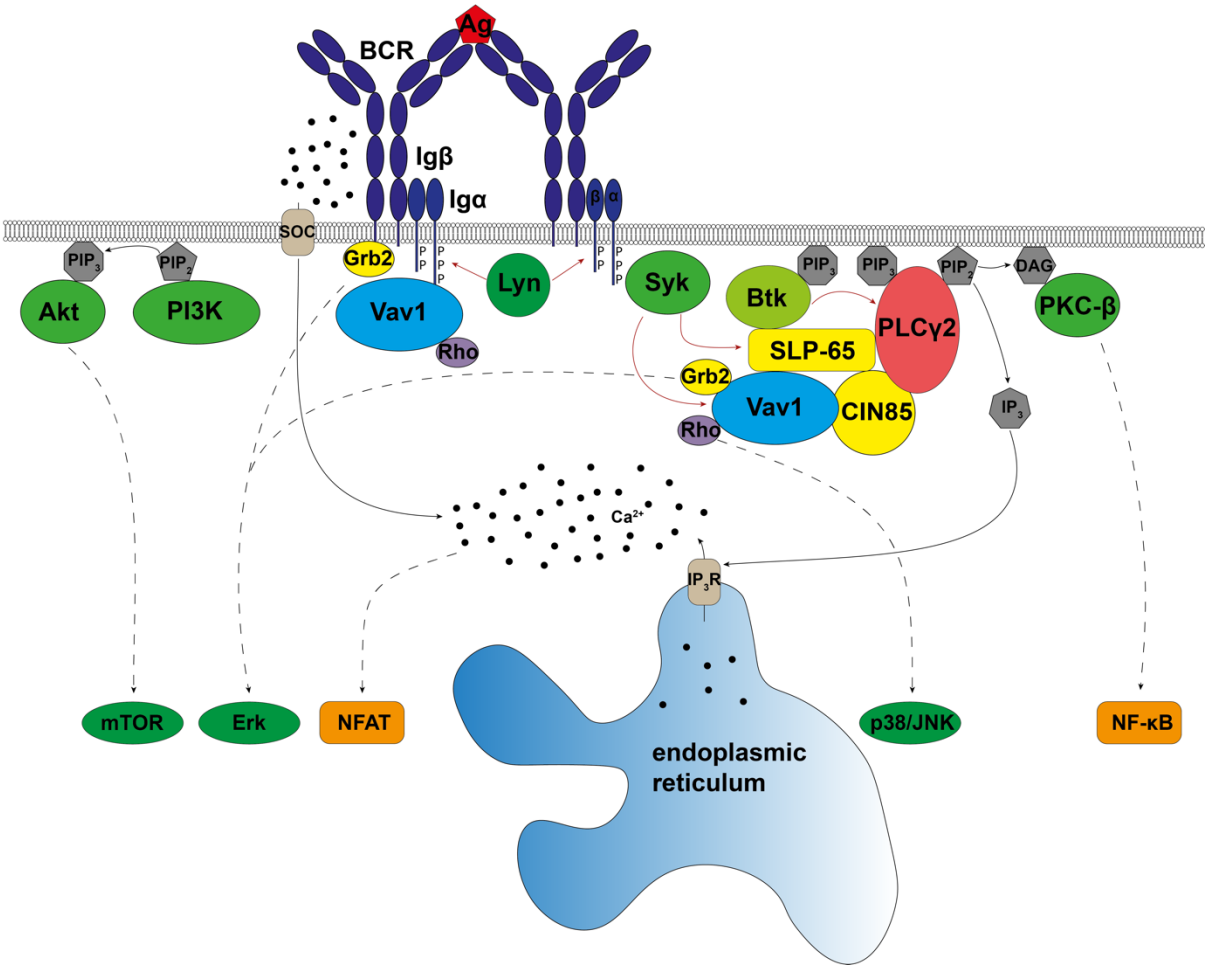

Figure 2.2 Schematic overview of the BCR-induced signaling cascade. The BCR signaling cascade is triggered by binding of the cognate antigen (Ag) to the BCR, mediating activation. Tyrosine residues inside and outside of ITAMs in Igα and Igβ are phosphorylated by Src family kinases like Lyn. Consequently, Syk and SLP-65 are recruited. Due to generation of binding sites for SH2 containing proteins by phosphorylation of SLP-65 through Syk, the Ca^{2+} initiation complex is formed consisting of Btk, PLCγ2, CIN85 and Vav1. As a result, Ca^{2+} is mobilized into the cytosol, mediating the nuclear translocation of the transcription factor NFAT. Additionally, the translocation of the transcription factor NF-κB into the nucleus is induced and MAPK like Erk, JNK and p38 are activated. Survival and proliferation are promoted via the PI3K/Akt pathway. Red arrows indicate phosphorylation processes, solid arrows indicate translocation processes and dashed arrows indicate multistep activation processes. Ca^{2+} is indicated as black dots. Kinases are colored in green, adaptor proteins in yellow, PLCγ2 in red, Vav1 in blue, Rho GTPases in purple, transcription factors in orange, Ca^{2+}-channels in light brown, phosphatidylinositols and relatives in dark grey, the BCR complex with Igα and Igβ in dark blue and the antigen in dark red.

However, a recent report using super resolution stimulated emission depletion (STED) microscopy showed that BCR clusters are formed after stimulation of the BCR, speaking for the crosslinking model[38]. Certainly, both models have in common that the signal is triggered by binding of antigen to the BCR (Figure 2.2). The membrane-anchored immunoglobulin itself is not capable of transducing any signals into the cytosol since it has no intracellular signal transduction domains. The signal transduction is enabled by the non-covalently but constantly associated integral Igα/Igβ heterodimer[19]. Activation of the BCR mediates phosphorylation of intracellular immunoreceptor tyrosine-based activation motifs (ITAMs) in Igα and Igβ by Src family kinases like Lyn and the kinase Syk is recruited to those phosphorylated tyrosines[39,40]. Due to this interaction, autoinhibition of Syk is relieved and tyrosine-rich regions that were previously masked by the own tandem Src-homology 2 (SH2) domains, become available. These tyrosines are auto-phosphorylated leading to full activation of Syk[40]. While Syk is specifically recruited to phosphorylated tyrosine residues of the ITAM in Igα and Igβ, the indispensable signaling protein SH2-domain-containing leukocyte adaptor protein of 65 kDa (SLP-65, also named BLNK) is recruited to the phosphorylated non-ITAM tyrosine 204, which is exclusively found in Igα[41–43]. On phosphorylation of SLP-65 by Syk, further docking sites are generated for additional SH2 domain-containing proteins[43]. Moreover, SLP-65 contains various proline-rich regions that serve as interaction motifs for SH3 domain-containing proteins[44]. These features make SLP-65 the central adaptor platform within the BCR signaling cascade[45]. Mice deficient for SLP-65 expression show strongly reduced numbers of B cells and disturbed BCR-induced signaling[46]. In line with this observation, SLP-65 deficient human DG75 B cells are barely capable of Ca^{2+} signaling compared to parental DG75 B cells[47]. Cbl-interacting protein of 85 kDa (CIN85) is a constant, BCR stimulation independent, interaction partner of SLP-65 and facilitates membrane recruitment of the SLP-65/CIN85 complex[48]. Absence of this complex in B cells leads to disturbed BCR-induced Ca^{2+}-mobilization and impaired activation of nuclear factor 'kappa-light-chain-enhancer' of activated B cells (NF-κB)[48]. Bruton's tyrosine kinase (Btk) and the phospholipase γ2 (PLCγ2), together with SLP-65 and CIN85, form the Ca^{2+}-initiation complex[49]. A distinct amount of both proteins, Btk and PLCγ2, are localized at the plasma membrane due to interactions with phosphatidyl-inositol-3,4,5-trisphosphate (PIP_3) through their PH domains[50,51]. They furthermore interact via their SH2 domains with the phosphorylated tyrosine residues of SLP-65[43,52]. In addition, Vav family members are part of this multimeric protein complex by recruitment via their SH2 domain to phosphorylated tyrosine residues of SLP-65, Syk or Igα[41,43,47]. This membrane-localized complex constitutes a branching point of several signaling axes within the BCR-induced signaling[21,49].

The kinase Btk activates the phospholipase PLCγ2, which subsequently cleaves phosphatidyl-inositol-4,5-bisphosphate (PIP_2) into diacylglycerol (DAG) and inositol-1,4,5-trisphosphate

(IP_3)[53]. While DAG remains in the plasma membrane, the soluble second messenger IP_3 diffuses into the cytosol and translocates to the plasma membrane of the endoplasmic reticulum (ER)[49]. Here, IP_3 binds to its IP_3-receptors, which are ligand-gated Ca^{2+}-channels[54]. As a consequence of this binding, the Ca^{2+}-channels are opened and Ca^{2+} is released from the ER into the cytoplasm[49]. This Ca^{2+}-flux is further supported by opening of store-operated Ca^{2+}-channels located within the plasma membrane through Ca^{2+}-dependent clustering of stromal interaction molecules (STIMs) and the Ca^{2+} release-activated Ca^{2+}-channel Orai[55]. Elevated intracellular Ca^{2+}-levels lead to the activation of the Ca^{2+}-dependent serine/threonine phosphatase Calcineurin. Calcineurin dephosphorylates the cytosolic transcription factor nuclear factor of activated T cells (NFAT), thereby releasing its retention in the cytosol due to constant phosphorylation and promoting its translocation into the nucleus[49].

At the plasma membrane, protein kinase C-β (PKC-β) is recruited to DAG[56]. Proper activation of PKC-β requires binding of Ca^{2+} to its C2 domain[49]. Phosphorylation of various adaptor proteins activates the transforming growth factor-β-activated kinase 1 (Tak1), which in turn phosphorylates and activates the inhibitor of NF-κB (IκB) kinase (IKK)[56]. Eventually, this kinase phosphorylates and thereby marks IκB, an inhibitory protein which is responsible for the cytosolic retention of NF-κB, for proteasomal degradation[57]. As a result, the transcription factor NF-κB translocates into the nucleus[49].

In addition to the previously described formation and effects of the Ca^{2+}-initiation complex, the adaptor protein growth factor receptor-bound protein 2 (Grb2) is upon stimulation directly recruited to the BCR and responsible for activation of the MAPK Erk[58,59]. Furthermore, activation of the BCR leads to membrane recruitment of phosphoinositide-3 kinase (PI3K) family members which phosphorylate their substrate PIP_2 to PIP_3[60]. Membrane-bound PIP_3 not only serves as membrane anchor for different PH domain-containing proteins like Btk or PLCγ2, it also recruits the kinase Akt (also named protein kinase B, PKB)[50,51,61]. Recruitment of Akt ultimately leads to the activation of metabolism, survival and proliferation pathways[60–62].

In summary, BCR signaling involves a complex interplay of different types of proteins to achieve activation of transcription factors such as NF-κB and NFAT, but also activation of MAPK like Erk, JNK and p38 as well as promotion of survival and proliferation (Figure 2.2). This signaling pathway is of enormous significance for each developmental stage of a B cell. Dysregulation might lead to severe diseases such as immunodeficiencies, autoimmunity and malignancies, therefore it is required to understand the underlying mechanism in detail[63–65].

2.4. The Vav family of guanine-nucleotide exchange factors

Vav family proteins belong to the less understood molecules within the BCR signaling cascade. However, in T cells Vav family members mediate activation of mitogen-activated protein

kinases (MAPK) such as c-Jun N-terminal kinase (JNK) and p38[66,67]. Vav1 and Vav2 double-deficient mice were described to be impeded in the development of B and T cells[68,69]. Moreover, loss of Vav1 expression in human DG75 B cells has severe negative effects on BCR-induced Ca^{2+}-mobilization[47]. However, the underlying mechanisms remain to date unknown[47,68,69]. In general, Vav family members are proteins of dual functions, they mediate GEF-activity towards Rho family members of small G proteins and exhibit adaptor function[70]. This two-pronged functionality is reflected in the secondary protein structure of Vav proteins (Figure 2.3). All family members share the same domain composition, in which the N-terminal domains (green frame) are responsible for the mediation and regulation of the GEF-activity and the C-terminal domains (blue frame) function as protein-protein interfaces which includes intramolecular and intermolecular interactions[71,72].

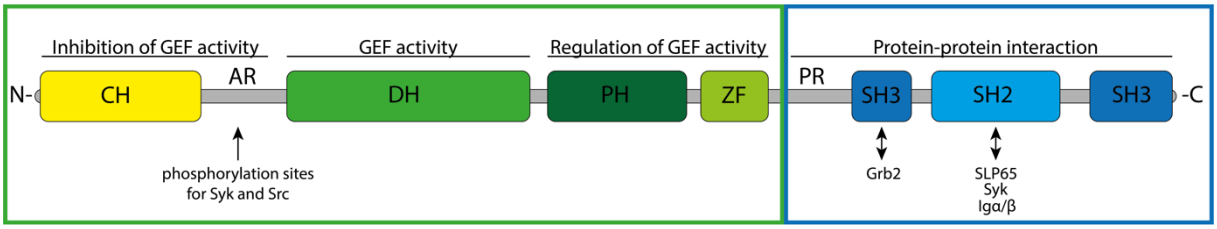

Figure 2.3 Schematic domain architecture of Vav family members. The individual domains of Vav family members and their function. Green frame: domains involved in GEF-activity. Blue frame: domains involved in protein-protein interaction. N = N-terminal end, C = C-terminal end, CH = Calponin-homology domain, AR = Acidic region, DH = Dbl-homology domain, PH = Pleckstrin-homology domain, ZF = Zinc finger region, PR = Proline Rich region, SH3 = Src-homology 3 domain, SH2 = Src-homology 2 domain.

Vav family members have been discovered between 1989 and 1999 by different groups[73–75]. Vav1, the first described isoform, was discovered while searching for new oncogenes. Since *VAV1* was the sixth oncogene found in this laboratory and the native language of the discoverer was Hebrew, they named the protein after the sixth letter of the Hebrew alphabet[73]. Although all three isoforms share similarities of 50% to 60% on amino acid level, expression is clearly cell type specific[71]. Vav2 and Vav3 are ubiquitously expressed in most cells of the human body whereas expression of Vav1 is limited to the hematopoietic lineage[71]. However, experiments in mice revealed redundancies in the function of Vav family members. Mice that lack expression of Vav1 barely show any abnormalities in B and T cell development or in BCR- and TCR-induced signaling compared to wild-type mice, whereas Vav1 and Vav2 double-deficient mice show significantly impaired B and T cell development and reduced BCR-induced Ca^{2+}-signaling[69,76]. Furthermore, these effects were even more pronounced upon loss of all three Vav family members in Vav1/Vav2/Vav3 triple-deficient mice[68]. In contrast to mice, generation of model systems in human B and T cell lines, DG75 and Jurkat, respectively, revealed that deletion of Vav1 leads to severely reduced BCR- and TCR-induced Ca^{2+}-mobilizations[47,77].

Collectively, these experiments in murine and human model systems have drawn attention to the research on Vav family members to understand their role in the generation of lymphocytes, BCR and TCR signaling. The underlying mechanism for Vav family members to contribute to lymphocyte development and their precise role within the BCR signaling cascade however remains unknown.

2.4.1. Vav family domain architecture and functions

Vav family members are multi-domain proteins with two functional sections. In brief, domains important for the GEF-activity are located within the N-terminal region of Vav family members and consist - from N-terminal to C-terminal - of Calponin-homology domain (CH domain), acidic region (AR), Dbl-homology domain (DH domain), Pleckstrin-homology domain (PH domain) and a zinc finger domain (ZF)[71]. The C-terminal region mediates protein-protein interactions and consists of a proline rich (PR) region followed by an SH2 domain flanked by one SH3 domain on each site (Figure 2.3)[71]. Each of the individual domains contribute to different extents to BCR-induced Ca^{2+}-mobilization, however, the underlying mechanisms remain widely unknown[47,72,78].

2.4.1.1. The adaptor part of Vav proteins

The C-terminal adaptor part of Vav mediates protein-protein and intramolecular interactions via a PR region, one SH2 domain and two SH3 domains[71]. SH2 domains interact with phosphorylated tyrosine residues of active signaling complexes, whereas SH3 domains interact with proline rich regions[79]. Adjacent amino acids closely located to the binding site of SH2 or SH3 domains and the surrounding amino acids of the tyrosine of the binding partner determine the specificity for recruitment of the SH2 and SH3 domains[79]. Thus, Vav family members are recruited to phosphorylated residues upon stimulation of the BCR through their SH2 domains, but they can also serve as additional binding platforms through their SH3 domains and their PR region[72].

Vav1 is specifically recruited to the BCR after stimulation to the integral signaling unit Igα or to Syk and SLP-65 through the SH2 domain[41,43,47,80]. Similarly, Vav1 is recruited to the TCR and its signaling components upon TCR-stimulation through the SH2 domain[81]. This recruitment is indispensable for BCR-induced Ca^{2+}-mobilization in DG75 B cells, since inactivation of the SH2 domain leads to BCR-induced Ca^{2+}-profiles representing Vav1-deficient DG75 B cells[47]. The N-terminal SH3 domain (hereinafter referred to as N-SH3) is known to engage in an atypical N-SH3-SH3 interaction with the adaptor protein Grb2[82]. Further interaction partners of the N-SH3 of Vav family members have not been described so far[72]. In contrast, the C-terminal SH3 domain (C-SH3) of Vav1 establishes intramolecular and intermolecular interactions[72]. Deletion of this domain leads to a loss of GEF-activity in Vav1[78]. A functional relevance of

known C-SH3 interaction partners for the GEF-activity of Vav family members, in the context of lymphocyte development or the antigen receptor signaling has not been described so far[83–85].

2.4.1.2. GEF-activity of Vav-family members

Vav family members activate small G proteins of the Rho family due to their GEF-activity that is mediated by a functional core consisting of their consecutively arranged DH, PH and ZF domains[86–88]. Upon recruitment of Vav1 to the BCR and its signaling components via its SH2 domain, Vav1 is phosphorylated and activated by Syk or Src family kinase members[80,89]. Both, the arrangement of the functional core unit and the stimulation depended recruitment via a SH2 domain are unique characteristics for GEFs towards Rho family small G proteins[72]. The GEF-activity of Vav family members is tightly controlled. Non-phosphorylated Vav proteins exhibit barely any GEF-activity due to their "closed" molecular structure mediated by interactions of the catalytic DH-PH-ZF core with the C-SH3 domain as well as the CH domain and the AR[72]. These interactions occlude binding sites for small G proteins and additionally force the catalytic core into a conformation that further prevents binding of Rho family members[72]. Furthermore, the PH domain within the catalytic core is in contact with the DH domain to stabilize the "closed" structure[72]. In addition, the PH domain influences the GEF-activity of Vav proteins by binding to phosphatidyl-inositols[90]. *In vitro* experiments revealed that binding of PIP_2 to the PH domain decreases the catalytic activity of Vav1 while binding of PIP_3 leads to an increased GEF-activity[91]. The AR of Vav proteins contains several negatively charged amino acid residues and forms an inhibitory loop in the "closed" state that blocks the active center of Vav proteins[78]. Currently, the role of the CH domain in the regulation of the GEF-activity remains to be elucidated in detail. Classical CH domains (type I and II) naturally occur as tandem CH domains and constitute evolutionary conserved actin binding domains to mediate binding to the actin cytoskeleton[92]. These conserved binding regions were lost during evolution for CH domain types III, IV and V[92]. Hence, the exact function of type III, IV, V CH domains has not been generalized so far and is proposed to be specific for each individual CH domain-containing protein[92]. Vav family members contain type III CH domains. Deletion of this domain resulted in a transformation potential of Vav1 for malignancies, which was manifested by an enhanced GEF-activity[78,93]. In contrast, studies in B and T cells revealed that loss of the CH domain leads to disturbed effector functions regarding to BCR and TCR-induced Ca^{2+}-mobilization or stimulation-dependent activation of NFAT in T cells[47,70,94]. Classical actin binding type I and II CH domains could not functionally replace the endogenous type III CH domain in Vav1 regarding BCR-induced Ca^{2+}-mobilization in DG75 B cells[47]. Thus, the function of the CH domain of Vav proteins for Ca^{2+}-mobilization after BCR stimulation is not to bind the actin cytoskeleton.

For activation, Vav proteins are phosphorylated on several tyrosine residues within different domains[80,89]. The AR of Vav proteins contains three tyrosines that are phosphorylated during this activation process. Due to introduction of additional negative charges in the AR, the structure of the inhibitory loop is resolved and an “open” conformation of Vav proteins is generated[78,95]. This conformational change to the “open” stage of Vav proteins is further supported by phosphorylation of two tyrosine residues within the ZF domain as well as the C-SH3 domain and ultimately leads to enhanced GEF-activity[72].

Experiments in mice expressing a GEF-inactive variant of Vav1 revealed that the GEF-activity of Vav proteins is important for selection of thymocytes and for optimal activation of T cells[96]. TCR-stimulated T cells of these mice showed reduced Rac1 activation and phosphorylation of Akt while TCR-induced Ca^{2+}-mobilization however was not affected by the GEF-inactive variant of Vav1[96]. In B cells, little is known about the role of the GEF-activity of Vav family members towards small G proteins of the Rho family. Vav-dependent activation of Rac is linked to cytoskeletal rearrangements and receptor internalization[97,98]. Furthermore, DG75 B cells expressing a Vav1-variant without GEF-activity showed similar BCR-induced Ca^{2+}-profiles as DG75 B cells deficient for Vav1[47,78,99]. Conclusively, these experiments indicate that the GEF-activity of Vav proteins might be important for lymphocyte development and activation.

2.4.1.2.1. The Rho family of small G proteins

The Rho family of small G proteins (or GTPases) belongs to the Ras superfamily and consists of 20 family members that share amino acid sequence homology between 45% and 95%[100,101]. They are grouped into 8 sub-families, all sharing the characteristic of a Rho-type GTPase-like domain[101,102]. In addition, a structural feature that distinguishes Rho GTPases from other small G proteins of the Ras superfamily is the insertion of the Rho insert region between the fifth β sheet and the fourth α helix[100–102]. Rho GTPases are involved in several cellular processes such as cytoskeletal rearrangement, cell motility and polarity, vesicle trafficking, cell cycle regulation and formation of axons[103]. Rho GTPases are regulated by three different types of proteins, GEFs, GTPase-activating proteins (GAPs) and guanine-nucleotide dissociation inhibitors (GDIs)[101]. GEFs catalyze the nucleotide exchange from guanosine diphosphate (GDP) to guanosine triphosphate (GTP), a soluble mediator required for activation of the small GTPases[104]. In contrast, GAPs increase the intrinsic GTP hydrolysis activity, promoting inactivation of small G proteins[101]. GDIs preserve the GDP-bound inactive state of Rho small G proteins in the cytosol, preventing their recruitment to adaptor proteins and activation[104]. *In vivo* studies in mice revealed that different members of Rho GTPases are critical for development, maturation and activation of lymphocytes, even though to different extents[105]. For example, mice that were deficient for Rac2 showed reduced B cell and plasma cell numbers and defects in BCR-induced signaling[106]. In contrast, mice deficient for Rac1 were

barely affected by the knockout in B cell development and activation[105]. Mice that were deficient for both, Rac1 and Rac2 exhibited an impeded development of B cells in early stages[107,108]. To understand the role of Vav proteins for BCR signaling, it is critical to understand which Vav isoform activates which Rho GTPases.

2.5. Phosphatidylinositol-4-phosphate 5 kinases (PIP5Ks)

The availability of PIP_2 is essential for BCR-induced signaling on two levels. PIP_2 as the substrate of PLCγ2 is required to induce Ca^{2+}-mobilization along with nuclear translocation of the transcription factors NFAT and NF-κB[21]. Moreover, PIP_2 is phosphorylated by PI3K for induction of the PI3K/Akt pathway[21]. Producers of PIP_2 are the phosphatidylinositol-4-phosphate 5-kinases (PIP5Ks), which phosphorylate phosphatidylinositol-4-phosphate (PI4P) at the D-5 position of the inositol ring to generate PIP_2[109]. Alternatively, PIP_2 is generated by phosphatidylinositol-5-phosphate 4-kinases (PIP4Ks) that phosphorylate phosphatidylinositol-5-phosphate (PI5P) at the D-4 position[110]. But since the intracellular abundance of PI4P is ten times higher than of PI5P, PIP5Ks represent the main producer of PIP_2[111]. PIP5Ks were first described in the 1980's and today three family members are known, PIP5Kα, PIP5Kβ and PIP5Kγ[112,113]. However, the cDNAs of each isoform were cloned in the late 1990's[114–116]. The activity of PIP5Ks is differentially regulated by different mechanisms for each isoform and they play an important role in a variety of signaling pathways[113]. Activation through Rho GTPases loaded with GTP is described by several groups and this activation is further supported by phosphorylation through Src family kinases, the latter at least for PIP5Kγ[117–119]. In addition, reports of groups investigating lymphocyte biology revealed a role of PIP5Ks in T cell activation and the formation of lipid rafts in the plasma membrane of T cells within the immunological synapse[120,121]. In B cells, it has been demonstrated that co-stimulation of the BCR and CD19, a co-receptor of B cells, leads to recruitment of Vav1 and PIP5Ks to CD19[122]. Furthermore, another group reported that upon stimulation of the BCR, PIP5Ks are recruited together with Btk to the stimulated BCR[123]. Both processes lead to locally elevated levels of PIP_2 for sufficient BCR signaling[122,123]. Consequently, PIP5Ks represent putative candidates as downstream molecules of the GEF-activity towards Rho GTPases of Vav family members.

2.6. Aims of this thesis

Using a cellular model system based on Vav1-deficient DG75 B cells, previous results of our lab demonstrated that loss of Vav1 severely diminished the ability to mobilize Ca^{2+} upon stimulation of the BCR. However, formation of the Ca^{2+}-initiation complex was not affected. We furthermore found that Vav1 and Vav3 supported BCR-induced Ca^{2+}-mobilization whereas Vav2 remained inactive[47]. In addition, Vav1 had to be recruited through its SH2 domain to the BCR or other signaling components to exhibit its function. Also, the CH domain was observed

to be essential for BCR-stimulated Ca^{2+}-flux into the cytosol[47]. However, the underlying mechanism for Vav family members to control Ca^{2+}-signaling yet remains to be elucidated. Therefore, the aim of this thesis was to investigate whether BCR-induced Ca^{2+}-mobilization is controlled or influenced by the GEF-activity of Vav family members which might influence the function of Rho GTPases. In detail, to address the question whether the GEF-activity is critical for BCR-induced signaling, I focused on the following issues on during this Ph.D. project:

1. To clarify whether differences in BCR-induced signaling capacities originate from different recruitments of Vav family members, I tested the association of Vav1, Vav2 and Vav3 to the stimulated BCR and its signaling components.

2. To reveal whether the interaction of Vav1 and Rac1 and the associated GEF-activity is required for BCR-induced signaling, I generated Vav family member variants with mutations within Vav1-Rac1 interaction interfaces and the resulting constructs were analyzed in Vav1-deficient DG75 B cells.

3. To get a clearer understanding of putative differential substrate preferences and the effects of the introduced mutations, the GEF-activity towards Rac1, RhoA and Cdc42 for all Vav family members and their respective mutant variants was determined.

4. To uncover whether the inability of Vav2 to support BCR-induced Ca^{2+}-mobilization derives from inhibitory effects of the acidic region, I examined this region in detail.

5. To get insights whether PIP5K family members are required for BCR-induced signaling as potential downstream effectors of the GEF-activity of Vav family members, I generated, genetically characterized and analyzed DG75 cells deficient for PIP5K family members.

6. To understand whether other signaling axes within BCR signaling depend on the presence of Vav family members and/or their GEF-activity, I tested BCR-induced signaling branches such as PI3K/Akt pathway, actin remodeling and activation of MAPK like p38 and Erk.

3. Material & Methods

3.1. Material

3.1.1. Laboratory equipment

Table 3.1 Laboratory equipment.

Name	Manufacturer
12-Tube Magnetic Separation Rack	NEB
Agarose Gel Electrophoresis system	Peqlab
Amaxa Nucleofector II	Lonza
Bacterial Incubator Kelvitron T	Heraeus
Bacterial Shaking Incubator Infors	Unitron
Balance BP 61	Sartorius
Balance TF 612	Sartorius
Cell Culture Incubator HeraCell 150	Heraeus
Cell Culture Safety Cabinet Herasafe	Heraeus
Centrifuge 5415D	Eppendorf
Centrifuge 5417R	Eppendorf
Centrifuge Multifuge 3 S-R	Heraeus
Chemi Lux Imager	Intas
Cytation 3 Plate Reader	BioTek
Cytometer LSRII	Becton Dickinson
Electrophoresis Power Supply	Amersham Biosciences
Electrophoresis System Hoefer SE600	Amersham Biosciences
Freezer HeraFreeze	Heraeus
Freezer Platilab 340	Angelantoni
Ice Machine	Ziegra
Inverted Microscope Axiovert 35	Zeiss
Magnetic stirrer M21/1	Framo Gerätetechnik
Mastercycler EP Gradient	Eppendorf
NanoDrop2000 Spectrophotometer	Thermo Scientific
Neubauer improved Counting Chamber	Brand
pH-Meter inoLab	WTW
Pipettes	Eppendorf
Rotator (Self-Made)	Werkstatt (UMG)
Shaker Duomax 1030	Heidolph

Shaker 3005	GFL
Test-Tube-Rotator 34528	Snijders
Thermomixer comfort	Eppendorf
Ultra-Low Temperatur Freezer MDF-C2156VAN	Panasonic
Ultrasonic Device Sonoplus	Bandelin
UV-Illuminator	Intas
Vortex Genie 2	Scientific Industries
Water Bath	GFL
Water Purification System Arium Pro	Sartorius
Western Blot Semidry Transfer Unit TE77	GE Healthcare

3.1.2. Consumables

Table 3.2 Consumables.

Name	Manufacturer
Cell Culture Dishes	Greiner Bio-One
Cell Culture Plates	Greiner Bio-One
Cell Culture Serological Pipettes	Greiner Bio-One
Cryo Tubes	Greiner Bio-One
Cuvettes	Roth
FACS Tubes	Sarstedt
Filter Tips	Greiner Bio-One
FLUOTRAC, 96-well plates	Greiner Bio-One
Nitrocellulose Membranes	Amersham Biosciences
Parafilm	Bemis
PCR Tubes	Sarstedt
Pipette Tips	Greiner Bio-One
Polypropylene Tubes	Greiner Bio-One
Reaction Tubes	Greiner Bio-One
Sterile Filters	Sarstedt
Whatman Blotting Paper	GE Healthcare

3.1.3. Software and data bases

Table 3.3 Software.

Application	Software	manufacturer
Agarose Gel Imaging	Gel Documentation Software	Intas
Citation Management Software	Mendeley	Elsevier
Flow Cytometry Data Acquisition	FACSDiva	Becton Dickinson
Flow Cytometry Data Analysis	FlowJo 7.6.5	Becton Dickinson
Graphing and statistical analysis	Prism 7	GraphPad
Illustration Software	Illustrator	Adobe
Image editing	Photoshop	Adobe
Sequencing Data Analysis	FinchTV	Geospiza
Sequencing Data Analysis	pDRAW32	Acaclone
Western Blot Data Acquisition	Chemostar Professional	Intas
Western Blot Data Analysis	LabImage 1D	Kapelanbio

Table 3.4 Data bases.

Data base	Application
http://primer3.ut.ee	Primer design
https://blast.ncbi.nlm.nih.gov/Blast.cgi	Sequence alignment
https://crispr.mit.edu/	CRISPR/Cas9 guide RNA design
https://www.ensembl.org/index.html	Genomic and mRNA data base
https://www.uniprot.org	Protein data base

3.1.4. Chemicals and reagents

All chemicals used for the preparation of buffers were purchased from Roth, Sigma or Merck if not stated otherwise. Any other chemicals and reagents are listed in Table 3.5.

Table 3.5 Chemicals and reagents.

Name	Manufacturer
10x Perm/Wash Buffer I	Becton Dickinson
100x Bovine Serum Albumin (BSA)	NEB
Agarose	Peqlab
Blue Prestained Protein Marker, Broad Range	NEB
Bodipy-FL-GDP	Thermo Scientific

CytoFix Fixation Buffer	Becton Dickinson
dNTPs Mix	NEB
DNA Ladder GeneRuler 1 kb	Fermentas
Fetal Calf Serum (FCS)	Anprotec
Gel Loading Dye (6x), purple	NEB
GTP	Thermo Scientific
Hexadimethrine Bromide (Polybrene)	Sigma
Indo-1 AM	Life Technologies
InstantBlue Coomassie Protein Stain	Expedeon
Isopropyl-β-D-thiogalactopyranosid (IPTG)	Sigma
L-Glutamine (200 mM)	Gibco
Lysophosphatidylcholine (LPC)	Sigma-Aldrich
NEB buffer 1.1, 2.1, 3.1 & CutSmart	NEB
Penicillin/Streptomycin (100x)	Gibco
Pluronic F-127	Life Technologies
Protease Inhibitor Cocktail (P2714)	Sigma
Protease Inhibitor Cocktail (cOmplete, EDTA free)	Roche
Puromycin	Invivogen
Roswell Park Memorial Institute (RPMI) 1640 Medium	Gibco
Sodium Pyruvate (100 mM)	Gibco
T4 Ligase Buffer	NEB
TransIT-293 Transfection Reagent	Mirus
Trypsin/EDTA (0.05%)	Gibco
5-Bromo-4-chloro-3-indolyl β-D-galactopyranoside (X-Gal)	Roth

3.1.5. Buffers and solutions

Antibody dilution solution	1% (w/v) BSA 0.01% (w/v) NaN_3 in TBS/T
Agar plates	2% (w/v) agar in LB-medium
Blocking solution	10% (w/v) BSA in TBS/T

Blotting buffer	48 mM Tris 39 mM Glycine 0.0375% (w/v) SDS 20% (v/v) Methanol in ddH_2O
ECL solution	4 ml ECL solution A 400 µl ECL solution B 1.5 µl H_2O_2 (30%)
ECL solution A	100 mM Tris-HCl (pH 8.6) 0.28 mM Luminol in ddH_2O
ECL solution B	6.7 mM p-coumaric acid in DMSO (stored in the dark)
Freezing media	10% (v/v) DMSO in FCS
GEF-assay buffer	20 mM Tris-HCl (pH 7.5) 50 mM NaCl 2 mM EDTA 100 µg/ml BSA 500 nM DTT 600 nM Bodipy-GDP in ddH_2O
Krebs-Ringer buffer	140 mM NaCl 10 mM HEPES (pH 7.4) 10 mM D-glucose 4 mM KCl 1 mM $MgCl_2$ 1 mM $CaCl_2$ (freshly added) in ddH_2O
Laemmli buffer (5x)	156.25 mM Tris-HCl (pH 6.8) 500 mM DTT 50% (v/v) Glycerol 15% (w/v) SDS 0.05 bromophenol blue in ddH_2O
Lysogeny broth (LB) medium	10 g/l Tryptone 5 g/l Yeast Extract 5 g/l NaCl (pH 7.0) in ddH_2O
Ni-NTA equilibration buffer	20 mM NaH_2PO_4 (pH 7.4) 300 mM NaCl 10 mM Imidazole 20% (v/v) Glycerol in ddH_2O

Ni-NTA wash buffer	20 mM NaH_2PO_4 (pH 7.4) 300 mM NaCl 20 mM Imidazole 20% (v/v) Glycerol in ddH_2O
NP-40 lysis buffer	137.5 mM NaCl 50 mM Tris-HCl (pH 7.8) 1 mM sodium-orthovanadate 0.5 mM EDTA 10% (v/v) Glycerol 1% (v/v) NP-40 1x Protease Inhibitor Cocktail (freshly added) in ddH_2O
pH10 elution buffer	50 mM Tris-HCl (pH 7.4) 300 mM NaCl 5 mM EDTA 250 mM Saccharose 500 mM Imidazole 20% (v/v) Glycerol in ddH_2O
pH10 high salt wash buffer	50 mM Tris-HCl (pH 7.4) 1.5 M NaCl 20 mM Imidazole 20% (v/v) Glycerol in ddH_2O
Phosphate buffered saline (PBS)	137 mM NaCl 4.3 mM Na_2HPO_4 2.7 mM KCl 1.4 mM KH_2PO_4 (pH 6.6) in ddH_2O
Resolving gel	375 mM Tris-HCl (pH 8.8) 3.5 mM SDS 10% (v/v) Acrylamide / Bisacrylamide in ddH_2O
RPMI media with 10% FCS (R10)	10% (v/v) heat inactivated FCS 1x PenStrep 1 mM sodium pyruvate 1 mM L-glutamine 50 µM β-mercaptoethanol in RPMI-1640 medium
RPMI media without FCS (R0)	1x PenStrep 1 mM sodium pyruvate 1 mM L-glutamine 50 µM β-mercaptoethanol in RPMI-1640 medium

SDS-PAGE buffer	25 mM Tris 192 mM Glycine 0.1% (w/v) SDS in ddH_2O
Stacking gel	125 mM Tris-HCl (pH 6.8) 3.5 mM SDS 10% (v/v) Acrylamide / Bisacrylamide in ddH_2O
TAE-buffer	40 mM Tris 20 mM glacial acetic acid 1 mM EDTA in ddH_2O
TAG-lysis buffer	10 mM Tris-HCl (pH 8.0) 50 mM KCl 0.45% (v/v) NP-40 0.45% (v/v) Tween 20 in ddH_2O
Terrific broth (TB) medium	24 g/l Yeast Extract 20 g/l Tryptone 0.4% (v/v) Glycerol 72 mM K_2HPO_4 17 mM KH_2PO_4 in ddH_2O
Tris buffered saline/Tween 20 (TBS/T)	137 mM NaCl 20 mM Tris-HCl (Ph 7.6) 0.1% (v/v) Tween 20 in ddH_2O

3.1.6. Reaction systems (kits)

Table 3.6 Ready-to-use reactions systems (kits).

Kit	Application	Manufacturer
Amaxa human B cell Nucleofector Kit	Nucleofection	Lonza
QiaPrep Spin MiniPrep Kit	Plasmid purification	Qiagen
TA cloning Kit	Cloning of PCR products	Invitrogen
Wizard SV Gel and PCR Clean-Up System	Agarose gel extraction	Promega

3.1.7. Enzymes

All enzymes were used according to the manufacturer's instructions.

Table 3.7 Enzymes.

Enzyme	Manufacturer
Calf intestine phosphatase (CIP)	NEB
Pfu Polymerase	Promega
Proteinase K	Macherey & Nagel
Q5 Polymerase	NEB
Restriction Endonucleases	NEB
T4 DNA Ligase	NEB
Taq Polymerase	NEB

3.1.8. Oligonucleotides

Synthetic DNA nucleotides were designed with Primer3, ordered at Eurofins Genomics and used according to the instructions by Primer3.

Table 3.8 Standard primer used for sequencing.

Name	Sequence (5' --> 3')	Purpose
M13_fwd	TGTAAAACGACGGCCAGT	Sequencing
M13_rev	CAGGAAACAGCTATGACC	Sequencing
MSCV_fwd	CCCTTGAACCTCCTCGTTCGACC	Sequencing
MSCV_rev	CAGACGTGCTACTTCCATTTGTC	Sequencing
N-eGFP_rev	CGTCGCCGTCCAGCTCGACCAG	Sequencing
QE-fwd	GTATCACGAGGCCCTTTCG	Sequencing
QE-rev	GTTCTGAGGTCATTACTGG	Sequencing
T7	TAATACGACTCACTATAGGG	Sequencing
U6_fwd	GAGGGCCTATTTCCCATGATTCC	Sequencing

Table 3.9 Primer used for cloning.

Name	Sequence (5' --> 3')	Purpose
AmplPIP5Ka_fwd	GGAGTTTTCTTCTGTGATCTTTTAGCCAC	Cloning of *PIP5K1A*'s exon 3 in pCR2.1
AmplPIP5Ka_rev	GAACTCCTGGCCTAAAATGATCTGC	Cloning of *PIP5K1A*'s exon 3 in pCR2.1
AmplE3PIP5Kc_fwd	CTCTCTGAAGTGTGCAGTGAGT	Cloning of *PIP5K1C*'s exon 3 in pCR2.1
AmplE3PIP5Kc_rev	TGAATCACATCTCAGTAAAACGGTT	Cloning of *PIP5K1C*'s exon 3 in pCR2.1
Ampl-E5-PIP5Kb_fwd	TGGATCTATGGTGGGACTAGTAAGC	Cloning of *PIP5K1B*'s exon 5 in pCR2.1

Ampl-E5-PIP5Kb_rev	TCTCCATATGGTCTTCCAGGCATTC	Cloning of *PIP5K1B*'s exon 5 in pCR2.1
mVav1-As170-BamHI_fwd	TAATGGATCCGGGGACGAGATCTACGAGGACCTAATG	Cloning of mVav1's GEF-mediating domains in pH10
mVav1-As575-HindBam_rev	TAATGGATCCAAGCTTTTACATGGTTCCTGCGAAATCTTGCCCA	Cloning of mVav1's GEF-mediating domains in pH10
PIP5Kb-AgeI_fwd	TAATACCGGTATGTCTTCTGCTGCTGAAAATGGAG	Cloning of PIP5Kβ in pCit-N1
PIP5Kb-AgeI_rev	TAATACCGGTAAATAGACGTCAAGCACAGAAGCATT	Cloning of PIP5Kβ in pCit-N1
Vav1-As170-BamHI_fwd	TAATGGATCCGGCGACGAGATCTATGAGGACCTCA	Cloning of Vav1's GEF-mediating domains in pH10
Vav1-As575-HindBam_rev	TAATGGATCCAAGCTTTTACATAGTTCCTGGGAAATCTTGCCCATGT	Cloning of Vav1's GEF-mediating domains in pH10
Vav3-As169-BamHI_fwd	TAATGGATCCGGTGGAGAAGTCTATGAGGACTTAATGAAGG	Cloning of Vav3's GEF-mediating domains in pH10
Vav3-As573-HindBam_rev	TAATGGATCCAAGCTTTTAGAGTGTCCCTTGTTCACCAGAATTAACTCT	Cloning of Vav3's GEF-mediating domains in pH10

Table 3.10 Primer used for site directed mutagenesis. Base pair substitutions are indicated by lowercase letters.

Name	Sequence (5' --> 3')	Purpose
mVav1-LKAA_fwd2	GCAGCGGGTGgcGgcGTACCACCTCC	Site directed mutagenesis of murine Vav1
mVav1-LKAA_rev2	GGAGGTGGTACgcCgcCACCCGCTGC	Site directed mutagenesis of murine Vav1
mVav1(pH10)-Y174D_fwd	TCCGGGGACGAGATCgACGAGGACCTAA	Site directed mutagenesis of murine Vav1 in pH10
mVav1(pH10)-Y174D_rev	GCGCATTAGGTCCTCGTcGATCTCGTCC	Site directed mutagenesis of murine Vav1 in pH10
PIP5KsCitM->Lfw	CTACCGGTCGCCACCcTGGTGAGCAAGGGCGAG	Site directed mutagenesis of Citrine tag
PIP5KsCitM->Lrev	CTCGCCCTTGCTCACCAgGGTGGCGACCGGTAG	Site directed mutagenesis of Citrine tag
Vav1-D376A_fwd	AACGAGGTCAAGCGAGcCAACGAGACAC	Site directed mutagenesis of Vav1
Vav1-D376A_rev	TCGCAGTGTCTCGTTGgCTCGCTTGACC	Site directed mutagenesis of Vav1
Vav1-E201A_fwd	CTGCCTGCGGGcGATCCAGCAGACGGAG	Site directed mutagenesis of Vav1
Vav1-E201A_rev	GTCTGCTGGATCgCCCGCAGGCAGCAGCAG	Site directed mutagenesis of Vav1
Vav1-E378A_fwd	GTCAAGCGAGACAACGcGACACTGCGAC	Site directed mutagenesis of Vav1
Vav1-E378A_rev	GATCTGTCGCAGTGTCgCGTTGTCTCGC	Site directed mutagenesis of Vav1
Vav1-K208A_fwd	GACGGAGGAGgcGTACACTGACACGCTG	Site directed mutagenesis of Vav1
Vav1-K208A_rev	GTGTCAGTGTACgcCTCCTCCGTCTGCTG	Site directed mutagenesis of Vav1
Vav1-K374A_fwd	TGCGTGAACGAGGTCgcGCGAGACAACG	Site directed mutagenesis of Vav1

Vav1-K374A_rev	TGTCTCGTTGTCTCGCgcGACCTCGTTC	Site directed mutagenesis of Vav1
Vav1-N371A_fwd	CTGGCTCAGTGCGTGgcCGAGGTCAAGC	Site directed mutagenesis of Vav1
Vav1-N371A_rev	TCGCTTGACCTCGgcCACGCACTGA	Site directed mutagenesis of Vav1
Vav1-Q331A_fwd	CTGATGGTGCCTATGgcGCGAGTTCTCA	Site directed mutagenesis of Vav1
Vav1-Q331A_rev	ATATTTGAGAACTCGCgcCATAGGCACC	Site directed mutagenesis of Vav1
Vav1-R375A_fwd	GTGAACGAGGTCAAGgcAGACAACGAGA	Site directed mutagenesis of Vav1
Vav1-R375A_rev	CAGTGTCTCGTTGTCTgcCTTGACCTCG	Site directed mutagenesis of Vav1
Vav1(pH10)-Y174D_fwd	TCCGGCGACGAGATCgATGAGGACCTCA	Site directed mutagenesis of Vav1 in pH10
Vav1(pH10)-Y174D_rev	GCGCATGAGGTCCTCATcGATCTCGTCG	Site directed mutagenesis of Vav1 in pH10
Vav2deltaAR-fwd	CAGAACAAAGGGATCAGCCCTTTTATGAAAATGGGCATGACTGAAGAT	Deletion of Acidic Region in Vav2
Vav2deltaAR-rev	ATCTTCAGTCATGCCCATTTTCATAAAAGGCCTGATCCCTTTGTTCTG	Deletion of Acidic Region in Vav2
Vav2-Y142D_fwd	AATGACGATGACGTCgACCGCAGCCTGG	Site directed mutagenesis of Vav2
Vav2-Y142D_rev	CTCCTCCAGGCTGCGGTcGACGTCATCG	Site directed mutagenesis of Vav2
Vav2-Y159D_fwd	CTGGGGGAGGACATCgACGACTGCGTCC	Site directed mutagenesis of Vav2
Vav2-Y159D_rev	ACACGGGACGCAGTCGTcGATGTCCTCC	Site directed mutagenesis of Vav2
Vav2-Y172D_fwd	GGAGGGGACGACATCgACGAGGACATCA	Site directed mutagenesis of Vav2
Vav2-Y172D_rev	CTTGATGATGTCCTCGTcGATGTCGTCC	Site directed mutagenesis of Vav2
Vav3-E199A_fwd	TCCGGTGGAGAAGTCgATGAGGACTTAA	Site directed mutagenesis of Vav3
Vav3-E199A_fwd	CTTCATTAAGTCCTCATcGACTTCTCCA	Site directed mutagenesis of Vav3
Vav3(pH10)-Y173D_fwd	AGTTGTTGTCTAGCAGcAATTAAGCAGA	Site directed mutagenesis of Vav3 in pH10
Vav3(pH10)-Y173D_fwd	TTCTGTCTGCTTAATTgCTGCTAGACAA	Site directed mutagenesis of Vav3 in pH10

Table 3.11 Primer used as sgRNA for CRISPR/Cas9-mediated genome editing.

Name	Sequence (5' --> 3')	Purpose
PIP5KA-E3-fwd	CACCGCATAGAAGTGTTGATTCCTC	sgRNA to CRISPR exon 3 of *PIP5K1A*
PIP5KA-E3-rev	AAACGAGGAATCAACACTTCTATG	sgRNA to CRISPR exon 3 of *PIP5K1A*
PIP5Kc-E3-fwd	CACCGCGGATGCGTCCACACCTCGA	sgRNA to CRISPR exon 3 of *PIP5K1C*

PIP5Kc-E3-rev	AAACTCGAGGTGTGGACGCATCCG C	sgRNA to CRISPR exon 3 of *PIP5K1C*
PIP5Kc-E4-fwd	CACCGCTGCATGAGCACGTCGCGTT	sgRNA to CRISPR exon 4 of *PIP5K1C*
PIP5Kc-E4-rev	AAACAACGCGACGTGCTCATGCAGC	sgRNA to CRISPR exon 4 of *PIP5K1C*
CRISPR-PIP5Kb-E5_fwd1	CACCGCTTGCTCCAAAACAATGACG	Upstream sgRNA to CRISPR exon 5 of *PIP5K1C*
CRISPR-PIP5Kb-E5_rev1	AAACCGTCATTGTTTTGGAGCAAGC	Upstream sgRNA to CRISPR exon 5 of *PIP5K1C*
CRISPR-PIP5Kb-E5_fwd2	CACCGTTGTGACAACCCCATATTGA	Downstream sgRNA to CRISPR exon 5 of *PIP5K1C*
CRISPR-PIP5Kb-E5_rev2	AAACTCAATATGGGGTTGTCACAAC	Downstream sgRNA to CRISPR exon 5 of *PIP5K1C*

3.1.9. Vectors and plasmids

Table 3.12 Plasmids, vectors and cDNAs used for cloning.

Name	Source	Application
pcDNA3.1-PIP5Kβ	GenScript	Cloning of PIP5Kβ
pCitrine-N1	Michael Engelke	C-terminal Citrine-tagging
pCR2.1	Invitrogen	Cloning
pH10-TEV	Hansjörg Götzke	His-tagged protein expression
pMSCV-Puro	Clontech	Protein expression
pRetroX-TetOne-Puro	Clontech	Inducible protein expression
pSpCas9(BB)-2A-GFP	Addgene	CRISPR/Cas9-mediated genome editing

Table 3.13 Retroviral expression plasmids.

Insert	Backbone	Source
eGFP	pMSCV-Puro	Michael Engelke
mVav1-Cit	pMSCV-Puro	Christoffer Hitzing
mVav1-Cit LK334/335AA	pMSCV-Puro	This work
PIP5Kα-Cit	pRetroX-TetOne-Puro	This work
PIP5Kβ-Cit	pRetroX-TetOne-Puro	This work
PIP5Kγ-Cit	pRetroX-TetOne-Puro	This work
Citrine	pRetroX-TetOne-Puro	This work
Vav1-Cit	pMSCV-Puro	Christoffer Hitzing
Vav1-Cit D376A	pMSCV-Puro	This work
Vav1-Cit E201A	pMSCV-Puro	This work
Vav1-Cit E201A E378A	pMSCV-Puro	This work

Vav1-Cit E201A N371A	pMSCV-Puro	This work
Vav1-Cit E378A	pMSCV-Puro	This work
Vav1-Cit K208A	pMSCV-Puro	This work
Vav1-Cit K374A	pMSCV-Puro	This work
Vav1-Cit L213Q	pMSCV-Puro	Christoffer Hitzing
Vav1-Cit N371A	pMSCV-Puro	This work
Vav1-Cit Q331A	pMSCV-Puro	This work
Vav1-Cit R375A	pMSCV-Puro	This work
Vav1Syk$(SH2)_2$-Cit	pMSCV-Puro	Christoffer Hitzing
Vav1Syk$(SH2)_2$-Cit E201A	pMSCV-Puro	This work
Vav1Syk$(SH2)_2$-Cit N371A	pMSCV-Puro	This work
Vav2-Cit	pMSCV-Puro	Christoffer Hitzing
Vav2ΔAR-Cit	pMSCV-Puro	This work
Vav2-Cit Y142D Y159D Y172D	pMSCV-Puro	This work
Vav3-Cit	pMSCV-Puro	Christoffer Hitzing
Vav3-Cit E199A	pMSCV-Puro	This work

Table 3.14 Plasmid used for transient transfection.

Insert	Backbone	Source
sgRNA (CRISPR exon 3 PIP5Kα)	pSpCas9(BB)-2A-GFP	This work
sgRNA (CRISPR exon 5 PIP5Kβ) upstream	pSpCas9(BB)-2A-GFP	This work
sgRNA (CRISPR exon 5 PIP5Kβ) downstream	pSpCas9(BB)-2A-GFP	This work
sgRNA (CRISPR exon 3 PIP5Kγ)	pSpCas9(BB)-2A-GFP	This work
sgRNA (CRISPR exon 4 PIP5Kγ)	pSpCas9(BB)-2A-GFP	This work

Table 3.15 Plasmids used for bacterial his-tagged fusion protein expression. Murine and human Vav1 constructs were expressed from amino acid 170 to 575 and human Vav3 constructs from amino acid 169 to 573, respectively.

Insert	Backbone	Source
mVav1 Y174D	pH10-TEV	This work
mVav1 Y174D LK334/335AA	pH10-TEV	This work
Vav1 Y174D	pH10-TEV	This work
Vav1 Y174D E201A	pH10-TEV	This work
Vav1 Y174D N371A	pH10-TEV	This work

Vav3 Y173D	pH10-TEV	This work
Vav3 Y173D E199A	pH10-TEV	This work

3.1.10. Antibodies

Table 3.16 Primary antibodies used for western blot analysis. Antibodies were diluted according to the manufacturer's recommendations in antibody dilution solution.

Antibody (clone)	Species/Isotype	Manufacturer
α Actin (15E9)	Rabbit	CST
α Actin (8H10D10)	Mouse IgG_{2b}	CST
α BLNK (SLP-65) (D8R3G)	Rabbit	CST
α CD79A (Igα) (EP3618)	Rabbit	Abcam
α Erk (16)	Mouse IgG_{2a}	Becton Dickinson
α phospho Erk (E10)	Mouse IgG_1	CST
α GFP (7.1 & 13.1)	Mouse IgG_1	Roche
α p38	Rabbit	CST
α phospho p38 (36/p38)	Mouse IgG_1	Becton Dickinson
α PIP5Kα	Rabbit	CST
α PIP5Kβ (F-4)	Mouse IgG_{2a}	Santa Cruz
α PIP5Kγ	Rabbit	CST
α Syk (4D10)	Mouse IgG_{2a}	Santa Cruz
α Vav1	Rabbit	CST

Table 3.17 Secondary antibodies used for western blot analysis. Antibodies were diluted 1:10000 in TBS/T.

Antibody	Species	Manufacturer
α mouse IgG_1-HRPO	Goat	Southern Biotech
α mouse IgG_{2a}-HRPO	Goat	Southern Biotech
α mouse IgG_{2b}-HRPO	Goat	Southern Biotech
α rabbit-HRPO	Goat	Southern Biotech

Table 3.18 Antibodies used for stimulation. Antibodies were used in a concentration of 20 µg/ml for stimulation.

Antibody	Species	Manufacturer
α human IgM (Fc5µ fragment specific)	Goat	Jackson ImmunoResearch

Table 3.19 Antibodies used for surface staining. Antibodies were labeled with AlexaFluor 647 and used according to the manufacturer's instructions.

Antibody	Species	Manufacturer
α human kappa light chain	Goat	Southern Biotech

Table 3.20 Antibodies used for intracellular staining. Antibodies were labeled with AlexaFluor 647 and used according to the manufacturer's instructions.

Antibody (clone)	Species/Isotype	Manufacturer
α phospho Akt (D9E)	Rabbit	CST
α phospho Erk (20A)	Mouse IgG_1	Becton Dickinson

3.1.11. Recombinant proteins

Table 3.21 Recombinant proteins. All recombinant proteins that were purchased at Cytoskeleton Inc. contained N-terminal His-tags. Phalloidin-AlexaFluor 647 was used according to the manufacturer's instructions.

Recombinant protein	Manufacturer
Cdc42	Cytoskeleton Inc.
Phalloidin-AlexaFluor 647	Molecular Probes
Rac1	Cytoskeleton Inc.
RhoA	Cytoskeleton Inc.
Vav2 GEF Protein (DH domain)	Cytoskeleton Inc.

3.1.12. Affinity purification systems

Table 3.22 Affinity purification systems.

Purification system	Species	Manufacturer
HisPur Ni-NTA Superflow Agarose	-	Thermo Scientific
GFP-Trap Magnetic Agarose	Alpaca	Chromotek

3.1.13. Inhibitors

Table 3.23 Inhibitors.

Inhibitor	Solvent	Manufacturer
EHop-016 (E-Hop)	DMSO	Calbiochem
Rhosin	DMSO	Calbiochem

3.1.14. Bacterial strains

Table 3.24 Chemically competent bacterial strains used.

Bacterial strain	Manufacturer	Purpose
E. coli TOP10F'	Invitrogen	Cloning/plasmid amplification
E. coli BL21 CodonPlus	Agilent Technologies	Protein expression

3.1.15. Mammalian cell lines

DG75 EcoBlast (EB)

Human Burkitt lymphoma DG75 B cells (DSMZ: ACC 83) were originally harvested from pleural effusion of a 10-year-old boy with refractory, terminal Burkitt lymphoma in 1975. This cell line is described to be negative for Epstein-Barr virus (EBV) and expresses membrane-bound IgM along with the κ light chain on the cell surface[124].

DG75EB cells are equipped with the receptor for Moloney murine leukemia virus (MMLV), the murine cationic amino acid transporter SLC7A1, by retroviral transduction. The cells were selected with the antibiotic blasticidin and used for retroviral gene transfer with MMLV-derived particles produced by the packaging cell line Platinum-E[125,126]. Since no differences were detected between DG75 and DG75EB cells regarding signaling pathways or culturing of these cells, DG75EB are henceforth referred to as DG75.

DG75EB Vav1$^{-/-}$#2

DG75EB Vav1$^{-/-}$#2 (hereinafter referred to as Vav1-deficient DG75) cells originated from DG75 cells and were made deficient for Vav1 by TALEN mutagenesis[47]. For analysis of Vav family members, these cells were retrovirally transduced with plasmids encoding for various Vav protein variants. All of the transduced variants of Vav proteins contained C-terminal Citrine tags. Citrine is a fluorescent protein with excitation at a wavelength of 516 nm and emission at 529 nm. Thus, protein expression of Citrine, Citrine-tagged proteins and eGFP (excitation at a wavelength of 488 nm and emission at 507 nm) is detectable by flow cytometry in the FITC channel[127,128].

Platinum-E (PlatE)

PlatE cells are retroviral packaging cells based on HEK293 cells. They contain the MMLV's *env*, *gag* & *pol* genes under the control of the EF1α promotor. Additionally, the insertion of internal ribosome entry sites (IRES) between those three genes ensures high titers of MMLV produced by these cells[126].

3.2. Methods

3.2.1. Molecular biology

3.2.1.1. Isolation and purification of nucleic acids

3.2.1.1.1. Isolation of genomic DNA

To isolate genomic DNA, 1 x 10^6 cells were lysed in 200 µl TAG-lysis buffer (for composition see section 3.1.5.). Subsequently, 1 µl of Proteinase K (20 mg/ml, Macherey & Nagel) was added and the mixture was incubated for 3 h at 56°C. This step was followed by heat-inactivation of Proteinase K at 95°C for 30 min. The isolated DNA was stored at -20°C.

3.2.1.1.2. Isolation of plasmid DNA

Plasmid DNA was purified from *E. coli* TOP10F' bacteria. One bacterial colony was inoculated in 4 ml of LB medium (for composition see section 3.1.5.) containing the respective selective antibiotic (ampicillin with 100 µg/ml or kanamycin with 30 µg/ml) and incubated overnight at 37°C in a bacterial shaker. Subsequently, plasmid DNA was isolated using QiaPrep Spin MiniPrep Kit (Qiagen) according to the manufacturer's instructions. DNA concentration and purity were determined using the NanoDrop2000 spectrophotometer.

3.2.1.2. Cloning techniques

In molecular biology, cloning is defined by transition of DNA fragments into different vectors for various purposes like sequencing or gene expression in distinct cells. The open reading frame (ORF) of a gene of interest is amplified by polymerase chain reaction (PCR) and either directly transferred into the final vector or transferred into an intermediate vector. This transfer is called cloning and requires generation of specific overhangs by restriction enzymes at both ends of the gene. Subsequently, DNA fragments with similar overhangs in the vector are ligated to form a plasmid.

3.2.1.2.1. Polymerase chain reaction

The PCR is a well-established method to amplify specific DNA fragments *in vitro*[129]. The amplicon is determined by primers. Generally, the PCR includes three steps. At first, the template DNA is denaturated, which allows annealing of primers in the second step. In the third and final step, the annealed primers are elongated using a polymerase. All three steps require different temperatures and the conditions of the PCR are adjusted to the used polymerase. Repetition of these three steps leads to amplification of the desired DNA fragment.

In this project, the Q5 polymerase was used to amplify DNA fragments according to the manufacturer's recommendations. Primers were designed for annealing temperatures of approx. 65°C using the online database Primer3. Furthermore, restriction sites were added to primers that were used for cloning.

Table 3.25 Standard PCR conditions. bp = base pairs, min = minutes, sec = seconds

Step	Temperature	Time	Cycles
Initial denaturation	98°C	2 min	1
Denaturation	98°C	20 sec	⎫
Annealing	65°C	30 sec	⎬ 35
Elongation	72°C	20 sec per 1000 bp	⎭
Final elongation	72°C	40 sec per 1000 bp	1

3.2.1.2.2. Agarose gel electrophoresis

Agarose gel electrophoresis was conducted to separate DNA fragments by size using 1% agarose gels containing 1 µg/ml ethidium bromide in TAE buffer (for composition see section 3.1.5.). Samples were mixed with one fifth of 6x DNA loading buffer (NEB) and subsequently loaded onto the agarose gel. Fragments were separated at 100 V, 110 mA for 50 min. To determine the size of the DNA fragments, a 1 kb DNA ladder (Fermentas) was used as a reference.

3.2.1.2.3. Agarose gel extraction

The desired DNA fragment was cut out after separation by agarose gel electrophoresis and the DNA was extracted using the Wizard SV Gel and PCR Clean Up System (Promega) according to the manufacturer's instructions.

3.2.1.2.4. TA cloning (Invitrogen)

25.5 µl of the isolated DNA were mixed with 3 µl of 10x ThermoPol buffer (NEB), 1 µl of dATPs (1 mM, NEB) and 0.5 µl of Taq polymerase. This mixture was incubated for 30 min at 72°C in a PCR cycler. This reaction generates adenine overhangs at the 3' end of the DNA fragments (A-tailing), which are required for ligation to an intermediate vector named pCR2.1 (Invitrogen). To ligate the A-tailed DNA fragments into pCR2.1, 4 µl of the A-tailing reaction were mixed with 3.5 µl of ddH_2O, 1 µl of 10x T4 Ligase buffer (NEB), 1 µl of linear pCR2.1 and 0.5 µl of T4 Ligase. The mixture was incubated overnight at 14°C.

3.2.1.2.5. Transformation of competent cells

Transformation of chemically competent *E. coli* TOP10F' was performed with 3.5 µl of the ligation reaction. After addition of the DNA, the bacteria were incubated for 30 min on ice followed by a heat shock for 45 sec at 42°C. Subsequently, the bacterial cells were cooled on ice for another 2 min before addition of 450 µl of prewarmed (37°C) LB medium and incubation for 1 h at 37°C with mild agitation. Afterwards, the bacteria were plated on agar plates containing 100 µg/ml of ampicillin or 30 µg/ml of kanamycin and incubated overnight at 37°C. Transformation of *E. coli* TOP10F' with plasmids that have a pCR2.1 backbone allows for blue-white-screening. Therefore, an agar dish was coated with 50 µl of X-Gal and IPTG before plating the bacteria. Successfully cloned colonies either remained white or became blue when TA cloning was not successful. Thus, white colonies were picked after over-night incubation and DNA was isolated according to chapter 3.2.1.1.2.

3.2.1.2.6. Sequencing of plasmids

After isolation of plasmid DNA from *E. coli* TOP10F' bacteria, the plasmid DNA of potential clones was sent for sequencing to confirm the insertion of the desired DNA fragment into pCR2.1. Briefly, 12 µl containing 800 - 1200 ng of DNA were mixed with 3 µl of the sequencing primers (10 µM). Sequencing was performed by the Seqlab company.

3.2.1.2.7. Restriction digestion of DNA for cloning into expression backbones

DNA fragments cloned into pCR2.1 cannot be used for expression, neither in bacterial nor in eukaryotic cells. Hence, the desired DNA fragments (= inserts) were cloned into three different expression backbones. Two backbones were used for protein expression in mammalian cell lines, pMSCV-Puro and pRetroX-TetOne-Puro (Clontech), and one for inducible protein expression in bacteria, pH10-TEV (kindly provided by Hansjörg Götzke, NanoTag Biotechnologies). Protein expression using the pMSCV-Puro backbone in mammalian cells leads to a permanent expression of the respective protein, whereas protein expression using pRetroX-TetOne-Puro is inducible with doxycycline.

Each backbone contains a unique multiple cloning site (MCS), hence restriction digestions need to be adapted to those. To generate complementary overhangs, the backbone and the pCR2.1 construct carrying the desired insert were digested for 2 h according to the manufacturer's instructions for each restriction enzyme. Depending from the insert, either one restriction enzyme cleaved at both ends of the insert or two different restriction enzymes were used for cleavage at either end of the inserts. Subsequently, the digested DNA was loaded onto an agarose gel. The DNA was separated within the gel and the band at the predicted size was isolated according to sections 3.2.1.2.2. and 3.2.1.2.3., respectively.

3.2.1.2.8. Treatment with calf intestine phosphatase

If only one restriction enzyme was used, incubation of the backbone with calf intestine phosphatase (CIP) became necessary to avoid any undesired re-ligation of the backbone instead of ligation with the insert during the ligation reaction. In brief, 1 µl of CIP was added to the digest, followed by an incubation of 1 h at 37°C. This step was skipped if two different restriction enzymes were used for cloning.

3.2.1.2.9. Cloning ligation

For ligation of the insert into the expression backbone, 4 µl of the cut out and purified insert were mixed with 3.5 µl of ddH_2O, 1 µl of linearized and purified backbone, 1 µl of 10x T4 Ligase buffer and 0.5 µl of T4 Ligase. Subsequently, the mixture was incubated overnight at 14°C followed by transformation and plasmid purification according to chapters 3.2.1.2.5. and 3.2.1.1.2., respectively. To confirm the correct insertion and orientation of the insert, the isolated plasmids of the potential clones were sequenced (described in section 3.2.1.2.6.).

3.2.1.2.10. Site directed mutagenesis

To investigate the importance of amino acids or regions within Vav family members, mutations or deletions were introduced into the respective isoforms. Those mutations were generated using specific primers through PCR using the Pfu polymerase (Promega). Primers for site directed mutagenesis were designed with one to four mismatches for the mutations and ten to fifteen complementary base pairs at each site to ensure annealing to the desired region.

Table 3.26 PCR reaction for site directed mutagenesis. bp = base pairs, min = minutes, sec = seconds

Step	Temperature	Time	Cycles
Initial denaturation	95°C	2 min	1
Denaturation	95°C	30 sec	25
Annealing	55°C	1 min	
Elongation	72°C	2 min per 1000 bp	
Final elongation	72°C	4 min per 1000 bp	1

During that process, the whole plasmid including the mutation was amplified by Pfu polymerase. Subsequently, the PCR mixture was digested with DpnI, an endonuclease that exclusively digests methylated DNA. Methylation is a process that occurs in both, bacteria and eukaryotes, but not during *in vitro* PCR. Accordingly, only the template DNA that lacked the mutation was digested but not the mutated amplified plasmids containing the desired mutation by the primers via PCR. The DpnI-digested DNA was afterwards transformed, purified and sequenced as described before in sections 3.2.1.2.5., 3.2.1.1.2. and 3.2.1.2.6., respectively.

3.2.2. Protein biochemistry

3.2.2.1. Preparation of cleared cellular lysates

Cleared cellular lysates (CCLs) were prepared from DG75 B cells to investigate expression of different proteins by western blot analysis. Before lysis, cells were washed twice in ice-cold PBS (for composition see section 3.1.5.). Then, 20 µl of NP-40 lysis buffer (for composition see section 3.1.5.) were used per 1 x 10^6 cells. For lysis, cells were incubated for 10 min on ice. The lysates were subsequently centrifuged at 20,000 x g at 4°C for 10 min to clear them from cell debris. Finally, the supernatants constituting the cleared lysates were mixed with one fourth of 5x Laemmli buffer (for composition see section 3.1.5.), boiled for 10 min at 95°C and were either used for SDS-PAGE for further analysis or stored at -20°C.

3.2.2.2. Stimulation of B cells

To examine and to determine interaction partners of Vav family members, which are recruited after stimulation of the BCR, 50 x 10^6 of the investigated cells were harvested. For starvation, cells were resuspended in 35 ml of R0 (for composition see section 3.1.5.) and were incubated for 30 min at 37°C and 5% CO_2. Before stimulation with 20 µg/ml anti-human IgM F(ab')$_2$ fragments, the volume of R0 was reduced to 1 ml by centrifugation. Cells were either left untreated or stimulated for 1, 3 or 10 min. Stimulation was stopped by centrifugation, R0 was removed, 1 ml of NP-40 lysis buffer was added and for lysis, treated cells were incubated for 10 min on ice, followed by clearance of the lysate by centrifugation (20,000 x g, 10 min, 4°C). 100 µl (equals 5 x 10^6 cells) were mixed with 25 µl of 5x Laemmli buffer, were boiled for 10 min at 95°C and stored at -20°C for later usage as input fractions. The remaining 900 µl of the CCL were used for immunoprecipitation assays.

3.2.2.3. Immunoprecipitation assays using GFP-Trap

To purify Vav family members and their interaction partners from CCLs, the GFP-Trap Magnetic Agarose System was used. As the name indicates, this system is suitable for purifications of GFP-coupled proteins or cognates like eGFP, YFP and Citrine (Cit). For this purpose, alpaca nanobodies coupled to magnetic agarose beads were purchased from Chromotek. Before addition of these nanobody-coupled beads to CCLs of unstimulated and BCR-stimulated cells, 25 µl of beads per sample were washed twice with ice-cold NP-40 lysis buffer for equilibration, followed by incubation for 2 h on a rotator at 4°C. The beads were then captured using a magnetic separation rack (NEB) and were washed four times with NP-40 lysis buffer after the supernatant had been removed. Proteins were afterwards eluted from the beads by addition of 40 µl 2x Laemmli buffer (diluted 1:2.5 from 5x Laemmli buffer). The eluates

containing the proteins of interest were boiled at 95°C for 10 min and either subjected to SDS-PAGE for further analysis or stored at -20°C.

3.2.2.4. Sodium dodecyl sulfate polyacrylamide gel electrophoresis

Sodium dodecyl sulfate polyacrylamide gel electrophoresis (SDS-PAGE) was used to separate denaturated and reduced proteins obtained from CCLs (see section 3.2.2.1.) or immunoprecipitation assays (see section 3.2.2.3.) by size[130]. Therefore, proteins in Laemmli buffer were loaded onto a 5% polyacrylamide stacking gel and were separated in a 10% polyacrylamide resolving gel (for compositions see section 3.1.5.). To determine the molecular weight of the analyzed proteins, a prestained protein ladder (NEB, broad range) was used.

3.2.2.5. Western Blot transfer

For identification of proteins with specific antibodies, proteins separated by SDS-PAGE were transferred onto a nitrocellulose membrane using western blot transfer[131]. Two Whatman papers, the gel and a nitrocellulose membrane were equilibrated in blotting buffer (for composition see section 3.1.5.). The gel was placed on top of the membrane between the two Whatman papers. The transfer was conducted at 230 V and 1 mA per cm^2 of membrane for 2 h.

3.2.2.6. Immunostaining

After successful transfer of the proteins onto the nitrocellulose membrane, the membrane was incubated for at least 3 h in blocking solution (for composition see section 3.1.5.) to block any unspecific binding of antibodies eventually resulting in undesired and unspecific staining. The antibodies were diluted according to the manufacturer's recommendations in antibody dilution solution (for composition see section 3.1.5.) and were incubated with the membrane overnight on a rocker at 4°C. After incubation, the membrane was washed three times for 15 min with TBS/T under constant agitation, followed by 1 h of incubation on a rocker at room temperature with horse-radish peroxidase (HRPO)-coupled secondary antibodies, that detect the constant region (Fc region) of the respective primary antibodies. After washing the membrane for three more times with TBS/T for 15 min, the proteins of interest stained with primary antibodies were visualized via the HRPO-coupled secondary antibodies using enhanced chemiluminescence (ECL) solution (for composition see section 3.1.5.) in combination with the Chemi Lux Imager (Intas).

3.2.2.7. Expression and purification of recombinant His-tagged fusion proteins

To generate His-tagged fusion protein, parts of ORFs of Vav family members, that encode for the domains which mediate the GEF-activity, were cloned into pH10-TEV backbone according to chapters 3.2.1.2.7. and 3.2.1.2.9. Correct in-frame insertion and presence of the stop-codon were checked by sequencing (described in chapter 3.2.1.2.6.).

2 ng of the resulting plasmid were transformed into *E. coli* BL21 CodonPlus bacteria (according to section 3.2.1.2.5.) for IPTG induced expression. Therefore, a single transformed colony was inoculated in 4 ml of LB medium supplemented with kanamycin (30 µg/ml) and incubated overnight at 37°C in a bacterial shaking incubator. Subsequently, the bacterial culture was transferred into 200 ml of TB medium supplemented with 30 µg/ml kanamycin (for composition see section 3.1.5.) before incubation at 37°C in a bacterial shaking incubator until the culture reached an OD_{595} of approx. 0.6. Afterwards, protein expression in bacteria was induced by addition of 100 nM IPTG and cells were incubated for 4 h at 25°C in a shaking incubator. Subsequently, the bacteria were pelleted by centrifugation (4,000 x g, 15 min, 4°C), the supernatant was discarded and the pellets were stored at -80°C.

For purification of the expressed recombinant His-tagged fusion protein, bacterial pellets were resuspended in 10 ml Ni-NTA equilibration buffer (for composition see section 3.1.5.) containing freshly added protease inhibitors (cOmplete, EDTA free). The cells were lysed by sonication (intensity: 75%, pulse: 5, duration: 30 sec) and lysis was subsequently supported by supplementation of Triton-X-100 in a final concentration of 1%. Bacterial lysates were then cleared by centrifugation (20,000 x g, 10 min, 4°C). In the meantime, 80 µl of HisPur Ni-NTA Superflow Agarose beads (50% slurry, Thermo Scientific) were equilibrated by washing them twice in Ni-NTA equilibration buffer (700 x g, 5 min, 4°C). The bacterial lysates were added to the beads and incubated for 4 h on a rotator at 4°C to purify the His-tagged proteins. After purification, the beads were washed three times with ice-cold Ni-NTA wash buffer and once in ice-cold pH10 high salt wash buffer (for compositions see section 3.1.5.). Elution of the purified protein was achieved using 200 µl pH10 elution buffer (for composition see section 3.1.5.) for 10 min at room temperature. To determine elution efficacy, 10 µl of the eluate were analyzed by SDS-PAGE (see section 3.2.2.4.) and staining with InstantBlue (Expedeon). Herein, BSA was used as a reference and the remaining 190 µl of eluted proteins were stored at 4°C.

3.2.2.8. *In vitro* GEF-activity assay

To determine the ability of Vav family members to catalyze the exchange of GDP to GTP for small G proteins of the Rho family, *in vitro* GEF-activity was determined using Bodipy-GDP (Thermo Scientific). Fluorescence of the Bodipy labeled GDP is excited at a wavelength of 503 nm with a detectable emission at 512 nm. Considerably higher intensities are achieved when

bound to small G proteins. Respectively, the exchange of GDP to GTP can be indirectly tracked by the loss of signal intensity. To measure GEF-activity, 400 nM of either Rac1, RhoA or Cdc42 was added to Bodipy-GDP containing GEF-assay buffer (for composition see section 3.1.5.) for 20 min at 25°C. To lock the loading of the Rho GTPase with Bodipy-GDP, $MgCl_2$ was added to a final concentration of 5 mM. Additionally, to allow the exchange to GTP, GTP was added to a final concentration of 500 nM. Per sample, 90 µl of the mixture was transferred into a FLUOTRAC 96-well plate (Greiner Bio-One) and fluorescence was measured every 30 sec for 2 min. The mean of those first 5 values represented the baseline. Then, 10 µl of purified GEF-mediating domains of Vav family members (for procedure see section 3.2.2.7.) with a concentration of 8 µM were added to the mixture and the fluorescence was measured for another 20 min.

3.2.3. Cell biology

3.2.3.1. Cell culture

3.2.3.1.1. Cell culture and maintenance of non-adherent cells

Non-adherent DG75 cells and all sub-clones derived from these cells were cultured in R10 (for composition see section 3.1.5.) at 37°C and 5% CO_2 in a cell culture incubator. Every two days, 1.5 x 10^6 cells were seeded in a culture dish with a diameter of 10 cm for maintenance. For experiments on cellular basis, a different number of cells was seeded for each experiment.

3.2.3.1.2. Cell culture and maintenance of adherent cells

Adherent PlatE cells were cultured in R10 at 37°C and 5% CO_2 in a cell culture incubator. For maintenance, cells were washed once with PBS and were detached using a 0.05% Trypsin/EDTA solution (Gibco). Every Monday, 1 x 10^6 cells were seeded in 10 cm cell culture dish and every Friday 2.5 x 10^6 cells. PlatE cells were exclusively used as a retroviral packaging cell line which allows infection of DG75 and sub-clones with MMLV-derived particles.

3.2.3.1.3. Storage and revitalization of cells

For long-term storage of mammalian cells, 10 x 10^6 cells were harvested by centrifugation (300 x g, 5 min, RT) and resuspended in 2 ml of freezing medium (for composition see section 3.1.5.). 1 ml of cell suspension per cryo tube were stored at -150°C.

Frozen cells were thawed at 37°C and were washed once with R10 before seeding in 10 ml of R10 medium for revitalization.

3.2.3.2. Transfection methods

3.2.3.2.1. Nucleofection (Amaxa)

Nucleofection was performed using the Amaxa human B cell Nucleofector Kit (Lonza) to introduce the plasmids for CRISPR/Cas9-mediated genome editing into the target cells. 2 x 10^6 cells were harvested by centrifugation (90 x g, 10 min, RT). Meanwhile, 82 µl of human B cell Nucleofector Solution were mixed with 18 µl of Supplement 1 as well as 2 µg of the desired plasmid. Subsequently, the cells were resuspended in this transfection mixture and were transferred into the provided cuvettes. Nucleofection was achieved using program T-015 of Amaxa Nucleofector II. After nucleofection, the cells were first transferred into 3 ml of prewarmed R10 using a Pasteur pipette and were then placed into a cell culture incubator.

3.2.3.2.2. Retroviral transduction

To overexpress particular proteins in DG75 B cells, plasmids were introduced into the genome of the cells through retroviral transduction. For this purpose, 3 x 10^5 cells of the retroviral packaging cell line PlatE were plated in 6 cm cell culture dishes three days before transfection. On the day of transfection, 8 µl of TransIT transfection solution (Mirus) were diluted in 250 µl of R0 medium, the mixture was incubated for 15 min at RT followed by addition of 4 µg of the plasmid encoding for the gene of interest. The preparation was further incubated for 30 min at RT. The R10 medium of PlatE cells was replaced with 2.5 ml fresh, pre-warmed R10, the transfection solution was added carefully, and PlatE cells were placed into a cell culture incubator for the production of viruses. Per transfection, 5 x 10^5 DG75 B cells or sub-clones (= target cells) were seeded in 10 ml of R10. 24 h later, 1.5 ml of pre-warmed R10 was added to virus-producing PlatE cells. Another 24 h later, target cells and virus containing supernatants of PlatE cells were centrifuged separately at 300 x g for 5 min at RT. The supernatants were discarded from the pelleted target cells, followed by resuspending these cells in 3.5 ml of the virus containing supernatant of PlatE cells. Subsequently, 1.5 ml of pre-warmed R10 and polybrene (final concentration 4 µg/ml) were added to the target cells before overnight incubation at 37°C and 5% CO_2. The next day, the virus containing medium for infection was replaced with fresh, pre-warmed R10. The following day, the R10 medium was replaced with R10 medium containing 1 µg/ml of the antibiotic puromycin for selection of transduced cells. The cells were cultured in R10 medium supplemented with puromycin for 10 days.

3.2.3.3. Flow cytometry

3.2.3.3.1. Expression analysis of ectopically expressed fluorescent proteins

To analyze expression of ectopically expressed fluorescent proteins, 5 x 10^5 cells were harvested and washed twice with PBS. The cells resuspended in 300 µl of PBS were subsequently analyzed by flow cytometry. Citrine and eGFP are fluorescent proteins. Citrine is excited at a wavelength of 516 nm and emits light at a wavelength of 529 nm, while eGFP is excited at a wavelength of 488 nm and emits light at a wavelength of 507 nm. Thus, protein expression of Citrine, Citrine-tagged proteins and is detectable by flow cytometry in the FITC channel[127,128].

3.2.3.3.2. Analysis of intracellular Ca^{2+}-concentration

To analyze the cytosolic Ca^{2+}-concentration in DG75 B cells and sub-clones, the fluorescent dye Indo-1 AM (Life Technologies) was used. This dye is excited at 350 nm and emits lights at two distinct wavelengths, dependent on whether or not Ca^{2+} is bound. If Ca^{2+} is bound to Indo-1, light at a wavelength of 400 nm (violet) is emitted, whereas the emitted light without Ca^{2+} is at a wavelength of 475 nm (blue). Hence, the ratio of the mean fluorescence intensities (MFI) of violet and blue light is representative for the cytosolic Ca^{2+}-concentration.

The day before the measurement, 1 x 10^6 cells were seeded in 10 ml R10. After 20 to 24 h, cells were harvested by centrifugation (300 x g, 5 min, RT), resuspended in 500 µl of R10 containing 1 µM of Indo-1 AM and 0.015% pluronic acid (Life Technologies) and incubated for 30 min at 30°C under mild agitation. The cells were then washed twice in 1 ml of Krebs-Ringer buffer (for composition see section 3.1.5.) and were finally resuspended in 650 µl of Krebs-Ringer buffer and rested for 30 min at 30°C with mild agitation. 300 µl of rested cells were transferred into FACS tubes and 25 sec of Indo-1 fluorescence were recorded for determination of the baseline, followed by stimulation with 20 µg/ml anti-human IgM $F(ab')_2$ fragments. In total, the fluorescence was recorded for 5 min. Additionally, the fluorescence of the cells in the FITC channel was recorded which allows gating for subsequent analysis. Data analysis was done with FlowJo, Microsoft Excel and GraphPad Prism.

3.2.3.3.3. Intracellular staining of phosphorylated proteins

Phosphorylation of Akt and Erk in BCR-stimulated DG75 B cells was determined by flow cytometry analysis through intracellular staining.

24 h before the measurement, 1.5 x 10^6 cells were seeded in 10 ml of R10 in 10 cm cell culture dishes. On the day of the measurement, the cells were harvested by centrifugation and resuspended in R0 to a concentration of 10 x 10^6 per ml. Per sample, 1 x 10^6 were rested for

30 min. Subsequently, the cells were either left untreated or stimulated with 20 µg/ml of anti-human IgM F(ab')$_2$ fragments for 3 min. Stimulation was stopped by addition of 100 µl CytoFix (Becton Dickinson). After 10 min of fixation at 37°C under mild agitation, the cells were pelleted by centrifugation (500 x g, 8 min, RT), resuspended in 400 µl Perm/Wash buffer I (Becton Dickinson) for permeabilization and incubated for 20 min at 22°C under mild agitation. Again, another 400 µl of Perm/Wash buffer I were added and the cells were pelleted (500 x g, 8 min, RT). During centrifugation, a master mix containing AlexaFluor 647 coupled phospho-specific antibodies was prepared according to the manufacturer's instructions in Perm/Wash buffer I. Pelleted cells were resuspended in 100 µl of staining master mix and incubated for 45 min at 22°C with mild agitation. After addition of 1 ml of Perm/Wash buffer to each sample, cells were centrifuged (500 x g, 8 min, RT) and resuspended in 300 µl Perm/Wash buffer I, followed by flow cytometry analysis. The gating strategy is shown in Figure 3.1 with Vav1-deficient DG75 B cells reconstituted with Vav1-Cit as an example. The MFI of red fluorescence (blue tinted peaks, third panels from the left) are related to protein phosphorylation and were used for calculations. Data analysis was done with FlowJo, Microsoft Excel and GraphPad Prism.

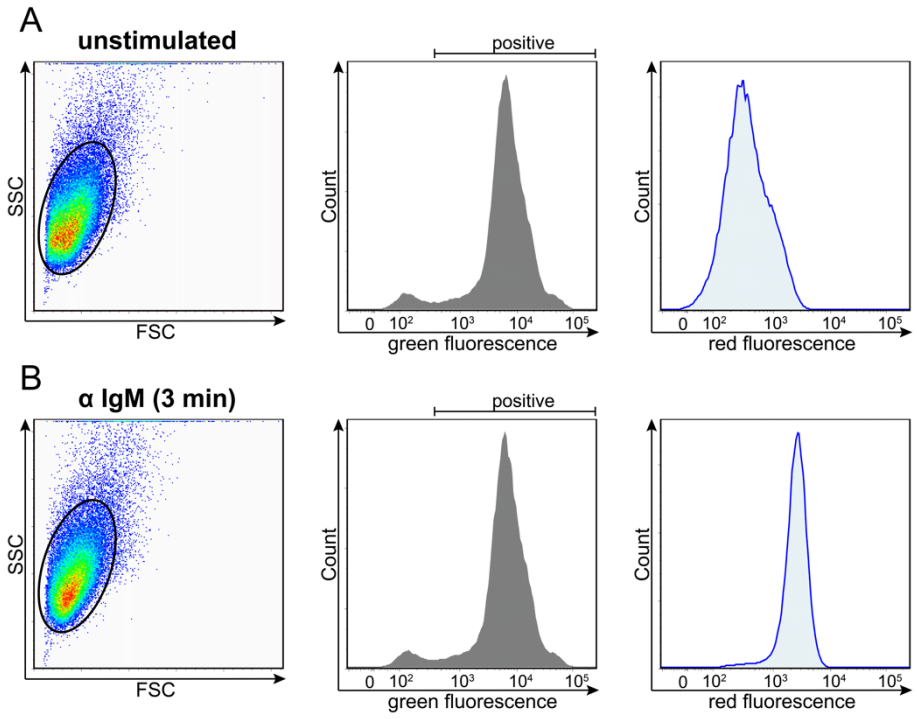

Figure 3.1 Gating strategy for intracellular staining of phosphorylated proteins. (A and B) Gating strategy for intracellular staining of phosphorylated Akt or Erk of unstimulated (A) or BCR-stimulated cells (B). Cells were harvested, left untreated or stimulated with 20 µg/ml of anti-human-IgM F(ab')$_2$ fragments (α IgM), followed by fixation, permeabilization and staining. Fluorescence (green and red) was measured for 50.000 events.

3.2.3.3.4. Actin polymerization assays

To analyze polymerization of globular actin (G-actin) to filamentary actin (F-actin), the fluorescently labeled (AlexaFluor 647) toxin phalloidin was used. This toxin isolated from poisonous *Amanita* mushrooms specifically stains F-actin[132,133].

2.5 x 10^6 of FITC-negative (DG75 or Vav1-deficient DG75 B cells) and 2.5 x 10^6 of FITC-positive (reconstituted Vav1-deficient DG75 B cells) were seeded in 10 ml of R10 in 10 cm cell culture dishes. The following day, 5 x 10^5 cells of each cell line were mixed in a 1:1 ratio in a total volume of 100 µl of R0 to ensure similar stimulation conditions. After a resting period of 20 min at 37°C, the cells were either left untreated or stimulated for 30 sec, 1, 3 or 7 min with 20 µg/ml of anti-human IgM F(ab')$_2$ fragments. Stimulation was stopped by addition of an equal volume of CytoFix containing 50 µg/ml lysophosphatidylcholine (LPC, Sigma-Aldrich) and 0.5 U phalloidin-AlexaFluor 647 (Thermo Scientific). Fixation, permeabilization and staining was achieved after 20 min of incubation at 37°C under mild agitation. Afterwards, cells were washed with 1.5 ml of PBS containing 2% FCS, followed by flow cytometry analysis. The gating strategy is shown in Figure 3.2 with Vav1-deficient DG75 B cells mixed with those cells reconstituted with Vav1-Cit as an example. The MFI of red fluorescence (black and blue tinted peaks, third panels from the left) are related to the amount of filamentary actin and were used for calculations. Data analysis was done with FlowJo, Microsoft Excel and GraphPad Prism.

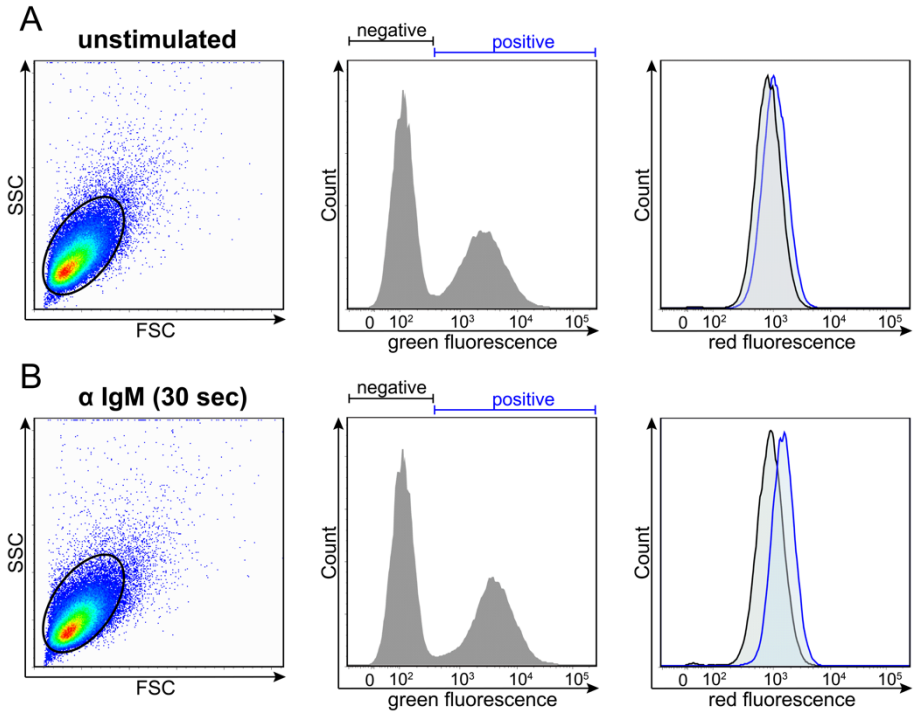

Figure 3.2 Gating strategy for actin polymerization assays. (A and B) Gating strategy for actin polymerization assays of unstimulated (A) or BCR-stimulated cells (B). Cells were harvested, left untreated or stimulated with 20 µg/ml of anti-human-IgM F(ab')$_2$ fragments (α IgM), followed by fixation, permeabilization and staining. Fluorescence (green and red) was measured for 100.000 events.

3.2.3.3.5. Receptor internalization assays

To measure stimulation-induced BCR internalization, the expression of membrane-bound IgM on the surface of DG75 B cells was measured using κ light chain specific antibodies labeled with AlexaFluor 647.

2.5 x 10^6 of FITC-negative (DG75 or Vav1-deficient DG75 B cells) and 2.5 x 10^6 of FITC-positive (reconstituted Vav1-deficient DG75 B cells) were seeded in 10 ml of R10 in 10 cm cell culture dishes. The next day, 5 x 10^5 cells of each cell line were mixed in a 1:1 ratio in a total volume of 100 µl of R0 to ensure similar stimulation conditions. After a resting period of 20 min at 37°C, the cells were either left untreated or stimulated for 5, 10, 15 or 20 min with 20 µg/ml anti-human IgM F(ab')$_2$ fragments. Stimulation was stopped by addition of 100 µl of CytoFix and the cells were incubated for 20 min at 37°C under mild agitation. Afterwards, the cells were washed with 1 ml of PBS containing 2% FCS, followed by an additional incubation period of 10 min on ice with anti-human κ light chain antibodies in PBS containing 2% FCS on ice. Subsequently, the cells were washed with 1.5 ml PBS containing 2% FCS and were subjected to flow cytometry analysis. The gating strategy is shown in Figure 3.3 with Vav1-deficient DG75 B cells mixed with those cells reconstituted with Vav1-Cit as an example. The MFI of red fluorescence (black and blue tinted peaks, third panels from the left) are related to the amount of IgM (BCR) left on the cell surface and were used for calculations. Data analysis was done with FlowJo, Microsoft Excel and GraphPad Prism.

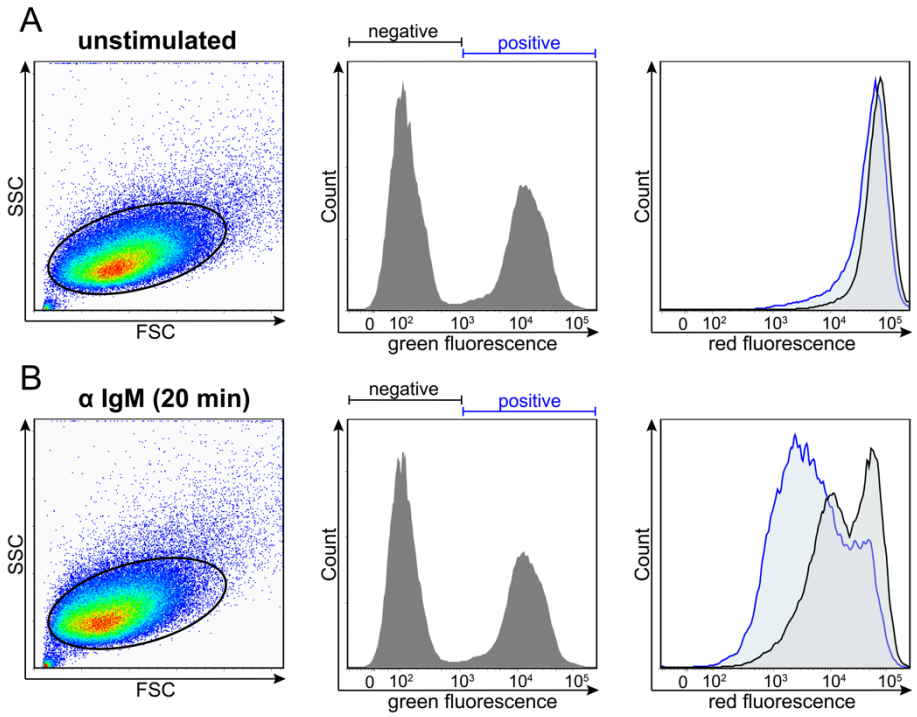

Figure 3.3 Gating strategy for receptor internalization assays. (A and B) Gating strategy for receptor internalization assays of unstimulated (A) or BCR-stimulated cells (B). Cells were harvested, left untreated or stimulated with 20 µg/ml of anti-human-IgM F(ab')$_2$ fragments (α IgM), followed by fixation and staining. Fluorescence (green and red) was measured for 100.000 events.

3.2.3.4. Genome editing techniques

3.2.3.4.1. CRISPR/Cas9-mediated genome editing

For CRISPR/Cas9-mediated genome editing and specific introduction of double strand breaks by Cas9, single guide RNAs (sgRNA) for were cloned into pSpCas9(BB)-2A-GFP (Addgene) and electroporated into the nucleus of DG75 B cells according to section 3.2.3.2.1. The Cas9-mediated double strand breaks are repaired by the non-homologous end joining (NHEJ) repair mechanism of the cells. In contrast to homology directed repair (HDR) mechanisms, NHEJ might cause mutations due to the lack of templates. For CRISPR/Cas9-mediated genome editing, this feature of NHEJ is used to introduce insertion or deletion (Indel) mutations into the genomic DNA, which ultimately may lead to frame shifts and premature stop codons[134]. Two days after nucleofection, GFP-positive cells were sorted (cell sorting facility, University Medical Center Göttingen). After recovery, 1 x 10^6 cells were harvested to isolate genomic DNA (see section 3.2.1.1.1.). The isolated genomic DNA served as a template for a PCR-based activity test of Cas9. For this purpose, an amplicon covering the targeted exon was amplified by PCR (see section 3.2.1.2.1.) and Cas9 activity was determined by restriction analysis or was directly identified through examination of a shift in the size of the resulting PCR product. When Cas9 activity was detected, single cells were plated on 96-well plates in 150 µl of R10 medium using the minimal dilution approach. Subsequently, the cells were cultured until a sufficient number of cells was reached for western blot analysis.

4. Results

Previous results in our lab identified a crucial role of Vav family members in BCR-induced Ca^{2+}-mobilization independent of phosphorylation of PLCγ2 or the formation of the Ca^{2+}-initiation complex. These results were obtained from a cellular model system based on Burkitt lymphoma-derived human DG75 B cells deficient for Vav1. Those Vav1-deficient DG75 B cells endogenously express only low amounts of Vav2 and barely any Vav3[47]. Furthermore, the results revealed that Vav1 and Vav3, but not Vav2, control the BCR-induced Ca^{2+}-influx into the cytosol and that Vav1 needs to be recruited to the BCR or its signaling components to execute its function[47]. However, the recruitment of Vav2 and Vav3 to the stimulated BCR and its signaling proteins and the underlying mechanism, by which Vav family members control Ca^{2+}-mobilization after stimulation of the BCR, remained unclear. Therefore, I analyzed the recruitment kinetics to the BCR and its signaling components of all Vav family members and their enzymatic GEF-activity. Moreover, potential molecules downstream of Vav were investigated. Additionally, I examined different signaling axes within the BCR signal cascade in order to determine further processes in which Vav family members might be involved.

4.1. Vav family members are recruited to the BCR and signaling components to different extents

Figure 4.1 shows the different signaling capacities for the three Vav isoforms. To this end, either Vav1 or Vav2 or Vav3 were individually expressed in Vav1-deficient DG75 B cells. All generated Vav-constructs were equipped with a C-terminal Citrine tag (Vav1-Cit, Vav2-Cit and Vav3-Cit). Vav1-deficient DG75 B cells expressing eGFP, which shares 97% amino acid similarities with Citrine, were used as negative control. They essentially represented Vav1-deficient cells but had undergone the same retroviral transduction and selection processes like cells transduced with Vav family members and mutants thereof. Fluorescence of the Citrine tag and the eGFP protein both directly correspond with the expression level of the respective protein. Thus, protein expression was determined by flow cytometry analysis and cells that were not successfully transduced were easily excluded by gating on FITC-positive cells.

The constructs encoding for wild-type Vav1 and Vav2 were expressed in amounts similar to eGFP. However, the construct encoding wild-type Vav3 was expressed approx. five times less efficiently (Figure 4.1 B). By monitoring the intracellular Ca^{2+}-concentration upon stimulation of the BCR (Figure 4.1 A), previously generated data of our group were successfully confirmed[47]. Wild-type Vav1 (blue line) and Vav3 (brown line) were able to compensate the loss of Vav1 in DG75 B cells, whereas cells expressing Vav2 (dark green line) showed similar BCR-induced Ca^{2+}-kinetics as the control cells expressing eGFP (green line).

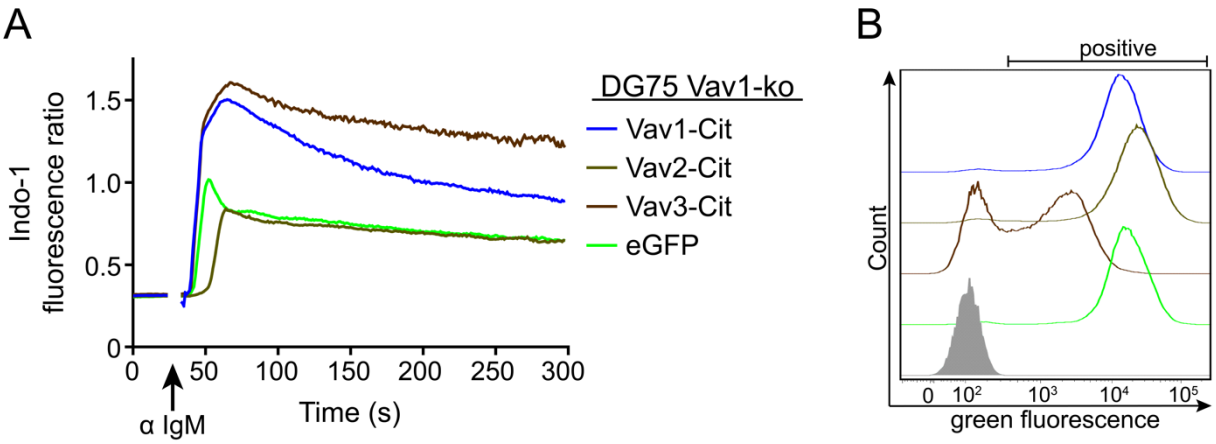

Figure 4.1 Vav1 and Vav3, but not Vav2, control BCR-induced Ca^{2+}-mobilization. (A) Analysis of intracellular BCR-induced Ca^{2+}-mobilization of Vav1-deficient DG75 B cells expressing either Vav1-Cit (blue line), Vav2-Cit (dark green line), Vav3-Cit (brown line) or eGFP (green line). Cells were loaded with the Ca^{2+}-sensitive fluorophore Indo-1 AM. After recording of basal Ca^{2+}-levels for 25 sec, the cells were stimulated with 20 µg/ml of anti-human-IgM $F(ab')_2$ fragments (α IgM) and the fluorescence was monitored for a total time of 5 min. The graphs are representative for 1 of 3 independent experiments. (B) Green fluorescence of cells analyzed in (A). The grey filled peak represents cells negative for green fluorescence.

To test whether the differences in BCR-induced Ca^{2+}-mobilization were due to different recruitment to the BCR or other signaling components, I analyzed the association of all three Vav family members with the activated BCR and proteins involved in its signaling cascade by affinity purification assays with the GFP-Trap Magnetic Agarose System (Chromotek). This system is suitable for both, the Citrine-tagged Vav fusion proteins and the eGFP protein. The resulting western blots of cleared cellular lysates (Figure 4.2 A and C, “Inputs”) and those of the purified proteins (Figure 4.2 B and D, “Affinity purifications”) were stained with antibodies to the known Vav interaction partners SLP-65 (BLNK) and Syk as proof of concept controls[41,80]. Additionally, the western blots were stained with antibodies against Igα (CD79A) which previously had been identified as interaction partner for Vav1 in our group[47]. For affinity purifications, barely any signal was detected for Syk, SLP-65 or Igα on western blots of unstimulated Vav1-deficient DG75 B cells expressing Citrine-tagged Vav1 (Figure 4.2 B, lane 1), indicating that Vav1 is hardly associated with any of the tested signaling proteins in resting B cells. The signals for SLP-65 and Igα (third and lower panel) were strongest after 1 min of BCR stimulation and the intensity decreased with the time of stimulation. The signal intensities of Syk (second panel) were highest for 1 and 3 min of BCR stimulation and slightly weaker for 10 min of stimulation. Western blots of Vav1-deficient DG75 B cells expressing Vav2-Cit (Figure 4.2 B, lanes 5 to 8) exhibited similar signal patterns, but with stronger intensities. However, by contrast, the band intensities of Syk (second panel) and SLP-65 (third panel) only marginally decreased with the time of stimulation, but the strength of the signal decreased with the time of stimulation for Igα (fourth panel). Western blots of DG75 cells deficient for Vav1 with reconstituted Citrine-tagged Vav3 (Figure 4.2 D, lanes 1 to 4) showed similar signal patterns as those from cells reconstituted with Vav1-Cit, but to a reduced extent. For Vav1

knockout DG75 B cells expressing eGFP (Figure 4.2 D, lanes 5 to 8) barely any signals were detected, except for Syk (second panel).

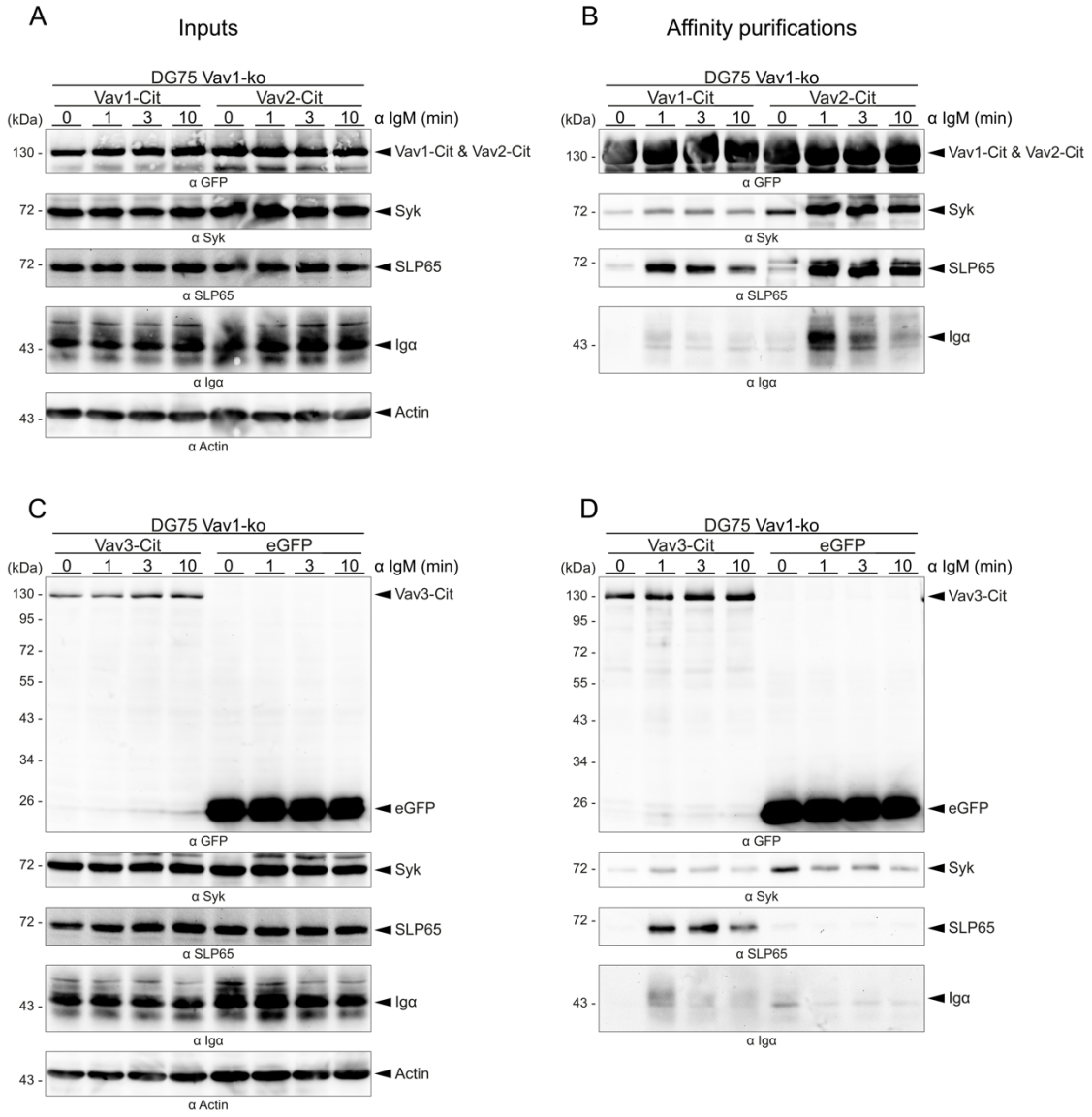

Figure 4.2 Differential recruitment kinetics of wild-type Vav family members. (A) and (C) Immunoblot analysis of cleared cellular lysates of Vav1-deficient DG75 B cells expressing either Vav1-Cit, Vav2-Cit, Vav3-Cit or eGFP. The cells were either left untreated or stimulated for 1, 3 or 10 min with 20 µg/ml of anti-human-IgM F(ab')$_2$ fragments (α IgM). Proteins were separated by SDS-PAGE and analyzed by western blot using antibodies specific for GFP, Sky, SLP-65, Igα and Actin, respectively. The molecular weight of marker proteins is indicated on the left in kDa. (B) and (D) Immunoblot analysis of immunoprecipitations of cells from (A) and (C) using GFP-Trap Magnetic Agarose beads. Subsequently, proteins were analyzed as in (A) and (C). The molecular weight of marker proteins is indicated on the left in kDa.

Recruitment kinetics of wild-type Vav family members to the stimulated BCR and its signaling components unveiled that the inability of Vav2 to support BCR-induced Ca^{2+}-mobilization in Vav1-deficient B cells (Figure 4.1 A, dark green line) is not caused by the absence of this protein at the BCR or signaling components such as SLP-65, Syk or Igα in BCR-stimulated B cells. In contrast, Vav2 is recruited more efficiently compared to Vav1 upon stimulation of the BCR (Figure 4.2 B and D).

4.2. The catalytic activity of Vav family members is required for BCR-induced Ca^{2+}-mobilization

Considering that Vav2 was not able to compensate for the loss of Vav1 regarding BCR-induced Ca^{2+}-mobilization in DG75 B cells, but was recruited to proteins involved in B cell antigen receptor signaling to an even higher extent compared to Vav1, I investigated the influence of Vav family-dependent GEF-activity on BCR-induced Ca^{2+}-mobilization. Since the ability of Vav proteins to interact with Rho GTPases is indispensable for the activation of these small G proteins, various amino acids of Vav1 which are known to form hydrogen bonds with Rac1 were mutated[86,87]. Furthermore, a mutant variant which is supposed to fully abrogate the GEF-activity of Vav1 was investigated[99].

4.2.1. Intact Rac1 binding sites are required for full BCR-induced Ca^{2+}-mobilization

The DH domain of Vav family members contains several amino acids which are responsible for the interaction with small G Proteins of the Rho family. Most of the studies that aimed to determine interaction sites between Vav proteins and Rho family members focused on Vav1 and Rac1. So far, three regions within the DH domain of Vav1 have been described to be required for the interaction with Rac1[86,87]. Based on these data, I generated variants of human Vav1, in which specific amino acids of the Vav1-Rac1 interaction interfaces were replaced with alanine. The first interaction interface is located at the N-terminus of the DH domain of Vav1 and consists of the amino acid glutamate at position 201. This amino acid forms a hydrogen bond to each of the amino acids tyrosine 32 and valine 36 of Rac1, respectively[86]. Hence, a Vav1 variant carrying the glutamate-to-alanine substitution at position 201 was expressed as Citrine-tagged fusion protein (Vav1-Cit E201A) in Vav1-deficient DG75 B cells and its ability to mobilize Ca^{2+} upon stimulation of the BCR was analyzed. In addition, leucine at position 213 was substituted with glutamine since this mutant has been widely used in the past as loss of function variant with regard to enzymatic activity of Vav1 (Vav1-Cit L213Q)[99]. To complete this set of mutations within the first interaction interface of Vav1 and Rac1, a lysine-to-alanine mutation was introduced at position 208 of Vav1 (Vav1-Cit K208A). This mutation served as a control since this amino acid is oppositely charged compared to glutamate at position 201 and is not described to be involved in the binding of Vav1 to Rac1. Thus, this mutation should not affect interactions of Rac1 and Vav1.

All mutant variants of Vav1 were expressed in Vav1-deficient cells, while Citrine-tagged wild type Vav1 and eGFP served as controls. Apart from the L213Q variant, all proteins were expressed in similar amounts. The Vav1-construct carrying the L213Q mutation was

expressed approx. ten times less efficiently compared to the other Vav1-constructs (Figure 4.3 B and C).

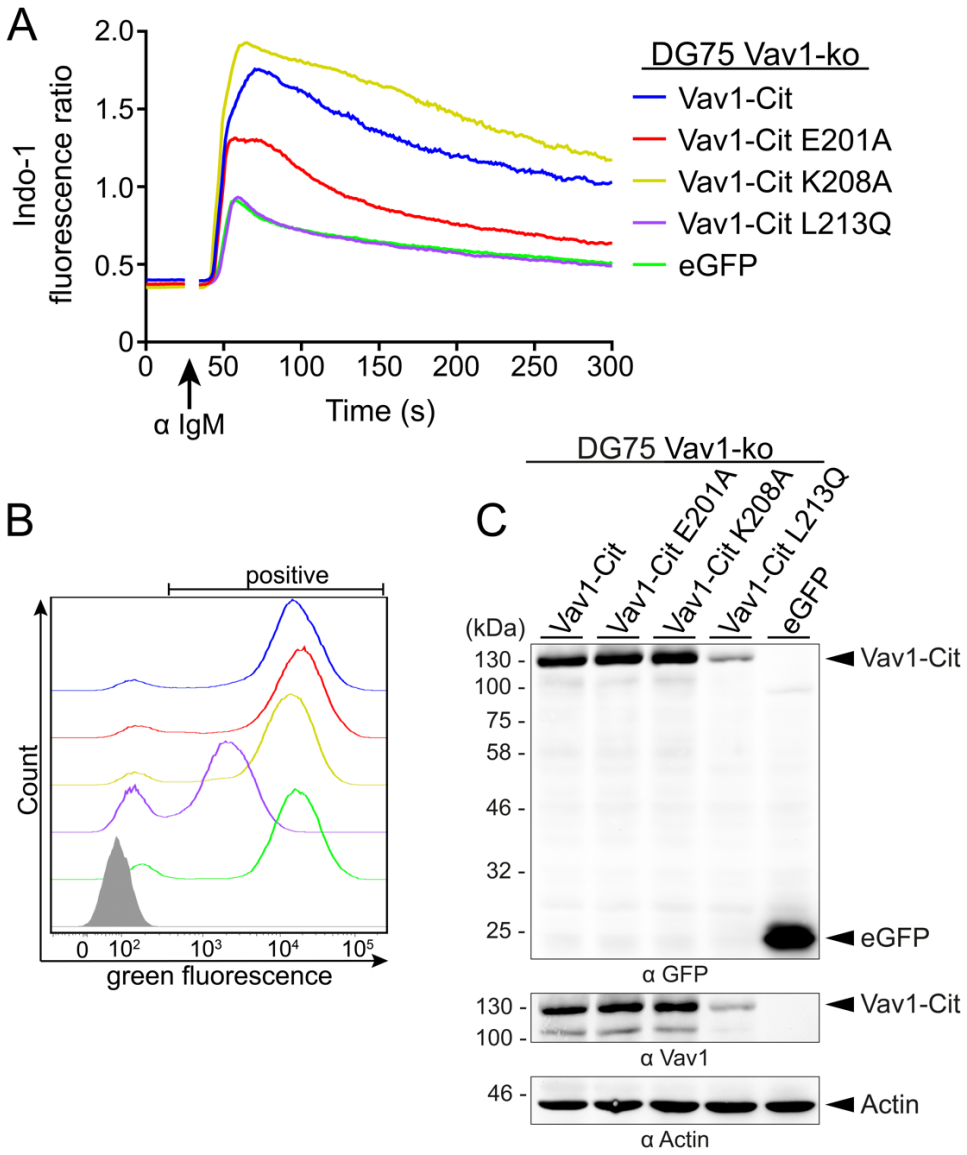

Figure 4.3 Mutation in Vav1-Rac1 interaction site diminish BCR-induced Ca^{2+}-mobilization. (A) Analysis of intracellular BCR-induced Ca^{2+}-mobilization of Vav1-deficient DG75 B cells expressing either Vav1-Cit (blue line), Vav1-Cit E201A (red line), Vav1-Cit K208A (dark yellow line), Vav1-Cit L213Q (purple line) or eGFP (green line). Cells were loaded with the Ca^{2+}-sensitive fluorophore Indo-1 AM. After recording of basal Ca^{2+}-levels for 25 sec, the cells were stimulated with 20 µg/ml of anti-human-IgM $F(ab')_2$ fragments (α IgM) and the fluorescence was monitored for a total time of 5 min. The graphs are representative for 1 of 3 independent experiments. (B) Green fluorescence of cells analyzed in (A). The grey filled peak represents cells negative for green fluorescence. (C) Immunoblot analysis of cleared cellular lysates of Vav1-deficient DG75 B cells expressing either Vav1-Cit, Vav1-Cit E201A, Vav1-Cit K208A, Vav1-Cit L213Q or eGFP. Proteins were separated by SDS-PAGE and analyzed by western blot using antibodies specific for GFP, Vav1 and Actin. The molecular weight of marker proteins is indicated on the left in kDa.

Expression data acquired by flow cytometry (Figure 4.3 B) strongly correlated with those obtained by western blot analyses (Figure 4.3 C) with specific antibodies to either GFP (upper panel) or Vav1 (middle panel). Staining for Actin (lower panel) was used as loading control. Intriguingly, the mutation in the Rac1 binding site of Vav1 at position 201 (Figure 4.3 A, red line) reduced the BCR-induced Ca^{2+}-mobilization approx. by half. In cells expressing the Vav1

L213Q variant (Figure 4.3 A, purple line), the Ca^{2+}-kinetics essentially represented the knockout phenotype of Vav1-deficient DG75 B cells expressing eGFP. The K208A mutation in Vav1 (Figure 4.3 A, dark yellow line) did not negatively affect BCR-induced Ca^{2+}-mobilization.

The second Rac1 interaction interface of Vav1 examined in the following experiments is located at the C-terminal end of the DH domain and consists of four amino acids: asparagine at position 371, lysine at position 374, arginine at position 375 and glutamate at position 378. These amino acids form hydrogen bonds with aspartate at position 65 and arginine at position 66 of Rac1[87].

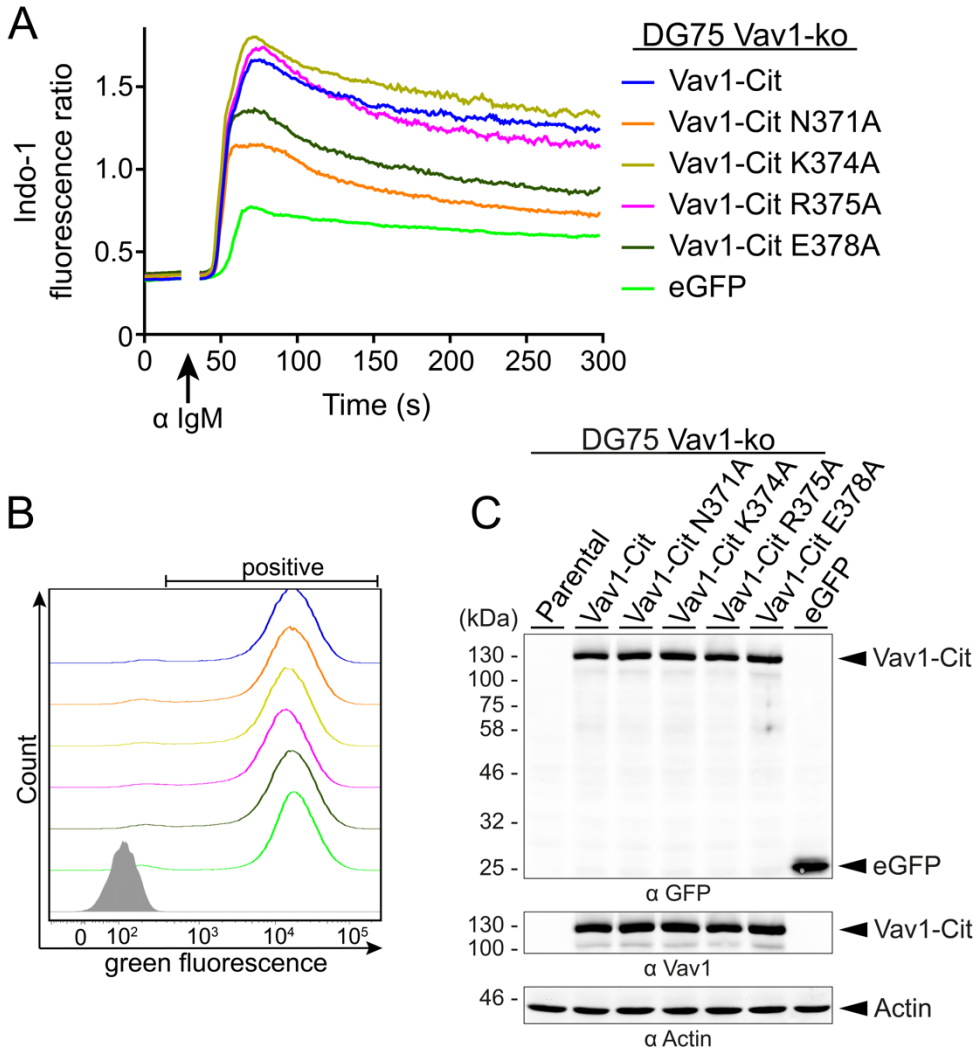

Figure 4.4 Mutations in Vav1-Rac1 interactions sites reduce BCR-induced Ca^{2+}-mobilization. (A) Analysis of intracellular BCR-induced Ca^{2+}-mobilization of Vav1-deficient DG75 B cells expressing either Vav1-Cit (blue line), Vav1-Cit N371A (orange line), Vav1-Cit K374A (olive-yellow line), Vav1-Cit R375A (pink line), Vav1-Cit E378A (dark green) or eGFP (green line). Cells were loaded with the Ca^{2+}-sensitive fluorophore Indo-1 AM. After recording of basal Ca^{2+}-levels for 25 sec, the cells were stimulated with 20 µg/ml of anti-human-IgM $F(ab')_2$ fragments (α IgM) and the fluorescence was monitored for a total time of 5 min. The graphs are representative for 1 of 3 independent experiments. (B) Green fluorescence of cells analyzed in (A). The grey filled peak represents cells negative for green fluorescence. (C) Immunoblot analysis of cleared cellular lysates of Vav1-deficient DG75 B cells expressing either Vav1-Cit, Vav1-Cit N371A, Vav1-Cit K374A, Vav1-Cit R375A, Vav1-Cit E378A or eGFP. Proteins were separated by SDS-PAGE and analyzed by western blot using antibodies specific for GFP, Vav1 and Actin. The molecular weight of marker proteins is indicated on the left in kDa.

Whereas lysine at position 374 of Vav1 forms only one hydrogen bond to Rac1, the other three amino acids each form two hydrogen bonds to Rac1[87]. To test whether also this interface is required for BCR-induced Ca^{2+}-mobilization, I substituted each of the mentioned amino acids in Vav1 with alanine and analyzed the resulting cells as before. All Citrine-tagged Vav1-constructs were expressed in similar amounts (Figure 4.4 B and C). The expression data acquired by flow cytometry (Figure 4.4 B) again corresponded to the data generated by western blot analysis (Figure 4.4 C). Because of this conformity, in the following only flow cytometry data are shown for expression of Vav variants (yet expression of Vav variants was routinely analyzed by western blot analysis to determine correct protein specificity and molecular weight). Analysis of BCR-induced Ca^{2+}-mobilization (Figure 4.4 A) revealed that introduction of alanine in Vav1 at positions 371 (N371A, orange line) or 378 (E378A, dark green line) severely attenuated BCR-induced Ca^{2+} flux. The Ca^{2+}-phenotypes of cells expressing Vav1-Cit with single amino acid substitutions on position 374 (K374A, olive-yellow line) or 375 (R375A, pink line) were almost similar to cells expressing wild-type Vav1-Cit (blue line). These results suggested that amino acids of Vav1 which form hydrogen bonds to Rac1 are important for BCR-induced Ca^{2+}-signaling.

The third interaction interface of Vav1 and Rac1 is located between the first and the second interface, but closer to the C-terminus of the DH domain of Vav1. It is constituted by the amino acid glutamine at position 331 and forms a hydrogen bond to asparagine 39 of Rac1[86]. Furthermore, three dimensional structural analysis of Vav1 revealed that aspartate 376 is not responsible for any interactions to Rac1, but forms intramolecular hydrogen bonds to threonine 539 and phenylalanine 540 within the zinc finger domain of Vav1[86,87]. To analyze whether BCR-induced Ca^{2+}-mobilization is affected by the third Vav1-Rac1 interface or by putative disruption of intramolecular hydrogen bonds, the respective amino acids at positions 331 and 376 were substituted with alanine. The resulting variants of Vav1 were expressed in Vav1-deficient DG75 B cells and again their capacity to mobilize Ca^{2+} upon stimulation of the BCR was tested.

The Citrine-tagged Vav1 protein carrying the D376A mutation (pink line) which forms two intramolecular hydrogen bonds, was expressed approx. four times less efficiently compared to wild-type Vav1-Cit (blue line), Vav1-Cit Q331A (olive line) or eGFP (green line) (Figure 4.5 B). In line with previous results (Figure 4.3 A and Figure 4.4 A), the construct carrying the Q331A mutation, affecting a Rac1 interaction site of Vav1 showed a diminished BCR-induced Ca^{2+}-mobilization (Figure 4.5 A, olive line). Almost the same reduction by half compared to Vav1-deficient cells that were reconstituted with wild-type Vav1 (Figure 4.5 A, blue line) was measured for those cells expressing Vav1 D376A protein (Figure 4.5 A, pink line).

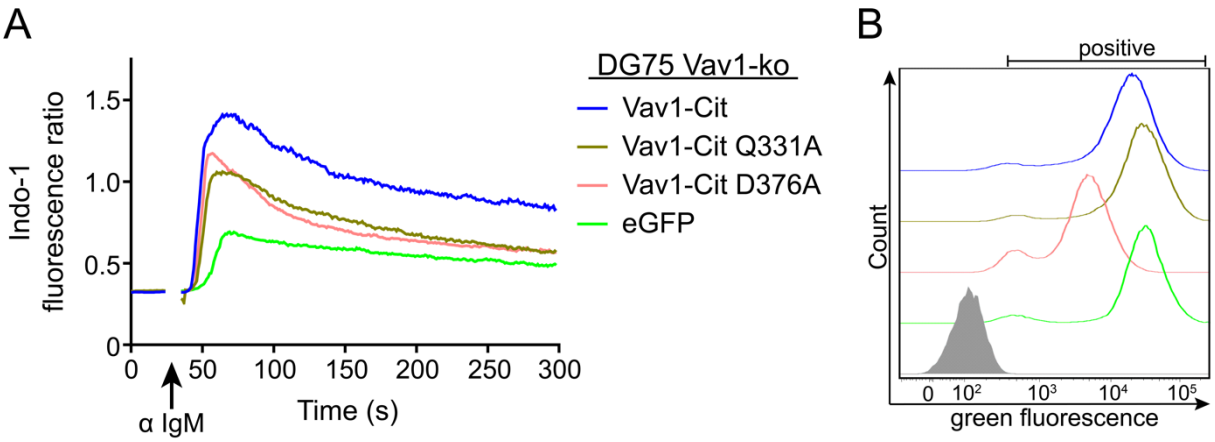

Figure 4.5 Mutation in Vav1-Rac1 interaction site or affection of the stability of Vav1 diminish BCR-induced Ca^{2+}-mobilization. (A) Analysis of intracellular BCR-induced Ca^{2+}-mobilization of Vav1-deficient DG75 B cells expressing either Vav1-Cit (blue line), Vav1-Cit Q331A (olive line), Vav1-Cit D376A (pink line) or eGFP (green line). Cells were loaded with the Ca^{2+}-sensitive fluorophore Indo-1 AM. After recording of basal Ca^{2+}-levels for 25 sec, the cells were stimulated with 20 µg/ml of anti-human-IgM $F(ab')_2$ fragments (α IgM) and the fluorescence was monitored for a total time of 5 min. The graphs are representative for 1 of 3 independent experiments. (B) Green fluorescence of cells analyzed in (A). The grey filled peak represents cells negative for green fluorescence.

Given that mutations at the N-terminus and mutations at the C-terminus of the DH domain of Vav1 within the Rac1 interaction interfaces diminished BCR-induced Ca^{2+}-mobilization, the question arose whether this drop in Ca^{2+}-influx can be further reduced. This question was addressed by generation of double-mutants carrying alanine substitutions in both termini of the DH domain. The resulting double-mutant variants of Vav1 were characterized by alanine residues at position 201 (E201A) and additionally either on position 371 (E201A N371A) or 378 (E201A E378A).

Both double-mutant Vav1 variants were expressed in amounts similar to the single amino substations and wild-type Vav1 (Figure 4.6 B and D). However, no further reduction of BCR-induced Ca^{2+}-mobilization was detected for Vav1 variants carrying amino acid substitutions to alanine either on positions 201 and 371 (Vav1-Cit E201A E371A, dark yellow line) or on positions 201 and 378 (Vav1-Cit E201 E378A, pink line). Furthermore, this experiment revealed that mutations in the second interaction interface of Vav1 for Rac1 (Figure 4.6 A and C, N371A, orange line and E378A, dark green line, respectively) reduced the Ca^{2+}-influx upon stimulation of the BCR to a stronger extent compared to the mutation in the first interaction interface (Figure 4.6 A and C, E201A, red line).

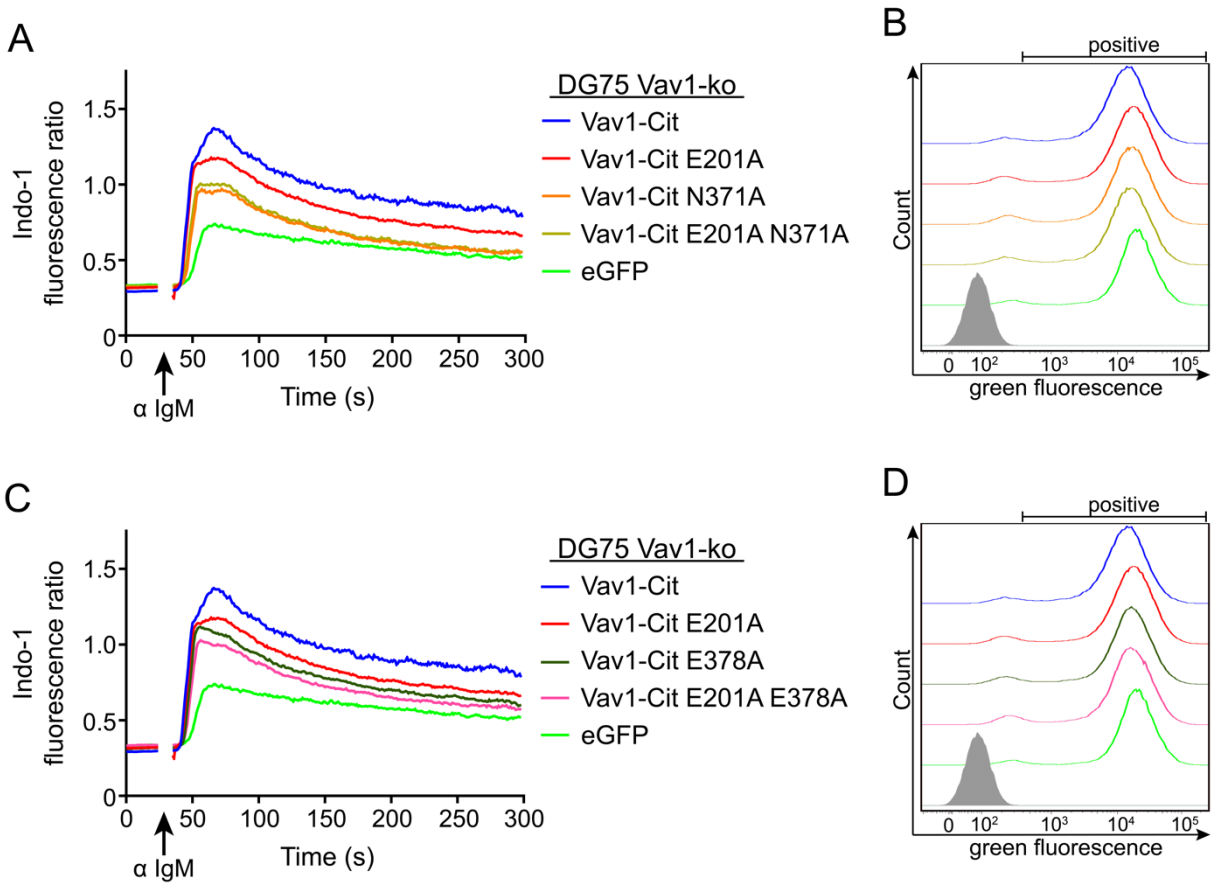

Figure 4.6 Double mutations in the Rac1 interaction site of Vav1 do not further reduce BCR-induced Ca^{2+}-mobilization as compared to single mutations. (A & C) Analysis of intracellular BCR-induced Ca^{2+}-mobilization of Vav1-deficient DG75 B cells expressing either Vav1-Cit (blue line), Vav1-Cit E201A (red line), Vav1-Cit N371A (orange line), Vav1-Cit E201A N371A (dark yellow line), E378A (dark green line), Vav1-Cit E201A E378A (pink line) or eGFP (green line). Cells were loaded with the Ca^{2+}-sensitive fluorophore Indo-1 AM. After recording of basal Ca^{2+}-levels for 25 sec, the cells were stimulated with 20 µg/ml of anti-human-IgM $F(ab')_2$ fragments (α IgM) and the fluorescence was monitored for a total time of 5 min. The graphs are representative for 1 of 3 independent experiments. (B) Green fluorescence of cells analyzed in (A) and (C), respectively. The grey filled peaks represent cells negative for green fluorescence.

Previous results of our group revealed that expression of murine wild-type Vav isoforms lead to similar BCR-induced Ca^{2+}-kinetics compared to their human counterparts in our human DG75 B cell model system[47]. For murine Vav1 (mVav1), an additional Rac1 interaction interface has been described, which consists of the amino acids leucine 334 and lysine 335. Mutations of these amino acids to alanine (LK334/335AA) have been reported to fully abolish the GEF-activity of mVav1 towards murine Rac1[96]. Based on these data, I generated a Citrine-tagged construct of mVav1 carrying the LK334/335AA double mutation and the resulting construct was expressed in Vav1-deficient DG75 B cells, while wild-type mVav1 and eGFP served as controls.

All variants of mVav1 were expressed in comparable amounts (Figure 4.7 B). However, while murine wild-type Vav1 was capable to compensate for the loss of human Vav1 in human DG75 B cells (Figure 4.7 A, purple line), cells expressing the murine LK334/335AA double-mutant variant (Figure 4.7 A, turquoise line) showed an attenuated BCR-induced Ca^{2+}-mobilization.

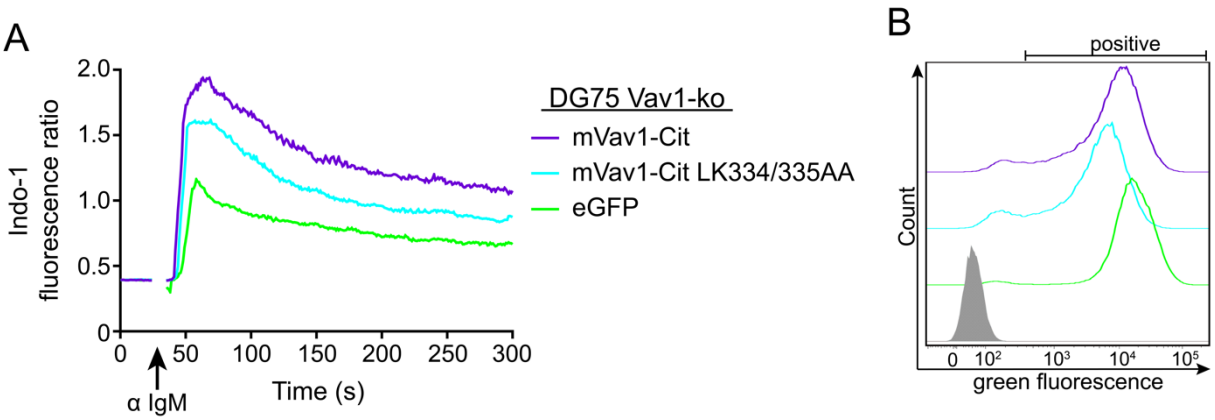

Figure 4.7 Mutations in mVav1-Rac1 interactions sites attenuate BCR-induced Ca^{2+}-mobilization. (A) Analysis of intracellular BCR-induced Ca^{2+}-mobilization of Vav1-deficient DG75 B cells expressing either mVav1-Cit (purple line), mVav1-Cit LK334/335AA (turquoise line) or eGFP (green line). Cells were loaded with the Ca^{2+}-sensitive fluorophore Indo-1 AM. After recording of basal Ca^{2+}-levels for 25 sec, the cells were stimulated with 20 µg/ml of anti-human-IgM $F(ab')_2$ fragments (α IgM) and the fluorescence was monitored for a total time of 5 min. The graphs are representative for 1 of 3 independent experiments. (B) Green fluorescence of cells analyzed in (A). The grey filled peak represents cells negative for green fluorescence.

On balance, various mutations on human or murine Vav1-Rac1 interaction sites reduced BCR-induced Ca^{2+}-mobilization approx. by half upon reconstitution compared to their respective wild-type counterparts in Vav1-deficient DG75 B cells. To test whether these amino acid substitutions are accompanied with altered GEF-activity of human and murine Vav1, the mediated enzymatic activity of the wild-type isoforms and mutant variants was tested.

4.2.2. Loss of GEF-activity of Vav1 and mVav1 results in diminished BCR-induced Ca^{2+}-mobilization in DG75 B cells

Having shown that mutations in Rac1 interaction interfaces of Vav1 caused diminished BCR-induced Ca^{2+}-mobilization and since an interaction of Vav1 and Rac1 is absolutely required for activation of GTPases, the hypothesis that the catalytic GEF-activity of Vav family members towards members of the Rho family is critical for this signaling pathway was postulated.

To examine this hypothesis, I established an *in vitro* GEF-activity assay which is based on the fluorophore Bodipy FL coupled to GDP (Bodipy-GDP) (for exact procedure see section 3.2.2.8.). To determine the ability of human and murine Vav1 to mediate the exchange from GDP to GTP for the most commonly used members of Rho GTPases in research, Rac1, RhoA and Cdc42, the GEF-mediating domains from amino acid 170 to 575 (acidic region to zinc finger domain) were expressed in *E. coli*, followed by purification (for exact procedure see section 3.2.2.7.). Besides the wild-type variants of human and murine Vav1, some of the mutations in the Vav1-Rac1 interface were introduced that caused a reduced BCR-induced Ca^{2+}-mobilization (E201A, Figure 4.3 A and N371A, Figure 4.4 A for human Vav1 and LK334/335AA, Figure 4.7 A for murine Vav1). Furthermore, to mimic the stimulated state of Vav1, I introduced a tyrosine-to-aspartate substitution at position 174 (Y174D). This amino

acid is known to be involved in the relief of autoinhibition upon phosphorylation by Src family kinases and to promote the GEF-activity of Vav1[95].

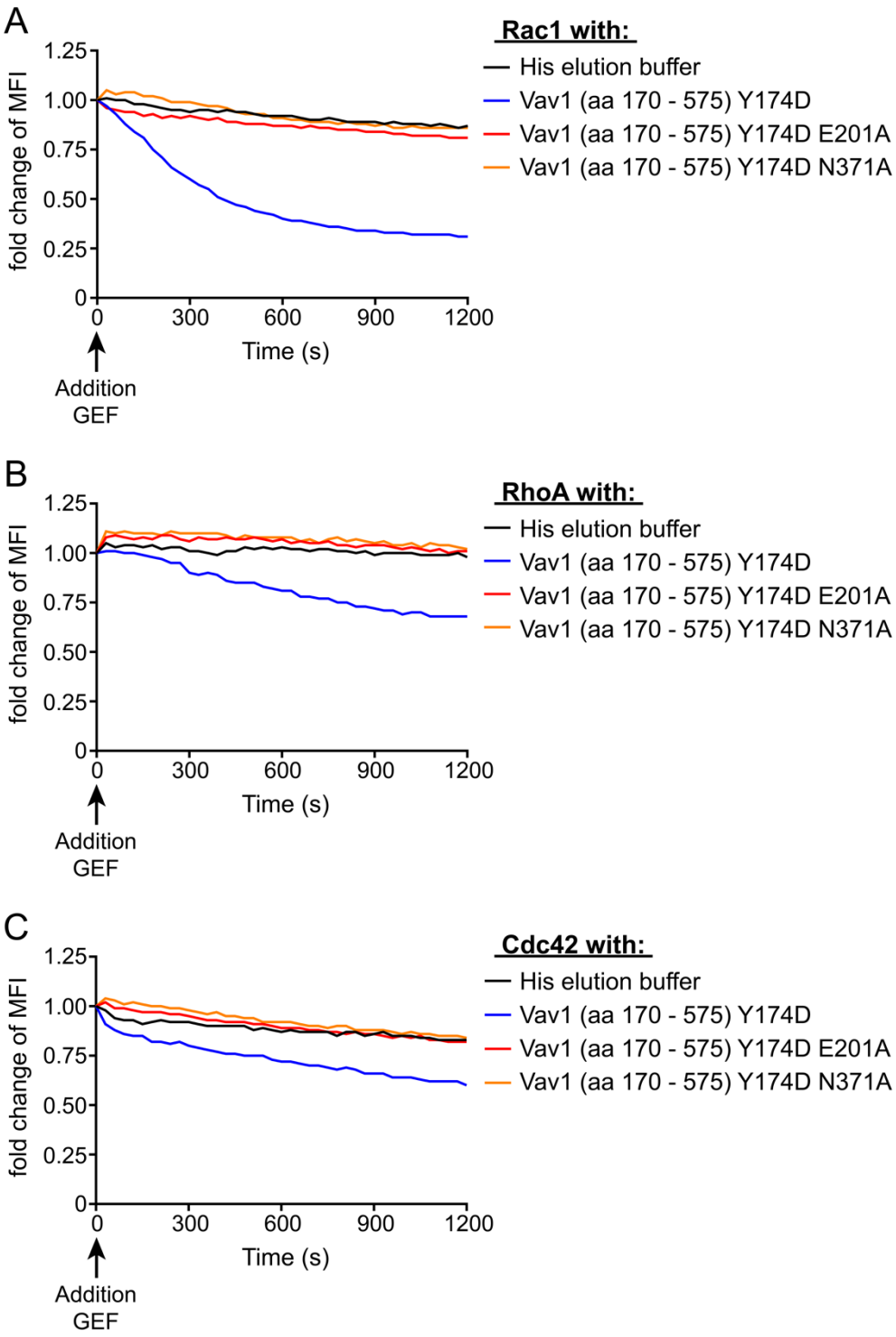

Figure 4.8 Mutations in Vav1-Rac1 interactions sites abolish GEF-activity of Vav1. (A, B and C) Analysis of GEF-activity of different variants of Vav1. The indicated small G proteins were loaded with 0,3 µM Bodipy-GDP. The mean of the first five measurements is timepoint 0. Upon addition of the indicated Vav1 variants or buffer, the fluorescence was measured every 30 sec for 20 min. All values are normalized to the mean value of timepoint 0. The graphs are representative for 1 of 3 independently performed experiments.

In line with previous results of another group, these experiments revealed that Vav1 exhibited the strongest GEF-activity towards Rac1 (Figure 4.8 A, blue line), an intermediate GEF-activity

towards RhoA (Figure 4.8 B, blue line) and little activity towards Cdc42 (Figure 4.8 C, blue line)[87]. Most strikingly, single amino acid substitutions to alanine either at position 201 (Vav1 E201A, Figure 4.8, red lines) or at position 371 (Vav1 N371A, Figure 4.8, orange lines) in Vav1 fully abolished Vav1-mediated GEF-activity towards all three tested Rho GTPases.

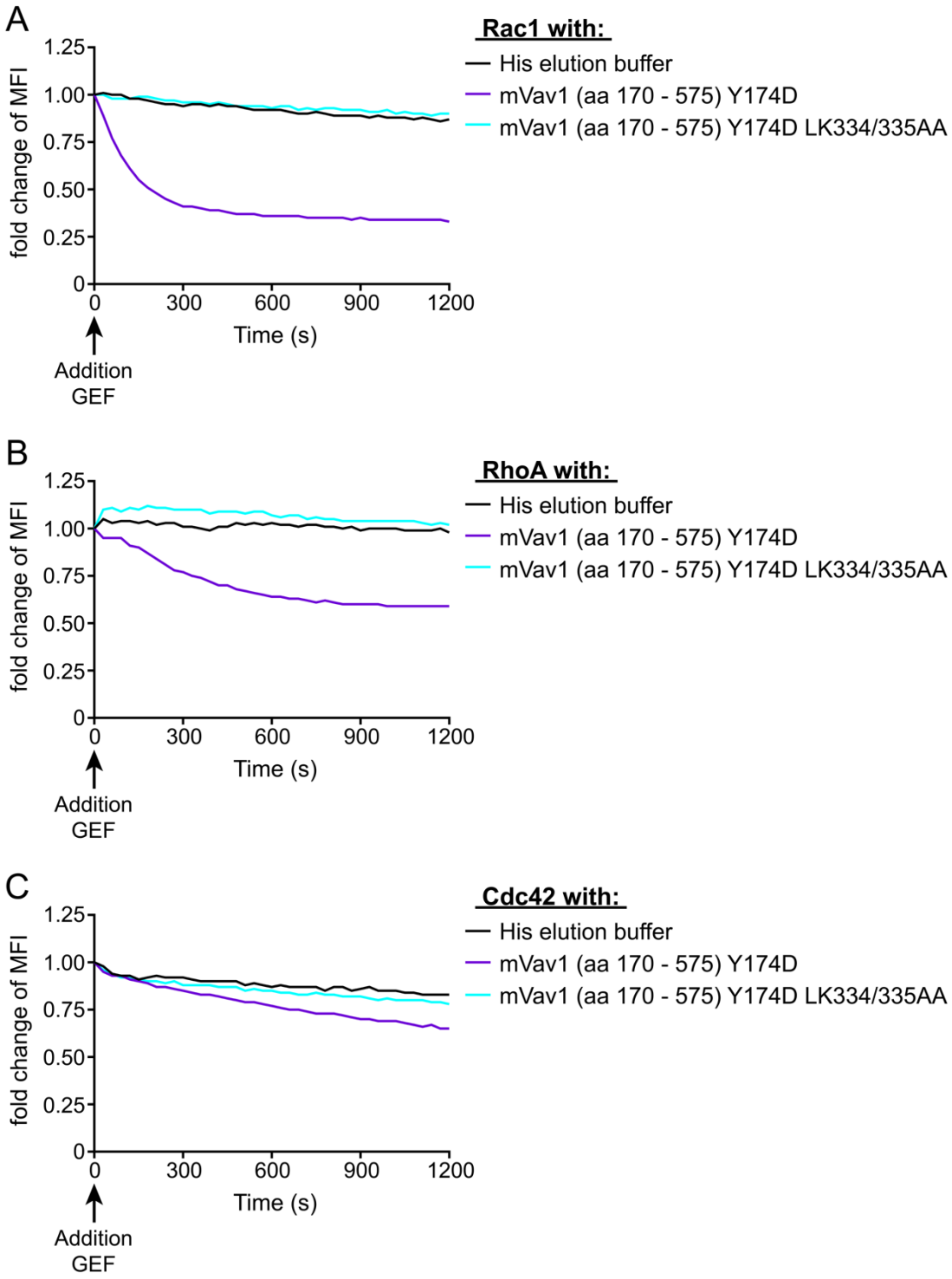

Figure 4.9 Mutations in mVav1-Rac1 interactions sites abolish GEF-activity of mVav1. (A, B and C) Analysis of GEF-activity of different variants of mVav1. The indicated small G proteins were loaded with 0,3 µM Bodipy-GDP. The mean of the first five measurements is timepoint 0. Upon addition of the indicated mVav1 variants or buffer, the fluorescence was measured every 30 sec for 20 min. All values are normalized to the mean value of timepoint 0. The graphs are representative for 1 of 3 independently performed experiments.

Next, I tested wild-type mVav1 as well as the LK334/335AA variant thereof. Barely any differences in the mediated activation of Rac1, RhoA or Cdc42 were detected between wild-type Vav1 (Figure 4.8) and wild-type mVav1 (Figure 4.9). Interestingly, mVav1 carrying amino acid substitutions to alanine at positions 334 and 335 lost the ability to catalyze the exchange from GDP to GTP for all three tested small G proteins of the Rho family.

In summary, alanine substitution of amino acids involved in binding of Vav1 to Rac1 either on the N- or the C-terminal end of the DH domain or alanine substitutions in described critical amino acids of mVav1 for the GEF-activity towards Rac1, fully abolish the mediated activation of Rac1, RhoA and Cdc42.

4.2.3. The GEF-activity of a Vav1 variant selectively recruited to the BCR and of Vav3 is required for full BCR-induced Ca^{2+}-mobilization

To further analyze the role of GEF-activity of Vav1 for BCR-induced Ca^{2+}-mobilization, an artificial Vav1-construct was used. The resulting protein, in which the endogenous SH2 domain was replaced by the tandem SH2 domains of Syk (Vav1Syk$(SH2)_2$), is specifically and exclusively recruited to Igα and Igβ upon stimulation of the BCR and causes an elevated Ca^{2+}-mobilization with barely any decrease within the first five min of stimulation compared to wild-type Vav1 (Figure 4.10 A, dark blue line)[47]. To test whether this sustained Ca^{2+}-phenotype is based on the GEF-activity of Vav1, I introduced the mutations E201A and N371A and the function of the resulting mutant variants were characterized in Vav1-deficient DG75 B cells as before.

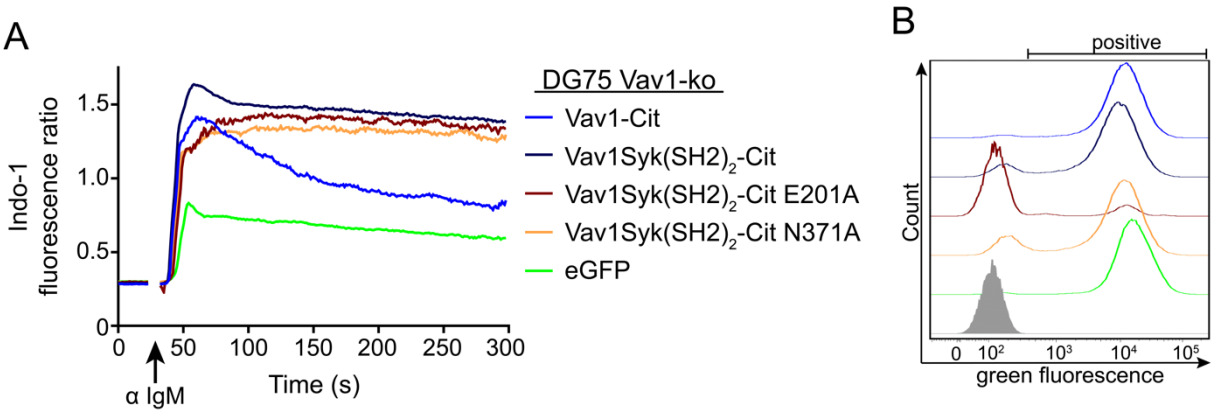

Figure 4.10 Mutations in Vav1-Rac1 interactions sites reduce BCR-induced Ca^{2+}-mobilization. (A) Analysis of intracellular BCR-induced Ca^{2+}-mobilization for Vav1-deficient DG75 B cells expressing either Vav1-Cit (blue line), Vav1Syk$(SH2)_2$-Cit (dark blue line), Vav1Syk$(SH2)_2$-Cit E201A (dark red line), Vav1Syk$(SH2)_2$-Cit N371A (light orange line) or eGFP (green line). Cells were loaded with the Ca^{2+}-sensitive fluorophore Indo-1 AM. After recording of basal Ca^{2+}-levels for 25 sec, cells were stimulated with 20 µg/ml of anti-human-IgM F(ab')$_2$ fragments (α IgM) and the fluorescence was monitored for a total time of 5 min. The graphs are representative for 1 of 3 independent experiments. (B) Green fluorescence of cells analyzed in (A). The grey filled peak represents cells negative for green fluorescence.

All generated constructs were expressed in similar amounts (Figure 4.10 B). Only few cells expressed Vav1Syk$(SH2)_2$ variant carrying the E201A mutation, but in a similar amount to cells

expressing the other constructs (dark red line). Analysis of BCR-induced Ca^{2+}-mobilization of the resulting cells (Figure 4.10 A) confirmed that the Vav1Syk$(SH2)_2$ chimera (dark blue line) exhibited enhanced Ca^{2+}-mobilization upon stimulation of the BCR compared to wild-type Vav1. This enhanced ability was partly reduced by the loss of GEF-activity (Vav1Syk$(SH2)_2$-Cit E201A, dark red line and Vav1Syk$(SH2)_2$-Cit N371A, light orange line). These two variants of Vav1Syk$(SH2)_2$ were still able to mobilize Ca^{2+} but showed a diminished peak in the first sec after stimulation of the BCR. The intracellular Ca^{2+}-concentration increased rather slowly and almost reached the level of Vav1Syk$(SH2)_2$ without loss-of-GEF-activity mutations 1 min after stimulation.

Considering that the loss of GEF-activity of human Vav1, murine Vav1 and Vav1Syk$(SH2)_2$ led to reduced Ca^{2+}-mobilization upon stimulation of the BCR, the question arose whether also the GEF-activity of Vav3 was required for BCR-induced Ca^{2+}-mobilization. Therefore, I introduced a single amino acid substitution at position 199 from glutamate to alanine in Vav3 (Vav3 E199A). This amino acid of Vav3 corresponds to glutamate at position 201 of Vav1 and showed a reduced ability in BCR-induced Ca^{2+}-mobilization (Figure 4.3 A). Furthermore, amino acid substitution at this position in Vav1 appeared to not exhibit any GEF-activity towards Rac1, RhoA or Cdc42 (Figure 4.8). The resulting construct was expressed as Citrine-tagged fusion protein in Vav1-deficient DG75 B cells, while expression of wild-type Vav3 and eGFP served as controls.

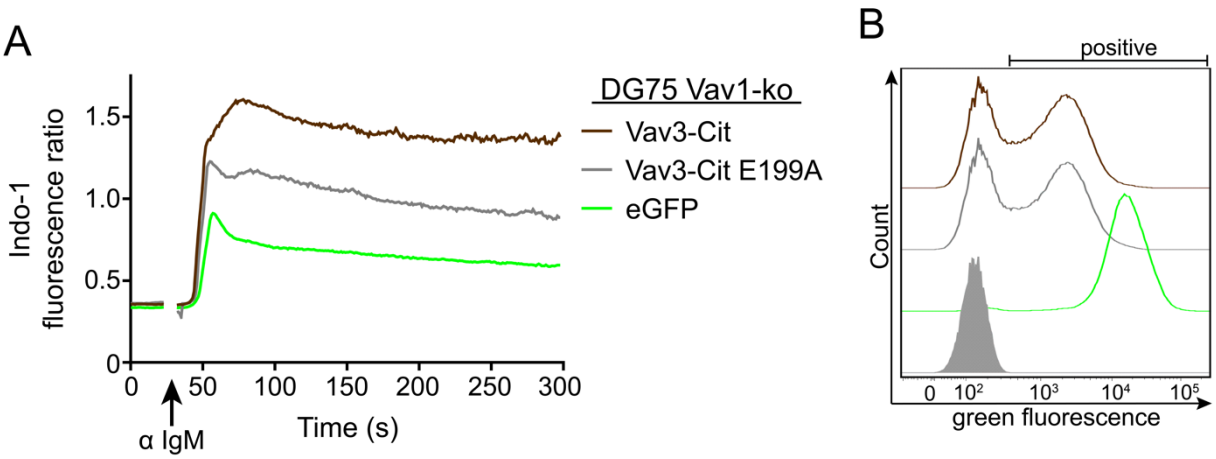

Figure 4.11 Mutation in Vav3-Rac1 interactions site attenuate BCR-induced Ca^{2+}-mobilization. (A) Analysis of intracellular BCR-induced Ca^{2+}-mobilization for Vav1-deficient DG75 B cells expressing either Vav3-Cit (brown line), Vav3-Cit E199A (grey line) or eGFP (green line). Cells were loaded with the Ca^{2+}-sensitive fluorophore Indo-1 AM. After recording of basal Ca^{2+}-levels for 25 sec, cells were stimulated with 20 µg/ml of anti-human-IgM F(ab')$_2$ fragments (α IgM) and the fluorescence was monitored for a total time of 5 min. The graphs are representative for 1 of 3 independent experiments. (B) Green fluorescence of cells analyzed in (A). The grey filled peak represents cells negative for green fluorescence.

Both Vav3 variants were expressed in similar amounts (Figure 4.11). Interestingly, Vav3 E199A (Figure 4.11 A, grey line) showed a reduced ability to mobilize Ca^{2+} upon stimulation of the BCR compared to wild-type Vav3 (Figure 4.11 A, brown line). The intracellular Ca^{2+}-concentration was reduced approx. by half throughout the measurement. To check whether

the differences in BCR-induced Ca^{2+}-mobilization were due to the loss of the catalytic GEF-activity, Vav3 variants were recombinantly expressed in bacteria and purified to perform *in vitro* GEF-activity assays as described before.

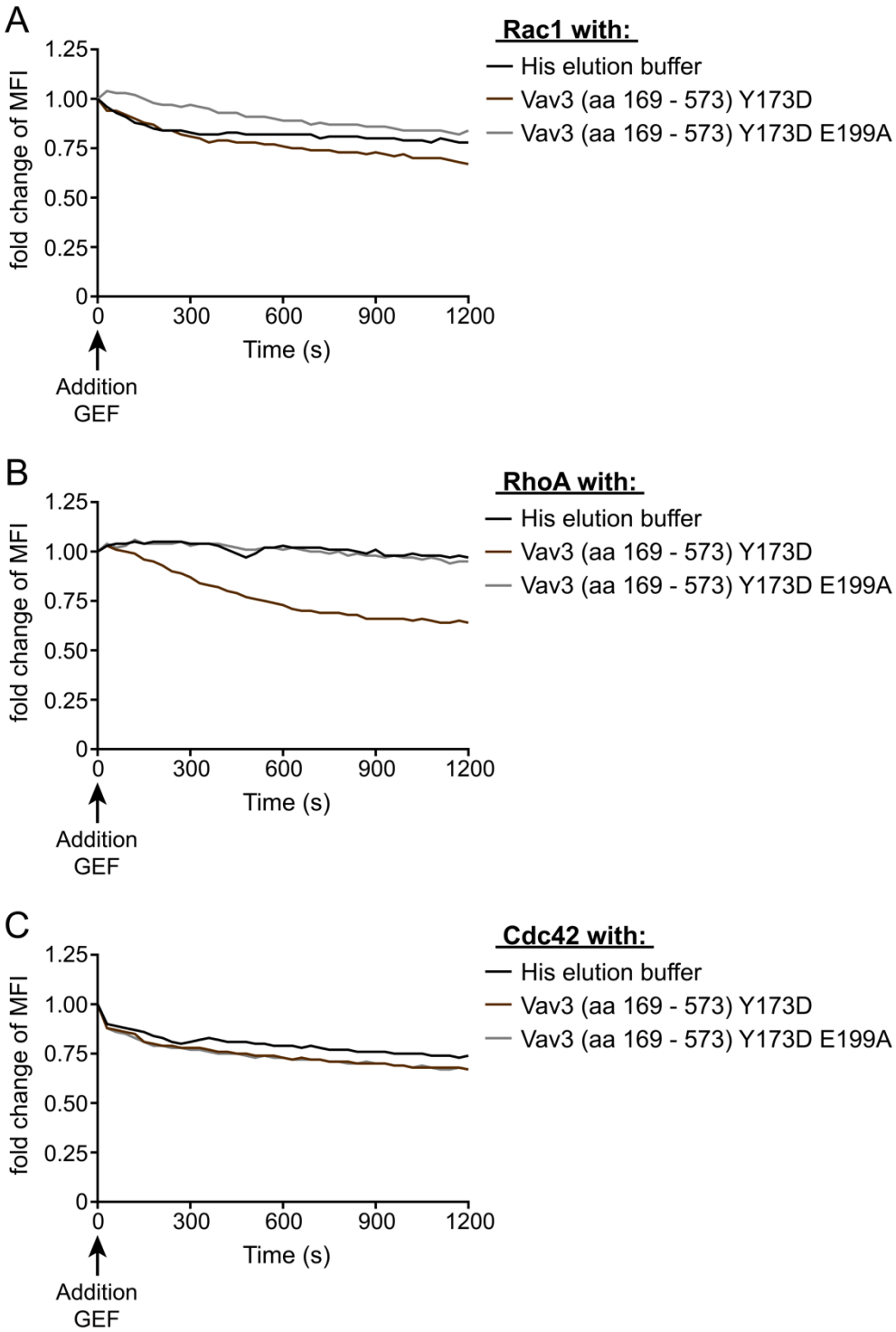

Figure 4.12 Mutation of the corresponding amino acid in Rac1 interaction site of Vav3 and Vav1 abolishes the GEF-activity of Vav3. (A, B and C) Analysis of GEF-activity of different variants of Vav3. The indicated small G proteins were loaded with 0,3 µM Bodipy-GDP. The mean of the first five measurements is timepoint 0. Upon addition of the indicated Vav3 variants or buffer, the fluorescence was measured every 30 sec for 20 min. All values are normalized to the mean value of timepoint 0. The graphs are representative for 1 of 3 independently performed experiments.

The cloned Vav3 constructs encompassed amino acids 169 to 573 of the human protein. As for Vav1, a tyrosine to aspartate substitution at position 173 (Y173D) within the acidic region was introduced to mimic phosphorylation of this residue. Analysis of the GEF-activity of Vav3 (Figure 4.12) revealed that the wild-type fragment of Vav3 (brown lines) barely exhibited any GEF-activity towards Rac1 or Cdc42, but showed moderate GEF-activity towards RhoA. This effect was similarly observed for human Vav1 (Figure 4.8) and mVav1 (Figure 4.9). This GEF-activity towards RhoA was fully abolished by the E199A single amino acid substitution (grey lines).

Having shown that the loss of GEF-activity towards Rac1, RhoA and Cdc42 of human and murine Vav1 and Vav3 led to reduced BCR-induced Ca^{2+}-kinetics, the role of the downstream Rho GTPases was examined.

4.2.4. Inhibition of small G proteins reduces BCR-induced Ca^{2+}-mobilization

So far, the results of this work demonstrated that the GEF-activity of Vav family members is critical for bona fide BCR-induced Ca^{2+}-mobilization. Rho GTPases are the substrates of the enzymatic GEF-activity of Vav family members resulting in activation of the small G proteins[72]. To further confirm the role of Vav proteins as GEFs within this signaling axis, activation of Rho family small G proteins was pharmacologically inhibited. Previous attempts in our lab to generate reliable knockout cell lines for Rho GTPases were rather less successful[47]. DG75 B cells deficient for either Rac1 or Rac2 were generated, B cell clones for RhoA deficient or Rac1 and Rac2 double-deficient were however not obtained[47]. Given that Rho family members share high similarities on amino acid level and that their functions particularly within the subfamilies are described to be redundant, the generated cell lines might not constitute the best model system for the loss of a subfamily[101,102]. Instead, activation of Rho GTPases was inhibited in DG75 parental cells and in Vav1-deficient DG75 cells by using two independent pharmacological inhibitors named EHop-016 (E-Hop) and Rhosin. E-Hop is described to be specific for Rac1 and Rac3 at low concentrations (≤ 5 µM). However, at higher concentrations it also inhibits the closely related Rho GTPase Cdc42[135]. Rhosin is reported to be specific for RhoA and RhoC[136]. Both, E-Hop and Rhosin bind to and thereby block binding sites of the respective Rho member to their GEFs[135,137].

Initially, the minimal effective concentrations for both inhibitors were acquired using DG75 parental cells. The concentrations ranged from 1 µM to 30 µM for E-Hop and 20 µM to 60 µM for Rhosin. The respective inhibitor was added at the indicated concentrations five min before the Ca^{2+}-measurement (Figure 4.13). Both inhibitors for Rho family members acted in a dose-dependent manner with E-Hop showing no effect at a concentration of 1 µM while BCR-induced Ca^{2+}-mobilization was completely abolished at a concentration of 30 µM (Figure

4.13 A). However, since the cells at an E-Hop concentration of 30 µM showed increased forward scatter/side scatter signals and slightly elevated baseline Ca^{2+}-levels, I conducted further experiments with a concentration of 20 µM.

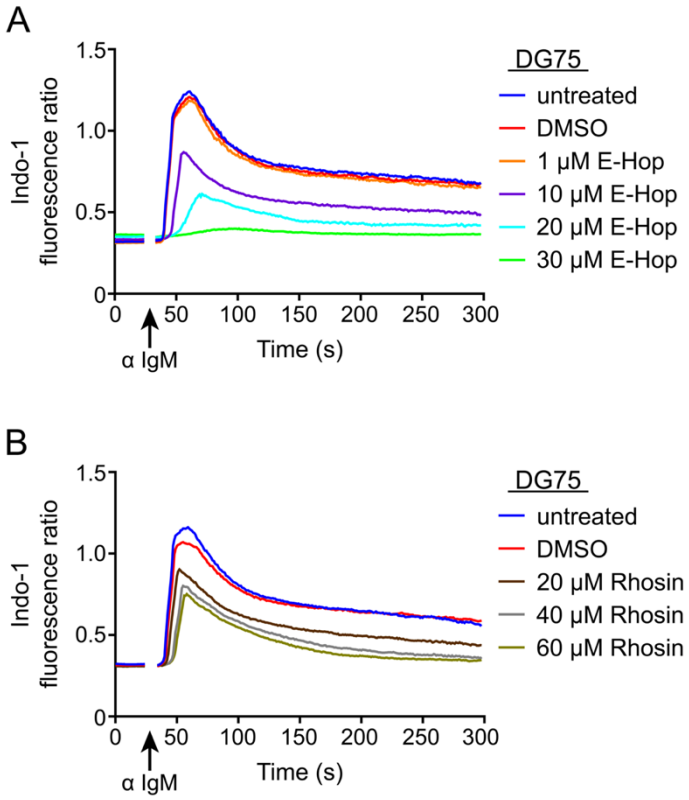

Figure 4.13 Rac1/RhoA/Cdc42 inhibitors reduce BCR-induced Ca^{2+}-mobilization. (A and B) Analysis of intracellular BCR-induced Ca^{2+}-mobilization for DG75 B cells. Cells were loaded with the Ca^{2+}-sensitive fluorophore Indo-1 AM. 5 min before stimulation, E-Hop or Rhosin were added at the indicated concentrations. After recording of basal Ca^{2+}-levels for 25 sec, cells were stimulated with 20 µg/ml of anti-human-IgM $F(ab')_2$ fragments (α IgM) and the fluorescence was monitored for a total time of 5 min. The graphs are representative for 1 of 3 independent experiments.

Inhibition of Rho family members with Rhosin also led to a reduced BCR-induced Ca^{2+}-mobilization (Figure 4.13 B). Pre-incubation of 20 µM Rhosin substantially reduced the ability to mobilize Ca^{2+} upon stimulation of the BCR (brown line). This reduction was further increased by addition of higher concentrations of Rhosin (grey and olive lines) without affecting the forward and side scatter of the cells. In contrast to E-Hop, inhibition with Rhosin did not affect the baseline of DG75 B cells. In the following, a concentration of 60 µM of Rhosin was applied in the subsequent experiments. Cytotoxic effects by the solvent DMSO were excluded by application of DMSO to the cells as vehicle control (blue and red lines).

Next, the effects on BCR-induced Ca^{2+}-mobilization resulting from inhibition of Rho family members through E-Hop and Rhosin with the previously determined concentrations were examined in parental DG75 cells and the Vav1-deficient subline (Figure 4.14).

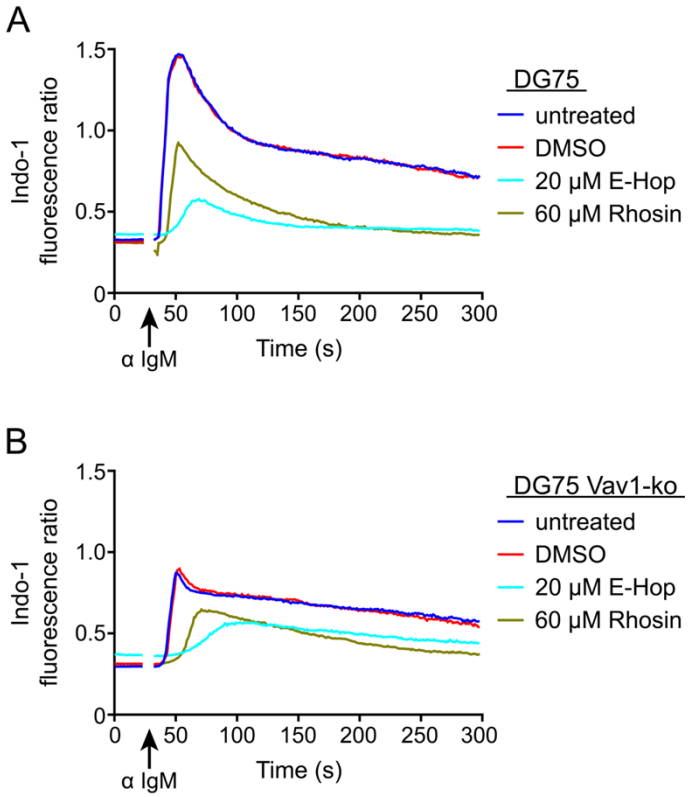

Figure 4.14 Rac1/RhoA/Cdc42 inhibitors reduce BCR-induced Ca^{2+}-mobilization. (A and B) Analysis of intracellular BCR-induced Ca^{2+}-mobilization for DG75 B cells in (A) and Vav1-deficient DG75 B cells in (B). Cells were loaded with the Ca^{2+}-sensitive fluorophore Indo-1 AM. 5 min before stimulation, E-Hop or Rhosin were added at the indicated concentrations. After recording of basal Ca^{2+}-levels for 25 sec, cells were stimulated with 20 µg/ml of anti-human-IgM $F(ab')_2$ fragments (α IgM) and the fluorescence was monitored for a total time of 5 min. The graphs are representative for 1 of 3 independent experiments.

Treatment of Vav1-deficient DG75 B cells with E-Hop and Rhosin negatively influenced their BCR-induced Ca^{2+}-mobilization, but to a lower extent compared to parental DG75 B cells (Figure 4.14 A and B). These results implied, that activation of Rho GTPases is required for BCR-induced Ca^{2+}-mobilization. However, this activation seemed not to be exclusively dependent on Vav1 since the Ca^{2+}-mobilization after BCR stimulation was also reduced upon pharmacological inhibition of Rho GTPases in Vav1-deficient DG75 B cells.

Collectively, loss of Vav-mediated GEF-activity achieved either through mutations in reported Rac1 interaction sites within Vav family members or via pharmacological inhibition of Rho GTPases substantially reduced BCR-induced Ca^{2+}-mobilization in DG75 B cells.

4.3. The acidic region of Vav2 prevents the support of this molecule for BCR-induced Ca^{2+}-mobilization in DG75 B cells

Previous results of this work strongly pointed to a role of the GEF-activity of Vav proteins on BCR-induced Ca^{2+}-signaling. Briefly, Vav1 and Vav3, but not Vav2 supported BCR-induced Ca^{2+}-mobilization in Vav1-deficient DG75 B cells. This finding together with previous results of

this thesis raised the question as to whether Vav2 was not able to compensate for the loss of Vav1 in Ca^{2+}-mobilization due to its ability to mediate GEF-activity. Either for all or just for specific members of the Rho family.

4.3.1. Deletion of the acidic region enables the ability of Vav2 for BCR-induced Ca^{2+}-mobilization in DG75 B cells

The acidic region in Vav family members is described as a negative regulatory module for their GEF-activity. As the name indicates, this region contains several negatively charged amino acid residues but also three tyrosines in each of the family members. Three-dimensional analysis revealed that this region forms an inhibitory loop that blocks the active center of the DH domain in resting cells[78]. Upon activation of Vav family members by Src family kinases, the tyrosine residues are phosphorylated, resulting in a disintegration of the auto-inhibited structure and an enhanced GEF-activity[95]. To test whether this resolution of auto-inhibition is crucial for BCR-induced Ca^{2+}-mobilization, I deleted the acidic region ranging from amino acid 130 to amino acid 183 in Vav2 and the resulting construct (Vav2ΔAR) was expressed as a Citrine-tagged fusion protein in Vav1-deficient DG75 B cells, while wild-type Vav2 and eGFP served as controls (Figure 4.15).

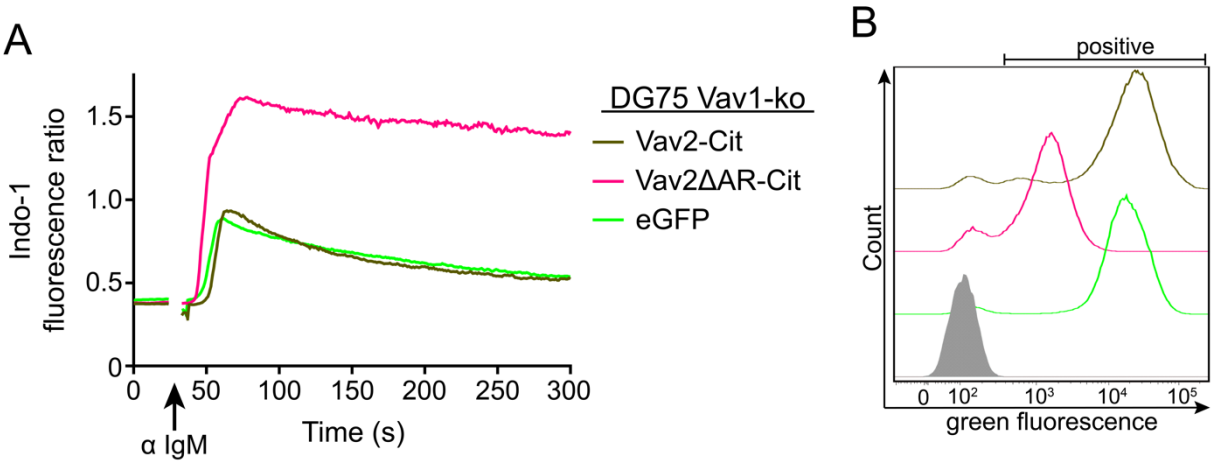

Figure 4.15 Deletion of the acidic region in Vav2 leads to strong BCR-induced Ca^{2+}-mobilization. (A) Analysis of intracellular BCR-induced Ca^{2+}-mobilization for Vav1-deficient DG75 B cells expressing either Vav2-Cit (dark green line), Vav2ΔAR-Cit (pink line) or eGFP (green line). Cells were loaded with the Ca^{2+}-sensitive fluorophore Indo-1 AM. After recording of basal Ca^{2+}-levels for 25 sec, cells were stimulated with 20 µg/ml of anti-human-IgM $F(ab')_2$ fragments (α IgM) and the fluorescence was monitored for a total time of 5 min. The graphs are representative for 1 of 3 independent experiments. (B) Green fluorescence of cells analyzed in (A). The grey filled peak represents cells negative for green fluorescence.

Most strikingly, even though Vav2ΔAR (pink lines) was expressed (Figure 4.15 B) approx. ten times less efficiently compared to wild-type Vav2 (dark green lines), this variant of Vav2 exhibited strong and sustained BCR-induced Ca^{2+}-mobilization (Figure 4.15 A). These data indicated that the ability of Vav2 to support Ca^{2+}-signaling upon stimulation of the BCR is prevented by its own acidic region.

4.3.2. Imitation of acidic region tyrosine phosphorylation in Vav2 allows BCR-induced Ca^{2+}-mobilization DG75 B cells

Since deletion of the acidic region turned Vav2 into an active molecule for Ca^{2+}-mobilization upon stimulation of the BCR, the underlying mechanism was analyzed in more detail. Because deletion of the entire acidic region was a significant alteration of Vav2, I selectively substituted potentially critical amino acids within this region of the protein. These critical amino acids are three tyrosines that are responsible for the structural resolution upon phosphorylation[95]. Hence, to mimic the phosphorylated state, the tyrosines at positions 142, 159 and 172 were substituted with aspartate, respectively, and the resulting variant was analyzed as a Citrine-tagged fusion protein in Vav1-deficient DG75 B cells as before (Figure 4.16).

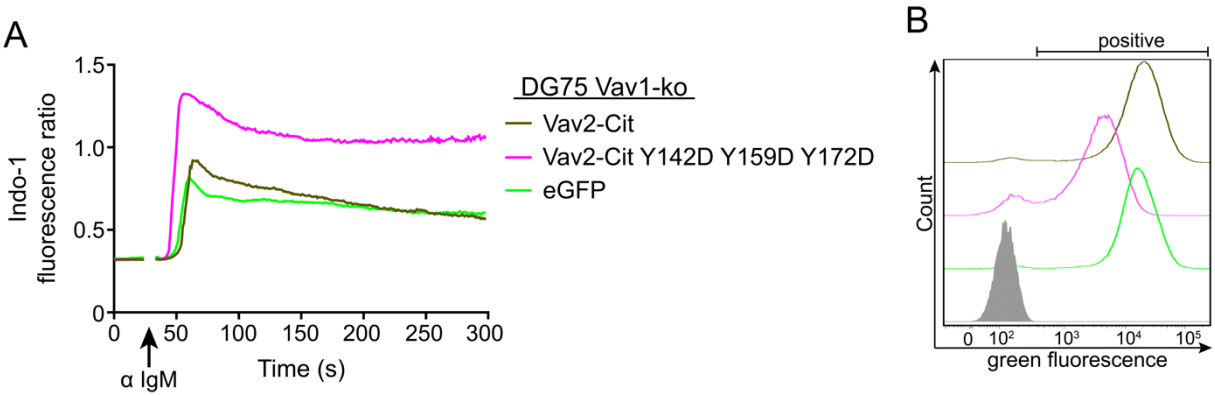

Figure 4.16 "Phosphorylation" of the acidic region of Vav2 leads to an increased BCR-induced Ca^{2+}-mobilization. (A) Analysis of intracellular BCR-induced Ca^{2+}-mobilization for Vav1-deficient DG75 B cells expressing either Vav2-Cit (dark green line), Vav2-Cit Y142D Y159D Y172D (magenta line) or eGFP (green line). Cells were loaded with the Ca^{2+}-sensitive fluorophore Indo-1 AM. After recording of basal Ca^{2+}-levels for 25 sec, cells were stimulated with 20 µg/ml of anti-human-IgM $F(ab')_2$ fragments (α IgM) and the fluorescence was monitored for a total time of 5 min. The graphs are representative for 1 of 3 independent experiments. (B) Green fluorescence of cells analyzed in (A). The grey filled peak represents cells negative for green fluorescence.

Like Vav2ΔAR, the Vav2 protein carrying the three tyrosine to aspartate amino acid substitutions within the acidic region (magenta line) was expressed five times less efficiently (Figure 4.16 B) compared to wild-type Vav2 (dark green line). Nevertheless, this variant of Vav2 was able to support BCR-induced Ca^{2+}-mobilization.

Both variants of Vav2, either without acidic or with "phosphorylated" acidic region, supported BCR-induced Ca^{2+}-mobilization in a sustained manner upon reconstitution in Vav1-deficient DG75 B cells. These experiments led to the question, whether those alterations in the acidic region of Vav2 corresponded to the ability to mediate GEF-activity of the Vav2 variants.

4.3.3. The DH domain of Vav2 activates Rac1 and Cdc42, but not RhoA

Next, the GEF-activity of the different Vav2 variants was supposed to be determined. Unfortunately, variants of Vav2 consisting of amino acids 168 to 581, which correspond to the constructs for Vav1 (Figure 4.8), mVav1 (Figure 4.9) or Vav3 (Figure 4.12), were not expressed

recombinantly and purified in amounts required for GEF-activity measurements. However, to get at least some insights into the GEF-activity of Vav2, I used a commercially available recombinant DH domain consisting of amino acids 189 to 374 of human Vav2 for determination of its GEF-activity (Figure 4.17).

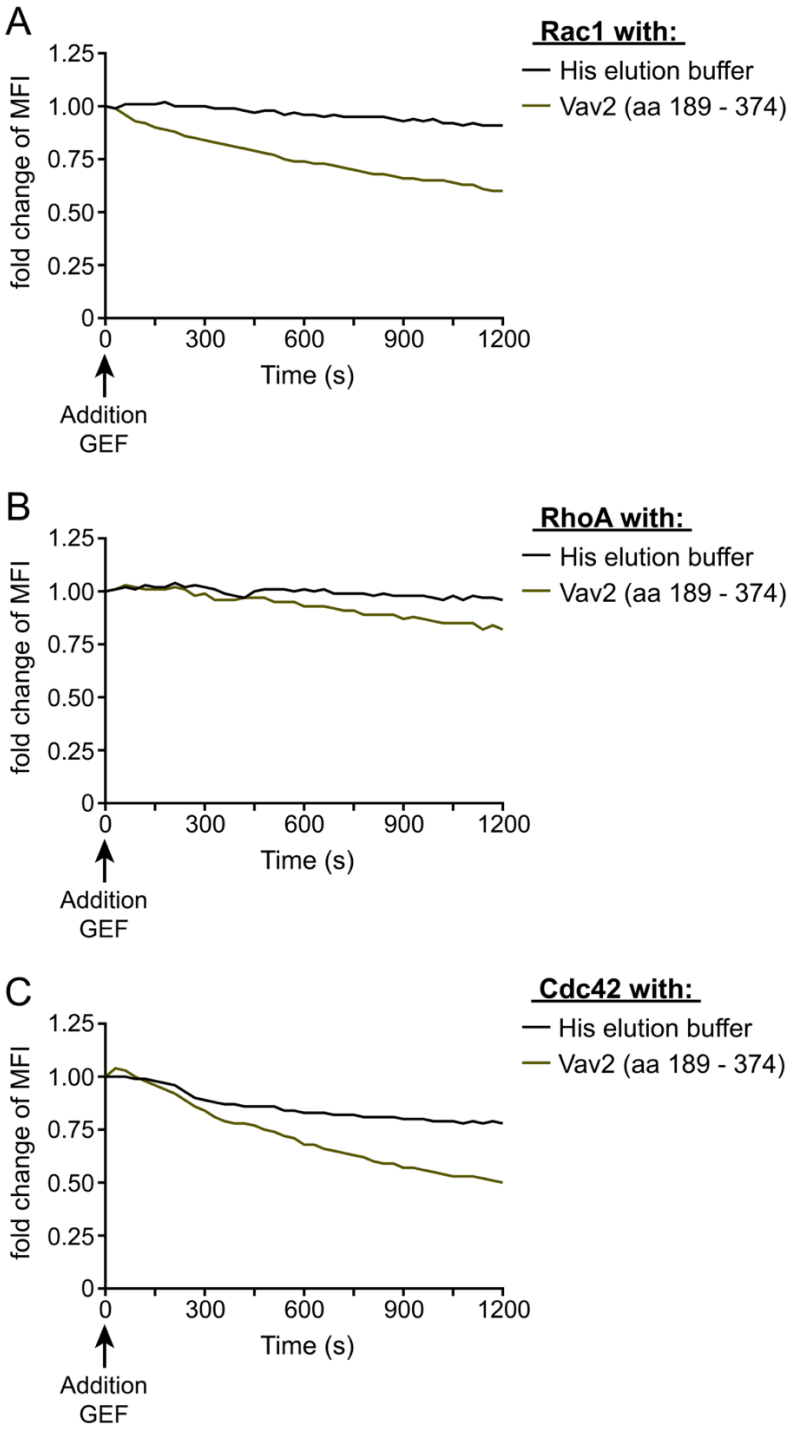

Figure 4.17 The DH domain of Vav2 mediates intermediate GEF-activity towards Rac1 and Cdc42, but shows barely any GEF-activity towards RhoA. (A, B and C) Analysis of GEF-activity of the DH domain of Vav2. The indicated small G proteins were loaded with 0,3 µM Bodipy-GDP. The mean of the first five measurements is timepoint 0. Upon addition of the DH domain of Vav2 or buffer, the fluorescence was measured every 30 sec for 20 min. All values are normalized to the mean value of timepoint 0. The graphs are representative for 1 of 3 independently performed experiments.

GEF-activity analysis revealed that the DH domain of Vav2 mediated intermediate activation of Rac1 and Cdc42, but hardly any towards RhoA (Figure 4.17).

In conclusion, the results in this chapter demonstrated that the acidic region of Vav2 limits its function in BCR-induced Ca^{2+}-mobilization in Vav1-deficient DG75 B cells. When the acidic region was deleted or when the phosphorylated state was mimicked through three amino acid substitutions from tyrosine to aspartate, Vav2 was turned into an active molecule for Ca^{2+}-influx into the cytosol upon stimulation of the BCR. Furthermore, the isolated DH domain of Vav2 was determined to have intermediate GEF-activity towards Rac1 and Cdc42, but barely any towards RhoA.

4.4. PIP5Ks as potential downstream molecules of activated Rho GTPases

Considering that the GEF-activity of Vav1 and Vav3 as well as activation of Rho family small G proteins were crucial for optimal BCR-induced Ca^{2+}-mobilization in DG75 B cells, the question arose which molecules could be potential downstream effectors of the small G proteins. One potential group of downstream targets were PIP5Ks and PIP4Ks, which are responsible for the generation of PIP_2, the substrate for PLCγ2[109,110]. Since the amount of PI4P in cells is ten times higher than the amount of PI5P and since activated small G proteins of the Rho family are reported to enhance the kinase activity of PIP5Ks, I started investigations on potential downstream targets with the PIP5Ks[111,117]. To date, three family members of PIP5Ks have been identified, named PIP5Kα, PIP5Kβ and PIP5Kγ[138].

4.4.1. Overexpression of PIP5Ks partially compensates for the loss of Vav1 in BCR-induced Ca^{2+}-mobilization

To examine whether PIP5Ks were able to recover for the loss of Vav1 regarding BCR-induced Ca^{2+}-mobilization, all three family members were expressed individually in Vav1-deficient DG75 cells. Since previous experiments in our group with PIP5Ks revealed that constitutive expression of these enzymes might be harmful to DG75 B cells, an inducible expression system was used. This system allows for expression of genes of interest upon addition of doxycycline. Cell lines containing the coding sequences for individual PIP5K isoforms were generated and gene expression was induced by addition of 1 µM doxycycline for 10 h. All PIP5Ks were equipped with a C-terminal Citrine tag. Accordingly, inducible expression of Citrine was used as a negative control (Figure 4.18).

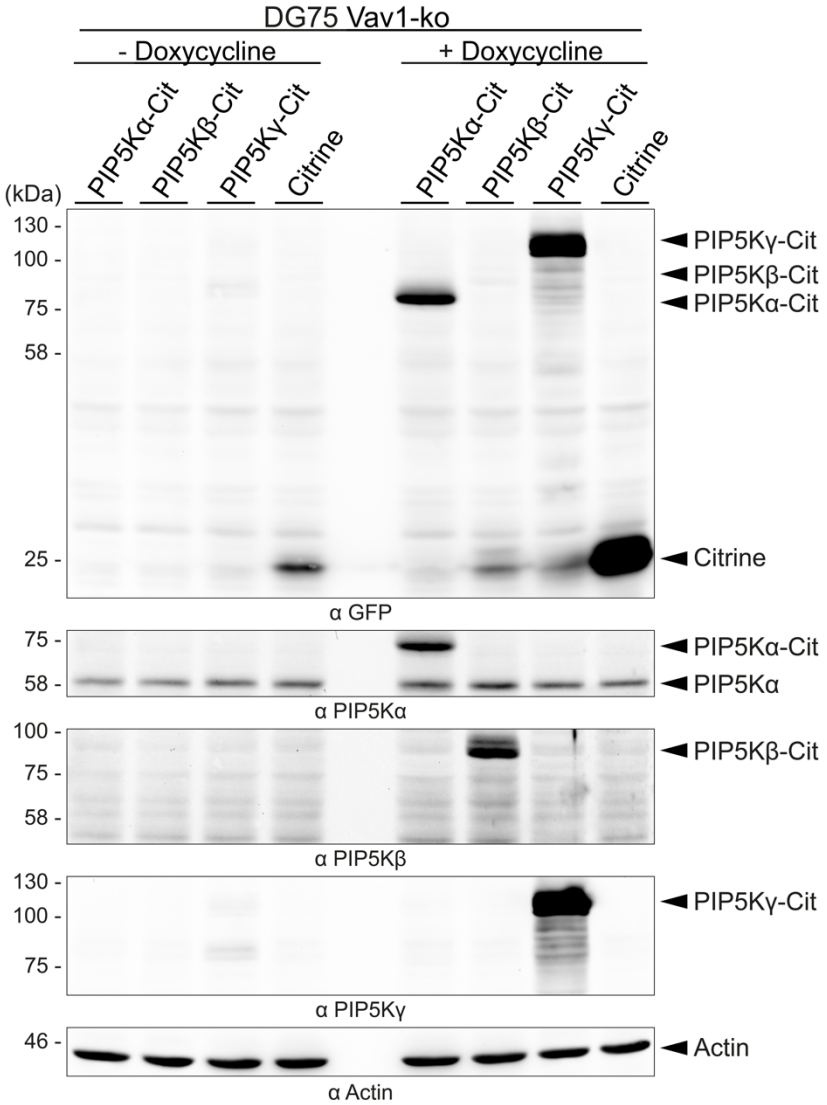

Figure 4.18 Validation of the induction model with doxycycline of PIP5K family members. Immunoblot analysis of cleared cellular lysates of Vav1-deficient DG75 B cells transduced with constructs for inducible expression of PIP5Kα, PIP5Kβ, PIP5Kγ or Citrine. The cells were either left untreated or were incubated with 1 µM of doxycycline 10 h before lysis. Proteins were separated by SDS-PAGE and analyzed by western blot using antibodies specific for GFP, PIP5Kα, PIP5Kβ, PIP5Kγ and Actin. The molecular weight of marker proteins is indicated on the left in kDa.

All three PIP5K isoforms were expressed to different extents upon doxycycline-induction (Figure 4.18, lanes 6 to 9). Without addition of doxycycline, no expression for PIP5K family members was detected (Figure 4.18, lanes 1 to 4). Signals for PIP5Kα and PIP5Kγ appeared at the predicted molecular weights after detection with antibodies for GFP (Figure 4.18, upper panel, lanes 6 and 8). Protein specificity as well as expression of PIP5Kβ was confirmed using specific antibodies to the respective family member (second, third and fourth panes, lanes 6 to 8). The only endogenously expressed isoform in Vav1-deficient DG75 B cells was PIP5Kα (second panel from the top).

Next, I investigated the effects of this exogenous expression of PIP5K family members for BCR-induced Ca^{2+}-mobilization in Vav1-deficient DG75 B cells. Hence, these cells were pre-

incubated for 10 h before the Ca^{2+}-measurement with 1 µM of doxycycline to induce protein expression.

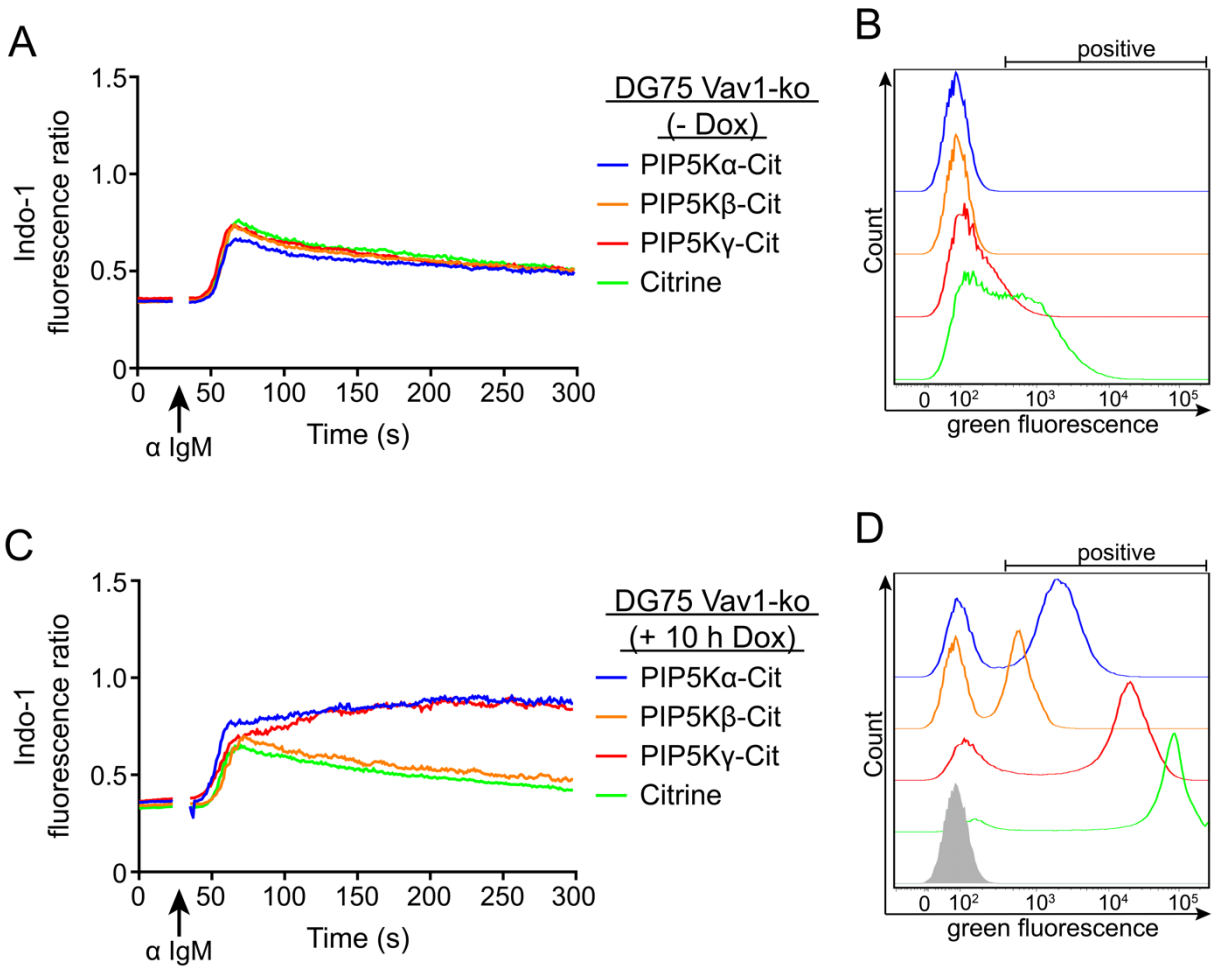

Figure 4.19 Expression of PIP5Kα or PIP5Kγ increase BCR-induced Ca^{2+}-mobilization in Vav1-deficient DG75 B cells. (A and C) Analysis of intracellular BCR-induced Ca^{2+}-mobilization for Vav1-deficient DG75 B cells with and without additional expression of PIP5Ks. The cells were either left untreated or were incubated for 10 h with 1 µM of doxycycline. Subsequently, cells were loaded with the Ca^{2+}-sensitive fluorophore Indo-1 AM. After recording of basal Ca^{2+}-levels for 25 sec, cells were stimulated with 20 µg/ml of anti-human-IgM $F(ab')_2$ fragments (α IgM) and the fluorescence was monitored for a total time of 5 min. The graphs are representative for 1 of 3 independent experiments. (B and D) Green fluorescence of cells analyzed in (A) and (C), respectively. The grey filled peaks represent cells negative for green fluorescence.

The expression data acquired by flow cytometry (Figure 4.19 B and D) in this experiment strongly correlated with those generated by western blot analysis (Figure 4.18). Without induction of protein expression with doxycycline, all cells showed the same Ca^{2+}-phenotype upon stimulation of the BCR (Figure 4.19 A), essentially representing DG75 B cells lacking expression of Vav1. Expression of either PIP5Kα (Figure 4.19 C, blue line) or PIP5Kγ (Figure 4.19 C, red line), yet not PIP5Kβ, led to a higher capacity to mobilize Ca^{2+} upon stimulation of the BCR. While the typical peak approx. 30 sec after BCR-stimulation was not restored, Vav1-deficient DG75 B cells expressing either PIP5Kα or PIP5Kγ showed constant increase of intracellular Ca^{2+}-concentrations after prolonged measurements.

4.4.2. Generation of PIP5Kα-deficient DG75 cells

Considering that PIP5Kα was the only endogenously expressed isoform of PIP5Ks in DG75 B cells (Figure 4.18) and that exogenous expression of PIP5Kα improved BCR-induced Ca^{2+}-mobilization in the absence of Vav1, I generated PIP5Kα-deficient DG75 B cells to further analyze a potential role of PIP5Ks within the Ca^{2+}-axis of BCR signaling. For the generation of PIP5Kα-deficient DG75 B cells, CRISPR/Cas9-mediated genome editing was used (for details see sections 3.2.3.2.1. and 3.2.3.4.1.). The resulting single cell clones were screened for expression of all PIP5K family members (Figure 4.20). As positive controls for PIP5Kβ and PIP5Kγ, either lysates from DG75 B cells inducibly expressing PIP5Kβ or from Jurkat T cells, respectively, were used (Figure 4.20).

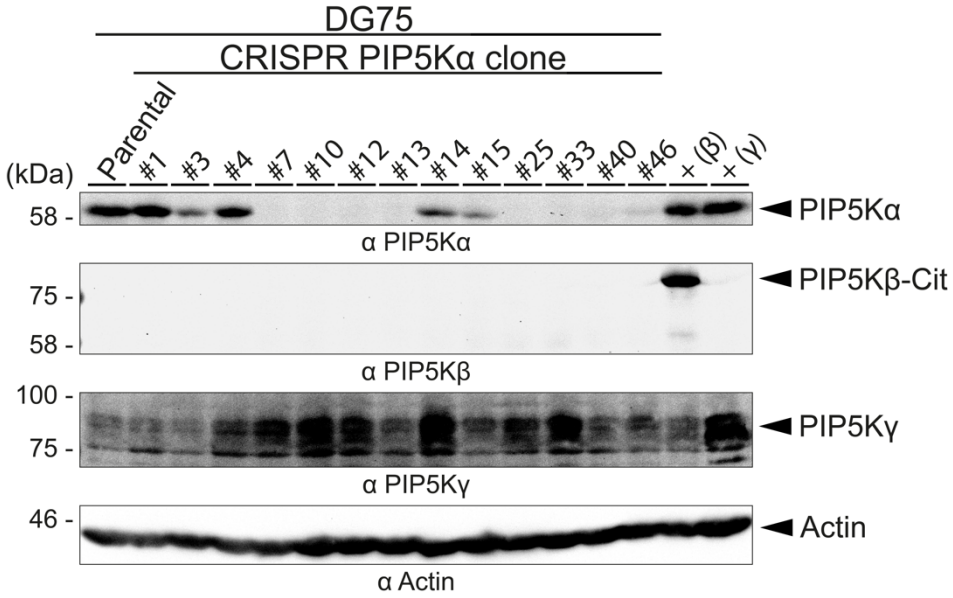

Figure 4.20 Generation of PIP5Kα-deficient DG75 B cells. Immunoblot analysis of cleared cellular lysates of DG75 B cell sub-clones transfected with plasmids to CRISPR PIP5Kα. Proteins were separated by SDS-PAGE and analyzed by western blot using antibodies specific for PIP5Kα, PIP5Kβ, PIP5Kγ and Actin. The molecular weight of marker proteins is indicated on the left in kDa. As a positive control for antibodies to PIP5Kβ (+ (β)), lysates from Vav1-deficient DG75 B cells with induced expression of Citrine-tagged PIP5Kβ were used. As a positive control for antibodies to PIP5Kγ (+ (γ)), lysates from Jurkat cells were used.

Staining with antibodies to PIP5Kα revealed that several clones (#7, #10, #12, #13, #25, #33, #40) had lost expression of PIP5Kα (Figure 4.20, upper panel). Intriguingly, while none of the clones expressed detectable amounts of PIP5Kβ (second panel from the top), staining with antibodies to PIP5Kγ (third panel from the top) showed that in almost all of the clones that lost expression of PIP5Kα, higher amounts of PIP5Kγ were detected in comparison to parental DG75 B cells.

Next, I analyzed the Ca^{2+}-mobilization kinetics of several PIP5Kα-deficient clones. Unfortunately, the tested DG75 sub-clones produced inconsistent results ranging from significantly impaired to considerably enhanced Ca^{2+}-kinetics compared to parental cells (Figure 4.21).

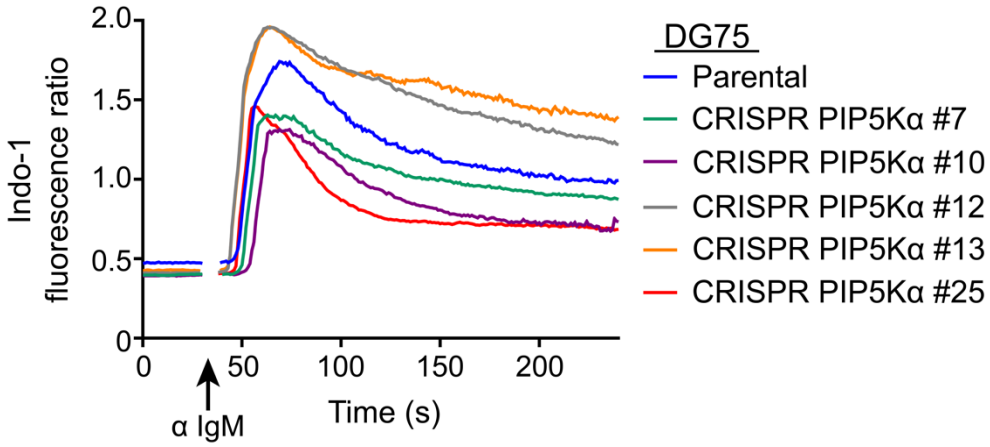

Figure 4.21 BCR-induced Ca^{2+}-phenotypes of PIP5Kα-deficient DG75 sub-clones. Analysis of intracellular BCR-induced Ca^{2+}-mobilization for DG75 B cells lacking the expression of PIP5Kα. Cells were loaded with the Ca^{2+}-sensitive fluorophore Indo-1 AM. After recording of basal Ca^{2+}-levels for 25 sec, cells were stimulated with 20 µg/ml of anti-human-IgM $F(ab')_2$ fragments (α IgM) and the fluorescence was monitored for a total time of 4 min.

Nevertheless, two of the obtained knockout clones were genetically analyzed, either showing higher (clone #13) or lower (clone #25) Ca^{2+}-mobilization upon BCR stimulation. For characterization, PCR amplicons covering the CRISPR/Cas9-targeted *PIP5K1A* exon 3 from genomic DNA of clones #13 and #25 were amplified and sequenced. Successful Cas9-mediated double strand breaks followed by erroneous cellular DNA repair was supposed to destroy a Bsu36I restriction site in that exon.

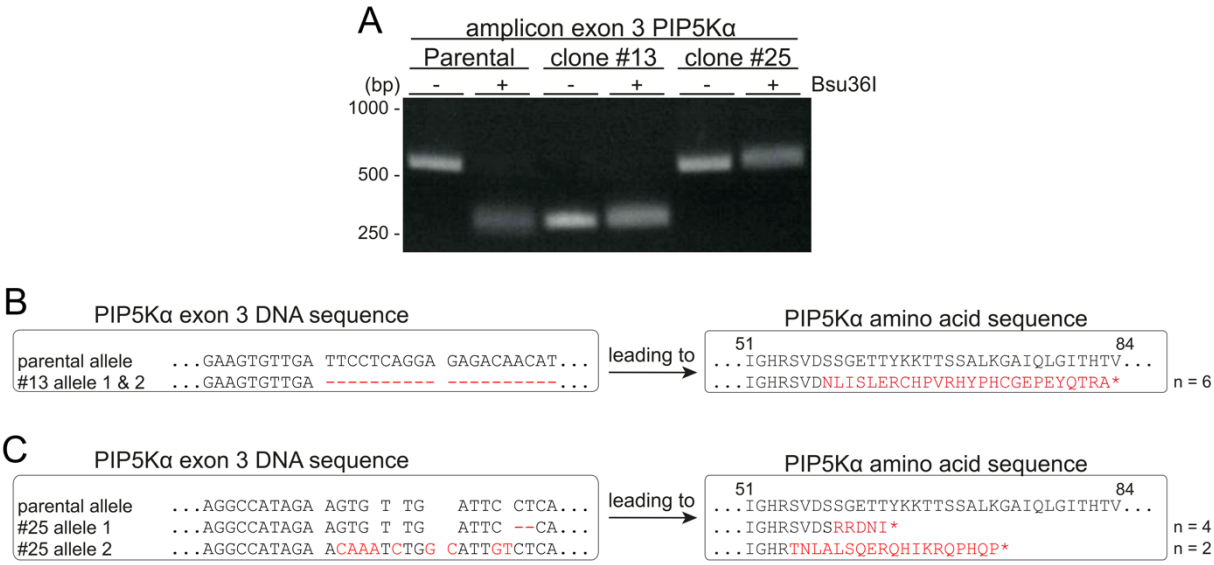

Figure 4.22 Genetic characterization of DG75 PIP5Kα knockout clones #13 and #25. (A) Restriction analysis of the amplicon covering exon 3 of *PIP5K1A*. The amplicon was amplified by PCR, the resulting DNA was separated by agarose gel electrophoresis and extracted from the gel. Half of the DNA was left untreated whereas the other half was incubated with Bsu36I. After this incubation period, the DNA was separated on an agarose gel and was visualized using ethidium bromide. The size of marker DNA is indicated on the left. (B and C) Sequencing data of exon 3 of *PIP5K1A* for clones #13 and #25. The amplicon was amplified by PCR, the resulting DNA was separated in an agarose gel and extracted from the gel. The DNA was cloned into the pCR2.1 plasmid and the insert was sequenced. Differences to the wild-type sequences are highlighted in red.

The size of the PCR product for parental cell and for PIP5Kα-deficient clone #25 matched the expected size of the amplicon (Figure 4.22 A, lanes 1 and 5), whereas the amplicon amplified

from genomic DNA of clone #13 however had a size of only about 300 base pairs (Figure 4.22 A, lane 3). While the parental derived amplicon was cleaved upon incubation with Bsu36I (lane 2), incubation with the same restriction enzyme did not affect the size of the amplicons for clones #13 and #25 (lanes 4 and 6). Clone #13 showed a deletion of approx. 300 base pairs on both alleles within the amplicon containing the targeted exon (Figure 4.22 B). This deletion led to a frame shift from amino acid 58 on protein level, which results in a truncated protein ranging to amino acid 84. For clone #25, on one allele a deletion of two base pairs was sequenced, which resulted in a frame shift from amino acid 59 and disrupted protein expression shortly afterwards. For the second allele of clone #25, several base pair substitutions and insertions occurred. Those alterations led to a frame shift starting from amino acid 55 and resulted in a premature stop codon at position 74.

Even though the generation of PIP5Kα-deficient DG75 B cells was successful, they showed inconsistencies regarding BCR-induced Ca^{2+}-mobilization. Since western blot analysis revealed that most of the resulting PIP5Kα-deficient DG75 B cell sub-clones showed elevated levels of PIP5Kγ, PIP5Kα and PIP5Kγ double-deficient DG75 B cells were generated.

4.4.3. Generation of DG75 B cells lacking expression of PIP5Kα and PIP5Kγ

In Vav1-deficient DG75 B cells, both isoforms, PIP5Kα and PIP5Kγ showed the same potency in enhancing BCR-induced Ca^{2+}-mobilization (Figure 4.19). I used the previously generated and characterized PIP5Kα-deficient DG75 clones #13 and #25 for nucleofection with plasmids targeting either exon 3 or exon 4 of the *PIP5K1C* gene for CRISPR/Cas9-mediated genome editing. The resulting single cell sub-clones originating from PIP5Kα-deficient clone #25 were screened for expression of PIP5Kγ using specific antibodies (Figure 4.23 A). Furthermore, the obtained clones lacking the expression of both, PIP5Kα and PIP5Kγ (Figure 4.23 B, C and D) were genetically characterized and checked for their ability to mobilize Ca^{2+} upon stimulation of the BCR (Figure 4.23 E). Genetic analysis of PIP5Kα-deficient clone #25 derived clones #1 and #5 lacking the expression of PIP5Kγ (Figure 4.23 A) revealed that in each clone both mutant alleles led to early frame shifts resulting in premature stop codons (Figure 4.23 C and D). However, the capacity to mobilize Ca^{2+} upon stimulation of the BCR was not altered for double-deficient DG75 B cells (Figure 4.23 E, turquoise and grey lines) compared to their parental precursor #25 with no expression of PIP5Kα (Figure 4.23 E, red line).

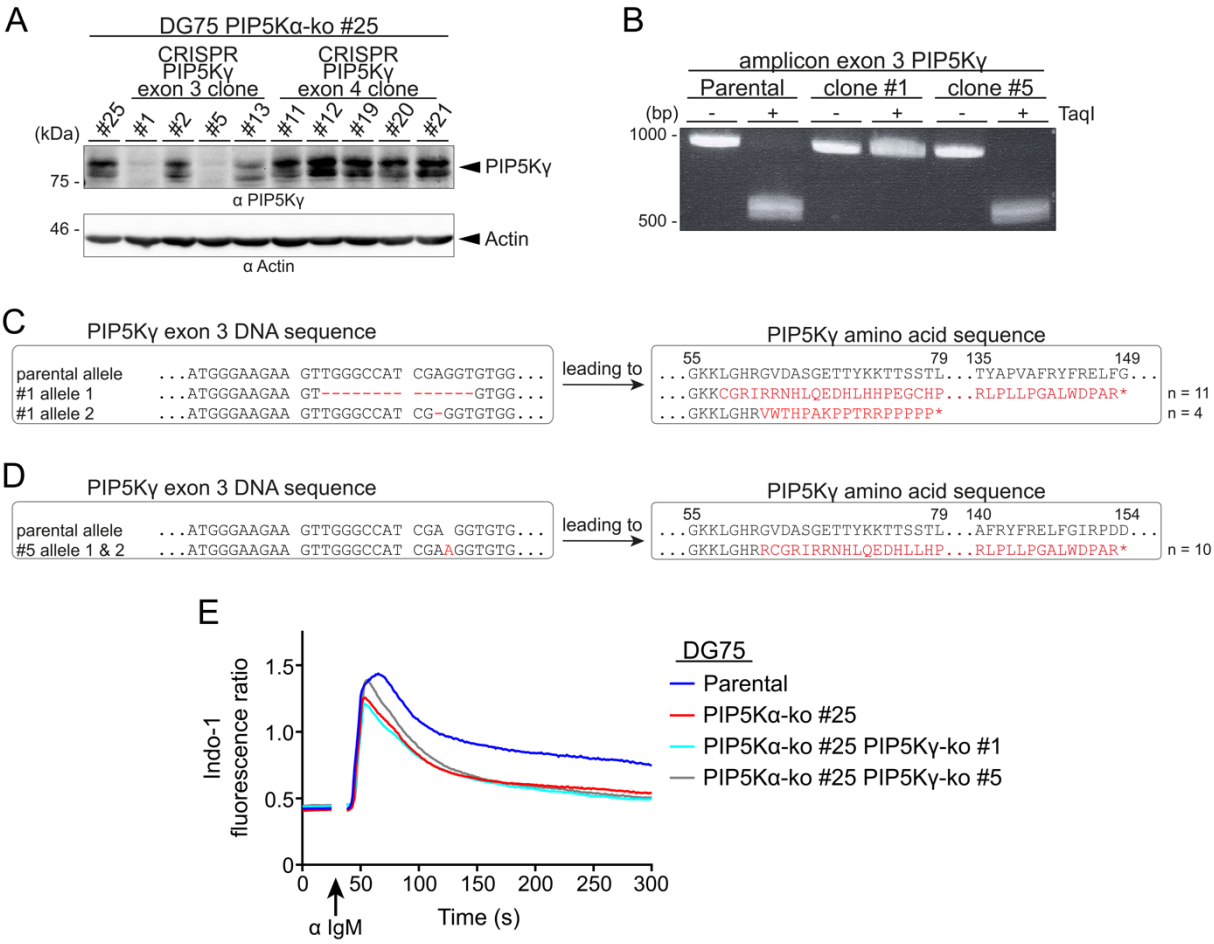

Figure 4.23 Targeting exon 3 of *PIP5KC* successfully generated double-deficient DG75 B cells for PIP5Kα and PIP5Kγ. (A) Immunoblot analysis of cleared cellular lysates of DG75 B cell sub-clones transfected with plasmids to CRISPR PIP5Kγ. Proteins were separated by SDS-PAGE and analyzed by western blot using antibodies specific for PIP5Kγ and Actin. The molecular weight of marker proteins is indicated on the left in kDa. (B) Restriction analysis of the amplicon covering exon 3 of *PIP5K1C*. The amplicon was amplified by PCR, the resulting DNA was separated by agarose gel electrophoresis and extracted from the gel. Half of the DNA was left untreated whereas the other half was incubated with TaqI. After this incubation period, the DNA was separated on an agarose gel and was visualized using ethidium bromide. The size of marker DNA is indicated on the left. (C and D) Sequencing data of exon 3 of *PIP5K1C* for clones #1 and #5. The amplicon was amplified by PCR, the resulting DNA was separated in an agarose gel and extracted from the gel. The DNA was cloned into the pCR2.1 plasmid and the insert was sequenced. Differences to the wild-type sequences are highlighted in red. (E) Analysis of intracellular BCR-induced Ca^{2+}-mobilization for DG75 B cells lacking the expression of PIP5Kα and PIP5Kγ. Cells were loaded with the Ca^{2+}-sensitive fluorophore Indo-1 AM. After recording of basal Ca^{2+}-levels for 25 sec, cells were stimulated with 20 µg/ml of anti-human-IgM $F(ab')_2$ fragments (α IgM) and the fluorescence was monitored for a total time of 5 min.

I repeated the same procedure to generate double-deficient cells for PIP5Kα and PIP5Kγ originating from PIP5Kα-deficient cell clone #13, this time targeting exon 3 of *PIP5K1C* (Figure 4.24).

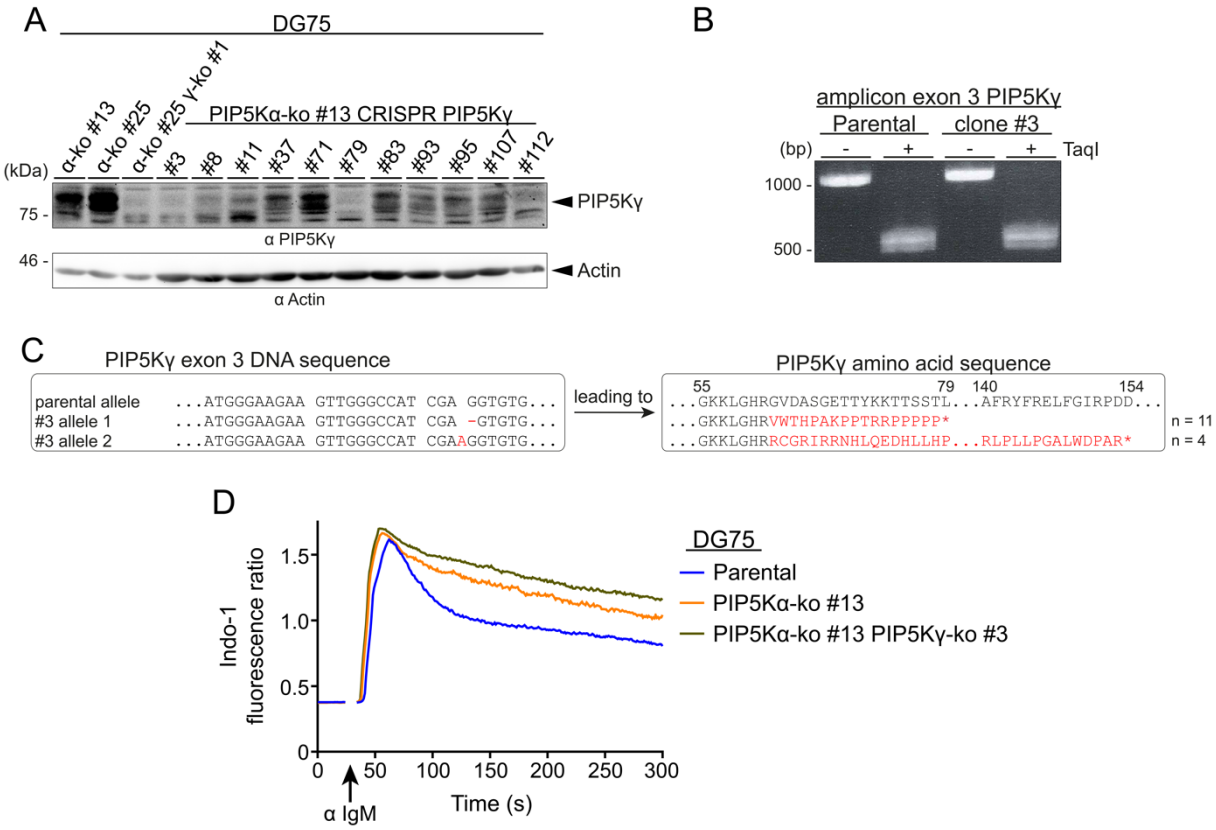

Figure 4.24 Targeting exon 3 of *PIP5KC* successfully generated double-deficient DG75 B cells for PIP5Kα and PIP5Kγ. (A) Immunoblot analysis of cleared cellular lysates of DG75 B cell sub-clones transfected with plasmids to CRISPR PIP5Kγ. Proteins were separated by SDS-PAGE and analyzed by western blot using antibodies specific for PIP5Kγ and Actin. The molecular weight of marker proteins is indicated on the left in kDa. (B) Restriction analysis of the amplicon covering exon 3 of *PIP5K1C*. The amplicon was amplified by PCR, the resulting DNA was separated by agarose gel electrophoresis and extracted from the gel. Half of the DNA was left untreated whereas the other half was incubated with TaqI. After this incubation period, the DNA was separated on an agarose gel and was visualized using ethidium bromide. The size of marker DNA is indicated on the left. (C) Sequencing data of exon 3 of *PIP5K1C* for clone #3. The amplicon was amplified by PCR, the resulting DNA was separated in an agarose gel and extracted from the gel. The DNA was cloned into the pCR2.1 plasmid and the insert was sequenced. Differences to the wild-type sequences are highlighted in red. (D) Analysis of intracellular BCR-induced Ca^{2+}-mobilization for DG75 B cells lacking the expression of PIP5Kα and PIP5Kγ. Cells were loaded with the Ca^{2+}-sensitive fluorophore Indo-1 AM. After recording of basal Ca^{2+}-levels for 25 sec, cells were stimulated with 20 µg/ml of anti-human-IgM F(ab')$_2$ fragments (α IgM) and the fluorescence was monitored for a total time of 5 min.

Genetic characterization (Figure 4.24 B and C) of the obtained PIP5Kα and PIP5Kγ double-deficient knockout clone #3 (Figure 4.24 A) revealed early frame shifts resulting in premature stop codons on both alleles. However, as before, the clone showed the same ability to mobilize Ca^{2+} upon stimulation of the BCR (Figure 4.24 D, olive line) compared to its PIP5Kα-deficient precursor #13 (Figure 4.24 D, orange line).

To verify the successful genetic inactivation of PIP5Kα and PIP5Kγ in the generated knockout clones and to investigate a possibly undesired upregulation of PIP5Kβ expression, western blot analyses were conducted for each of the PIP5K family members (Figure 4.25).

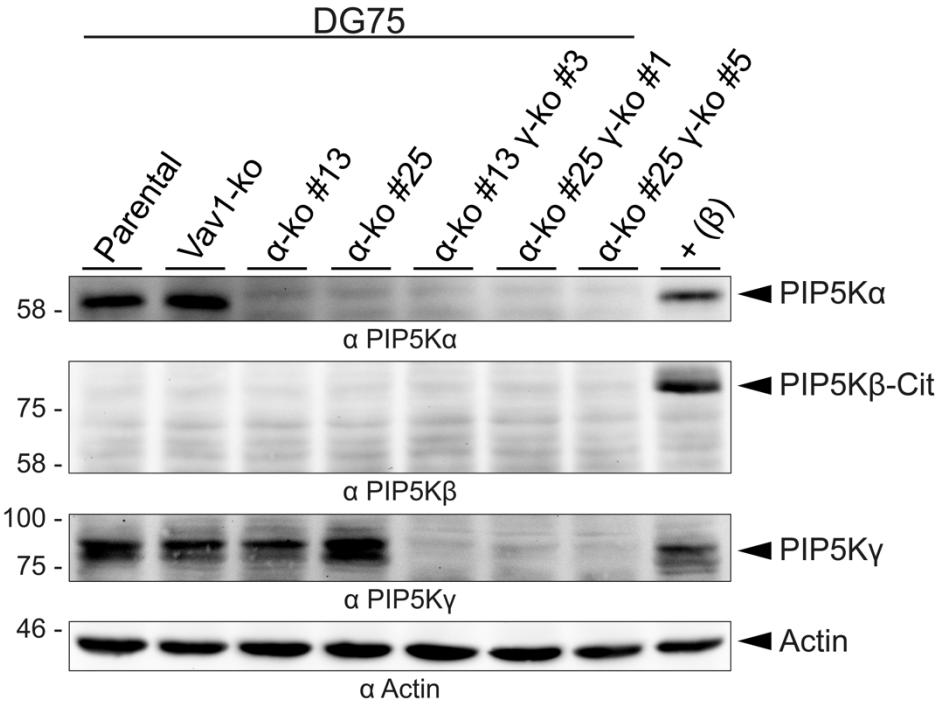

Figure 4.25 PIP5Kα and PIP5Kγ double-deficient DG75 B cells do not express any member of the PIP5K family. Immunoblot analysis of cleared cellular lysates of parental DG75 B cells or DG75 B cells deficient for either Vav1, PIP5Kα (α-ko) or PIP5Kα and PIP5Kγ (γ-ko). Proteins were separated by SDS-PAGE and analyzed by western blot using antibodies specific for PIP5Kα, PIP5Kβ, PIP5Kγ and Actin. The molecular weight of marker proteins is indicated on the left in kDa. As a positive control for antibodies to PIP5Kβ (+ (β)), lysates from Vav1-deficient DG75 B cells with induced expression of Citrine-tagged PIP5Kβ were used.

None of the three generated PIP5Kα and PIP5Kγ double-deficient DG75 B cell clones (Figure 4.25, lanes 5 to 7), either originating from PIP5Kα-deficient clone #13 (Figure 4.25, lane 3) or from clone #25 (Figure 4.25, lanes 4), expressed detectable amounts of PIP5K family members, thus most likely representing total PIP5K-negative cells.

4.4.4. Generation of DG75 cells deficient for all three members of the PIP5K family, PIP5Kα, PIP5Kβ and PIP5Kγ

The previously generated PIP5Kα and PIP5Kγ double-deficient DG75 B cells showed heterogeneous BCR-induced Ca^{2+}-profiles. Although induced expression of PIP5Kβ did not affect BCR-induced Ca^{2+}-mobilization in Vav1-deficient B cells (Figure 4.19), I generated DG75 B cells deficient for expression of all PIP5K family members, PIP5Kα, PIP5Kβ and PIP5Kγ, to exclude any effects that might be mediated by PIP5Kβ (even though this isoform was not detected in DG75 B cells by western blot analysis). The previously generated PIP5Kα and PIP5Kγ double-deficient cell clone #3, derived from PIP5Kα-deficient clone #13 ($PIP5K\alpha^{-/-}$#13 $PIP5K\gamma^{-/-}$#3), and clone #1 originating from PIP5Kα-deficient clone #25 ($PIP5K\alpha^{-/-}$#25 $PIP5K\gamma^{-/-}$#1) were used for these experiments. Since no endogenous expression of PIP5Kβ was detectable in neither of the tested cell lines by western blot analysis, I deleted the whole exon 5 of *PIP5K1B*. Deletion of the whole exon allows screening for knockout cells via PCR due to a predictable shift of the amplified amplicon and further promotes an early frame shift followed

by a premature stop codon. Hence, two sgRNAs were designed, one which guides Cas9 to the intronic downstream region and another one that guides Cas9 to the intronic upstream region of exon 5 in the *PIP5K1B* locus.

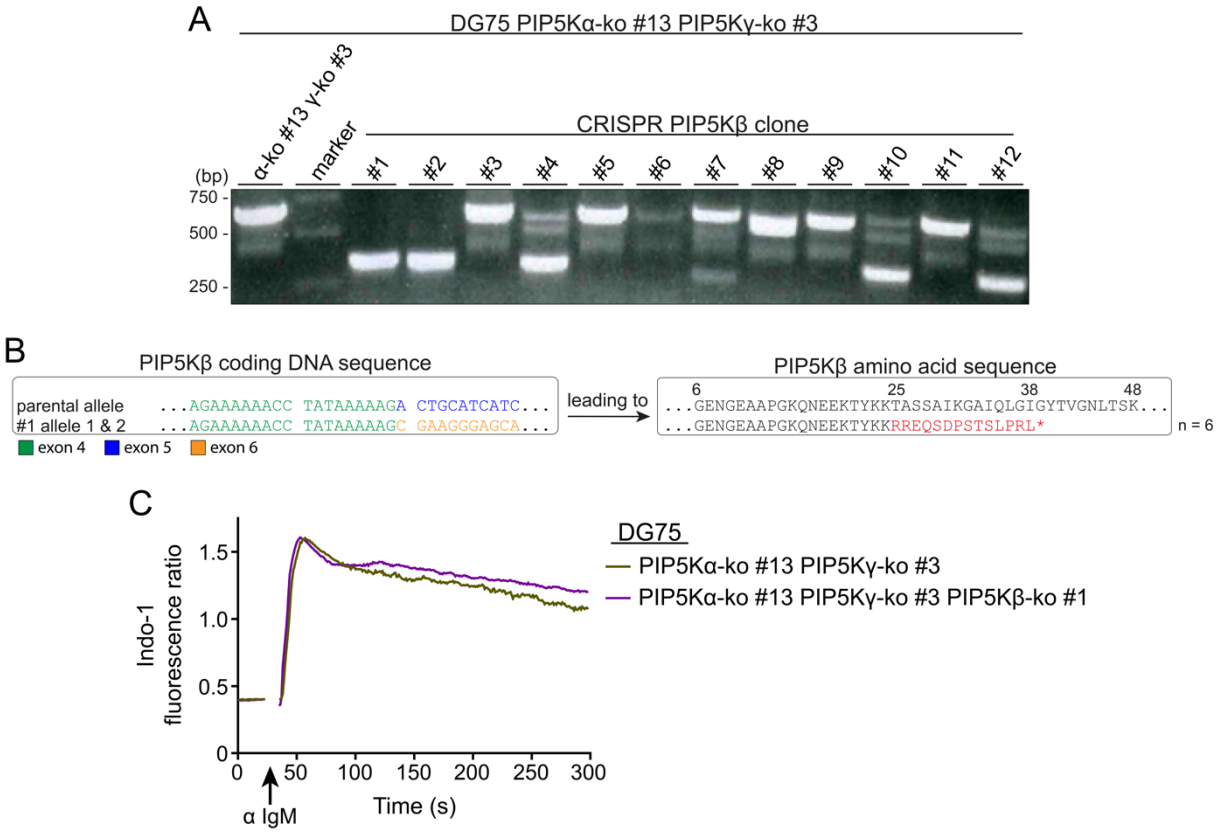

Figure 4.26 Successful generation of DG75 B cells deficient for all members of the PIP5K family derived from PIP5Kα-deficient cell clone #13. (A) PCR-based screening of DG75 sub-clones transfected with sgRNAs to delete exon 5 of *PIP5K1B*. The amplicon was amplified by PCR, the resulting DNA was separated by agarose gel electrophoresis and DNA was visualized using ethidium bromide. The size of marker DNA is indicated on the left. (B) Sequencing data of exon 5 of *PIP5K1B* for clone #1. The amplicon was amplified by PCR, the resulting DNA was separated in an agarose gel and extracted from the gel. The DNA was cloned into the pCR2.1 plasmid and the insert was sequenced. Base pairs of exon 4 are displayed in green, those of exon 5 in blue and those of exon 6 in orange. Differences to the wild-type protein sequence are highlighted in red. (C) Analysis of intracellular BCR-induced Ca^{2+}-mobilization for DG75 B cells lacking the expression of PIP5K family members. Cells were loaded with the Ca^{2+}-sensitive fluorophore Indo-1 AM. After recording of basal Ca^{2+}-levels for 25 sec, cells were stimulated with 20 µg/ml of anti-human-IgM F(ab')$_2$ fragments (α IgM) and the fluorescence was monitored for a total time of 5 min.

The predicted size of the amplicon surrounding exon 5 of *PIP5K1B* was approx. 660 base pairs (Figure 4.26 A, lane 1). When exon 5 was successfully deleted, the size of the amplicon was predicted to decrease about 360 base pairs. For clones #1 and #2 (Figure 4.26 A, lanes 3 and 4), this expected shift in the size of the amplicon was observed. Clones #4, #10 and #12 (Figure 4.26 A, lanes 6, 12 and 14) showed a prominent band at the size of 360 base pairs, but also weaker bands corresponding to 660 base pairs. Further characterization of the resulting clone #1 (PIP5K$\alpha^{-/-}$#13 PIP5K$\gamma^{-/-}$#3 PIP5K$\beta^{-/-}$#1) revealed that the deletion of exon 5 in *PIP5K1B* was successful (Figure 4.26 B). However, no differences in the ability to mobilize Ca^{2+} upon stimulation of the BCR were found compared to double-deficient PIP5Kα and PIP5Kγ deficient cells from which this clone originated (Figure 4.26 C, purple and olive lines).

Next, the same procedure was used to generate and characterize triple-deficient DG75 B cells for all members of the PIP5Ks originating from DG75 PIP5Kα$^{-/-}$#25 PIP5Kγ$^{-/-}$#1 (Figure 4.27).

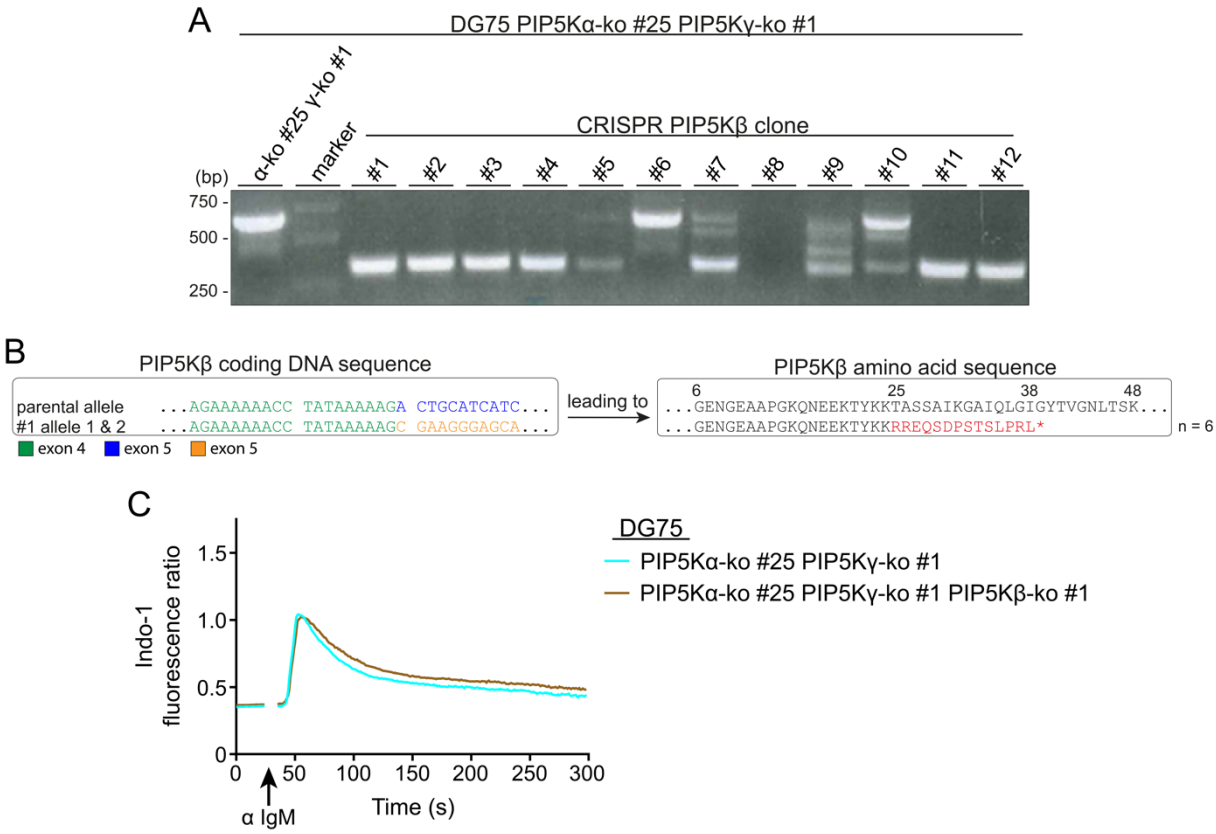

Figure 4.27 Successful generation of DG75 B cells deficient for all members of the PIP5K family derived from PIP5Kα-deficient cell clone #25. (A) PCR-based screening of DG75 sub-clones transfected with sgRNAs to delete exon 5 of *PIP5K1B*. The amplicon was amplified by PCR, the resulting DNA was separated by agarose gel electrophoresis and DNA was visualized using ethidium bromide. The size of marker DNA is indicated on the left. (B) Sequencing data of exon 5 of *PIP5K1B* for clone #1. The amplicon was amplified by PCR, the resulting DNA was separated in an agarose gel and extracted from the gel. The DNA was cloned into the pCR2.1 plasmid and the insert was sequenced. Base pairs of exon 4 are displayed in green, those of exon 5 in blue and those of exon 6 in orange. Differences to the wild-type protein sequence are highlighted in red. (D) Analysis of intracellular BCR-induced Ca^{2+}-mobilization for DG75 B cells lacking the expression of PIP5K family members. Cells were loaded with the Ca^{2+}-sensitive fluorophore Indo-1 AM. After recording of basal Ca^{2+}-levels for 25 sec, cells were stimulated with 20 µg/ml of anti-human-IgM F(ab')$_2$ fragments (α IgM) and the fluorescence was monitored for a total time of 5 min.

Deletion of exon 5 within *PIP5K1B* was proven by PCR in clones #1 to #4, #11 and #12 (Figure 4.27 A, lanes 3 to 6, 13 and 14). Sequencing of clone #1 (PIP5Kα$^{-/-}$#25 PIP5Kγ$^{-/-}$#1 PIP5Kβ$^{-/-}$ #1) additionally confirmed that the deletion had indeed occurred in this clone (Figure 4.27 B). BCR-induced Ca^{2+}-mobilization (Figure 4.27 C, brown line) however seemed not to be different compared to DG75 PIP5Kα$^{-/-}$#25 PIP5Kγ$^{-/-}$#1 double-deficient cells (Figure 4.27 C, turquoise line).

Finally, I analyzed expression levels of the PIP5K family members of the previously generated and genetically characterized PIP5Ks-deficient sub-clones on protein level by western blot analysis.

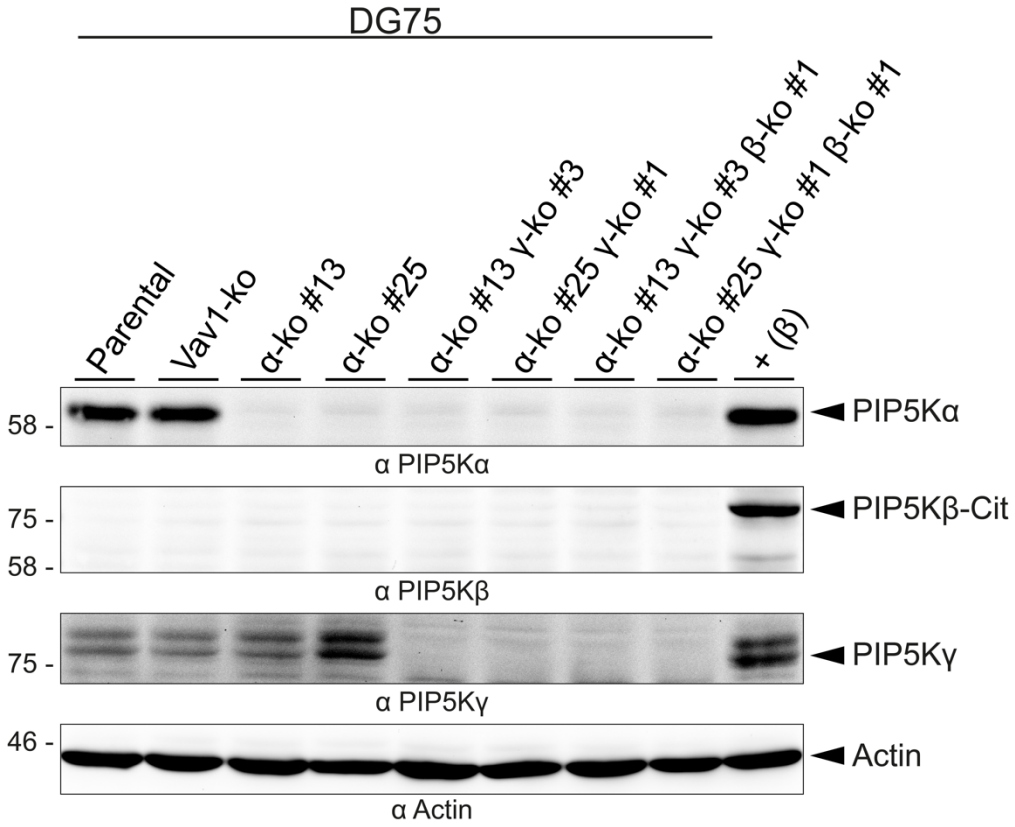

Figure 4.28 No detection of PIP5K family members in triple-deficient DG75 B cells. Immunoblot analysis of cleared cellular lysates of parental DG75 B cells or DG75 B cells deficient for either Vav1, PIP5Kα (α-ko), PIP5Kα and PIP5Kγ (γ-ko) or PIP5Kα, PIP5Kγ and PIP5Kβ (β-ko). Proteins were separated by SDS-PAGE and analyzed by western blot using antibodies specific for PIP5Kα, PIP5Kβ, PIP5Kγ and Actin. The molecular weight of marker proteins is indicated on the left in kDa. As a positive control for antibodies to PIP5Kβ (+ (β)), lysates from Vav1-deficient DG75 B cells with induced expression of Citrine-tagged PIP5Kβ were used.

Western Blot analysis (Figure 4.28) showed that PIP5Kα was only expressed by parental DG75 B cells and Vav1-deficient DG75 B cells (upper panel, lanes 1 and 2). PIP5Kβ was not expressed in neither of the tested cell clones (second panel from the top). PIP5Kγ was expressed at low levels in parental DG75 B cells as well as Vav1-deficient DG75 B cells and in PIP5Kα-deficient DG75 B cell clone #13 (third panel, lanes 1 to 3). PIP5Kγ appeared to be stronger in DG75 PIP5Kα$^{-/-}$#25 (third panel, lane 4). All other tested cell clones did not express PIP5Kγ.

In summary, this chapter showed that expression of either PIP5Kα or PIP5Kγ enhances BCR-induced Ca^{2+}-mobilization in Vav1-deficient DG75 B cells after prolonged times of stimulation. Moreover, genetically determined DG75 single cell clones deficient for all three known members of the PIP5K family were successfully generated. Although the resulting triple knockout cell clones were not able to express functional PIP5K enzymes, they exhibited inconsistent BCR-induced Ca^{2+}-phenotypes. However, these experiments indicated that expression of PIP5Ks in DG75 B cells is dispensable for BCR-induced signaling.

4.5. Vav family members constitute branching points for distinct BCR signaling pathways

Considering that Vav family members supported BCR-induced Ca^{2+}-mobilization to different extents, the question arose whether other signaling axes of the BCR signaling cascade (Figure 2.2) are affected by the loss of Vav1 and whether they are also differentially regulated by distinct Vav family members.

Previous reports showed that Vav family members are involved in the activation of MAPK like JNK, p38 and Erk by activating upstream MEKs through their GEF-mediated activation of Rho GTPases[66,99]. Furthermore, various groups published a connection between Vav and cytoskeletal rearrangement, a process essentially depending on small G proteins of the Rho family[75,97,139]. Finally, correlations between Vav3 and the activation of the PI3K/Akt pathway are reported in a chicken B cell line[140].

4.5.1. BCR-induced actin remodeling is controlled by Vav family members

The actin cytoskeleton plays a crucial role in BCR signaling. In the resting B cell, the BCR is anchored through interactions between Igβ and the cytoskeleton, limiting diffusion of the BCR. Upon stimulation of the BCR, actin remodeling is induced and mobility of the BCR is enhanced. Hence, the cytoskeletal organization is important for the resting as well as for the activated state of B cells[75,97,139,141,142].

To analyze BCR-induced actin remodeling, I used fluorescently labeled Phalloidin that binds filamentary actin (F-actin) but not globular actin (G-actin). Thus, fluorescence signal intensities correlate to the amount of filamentary actin in the analyzed cells (for detailed procedure see section 3.2.3.3.4.).

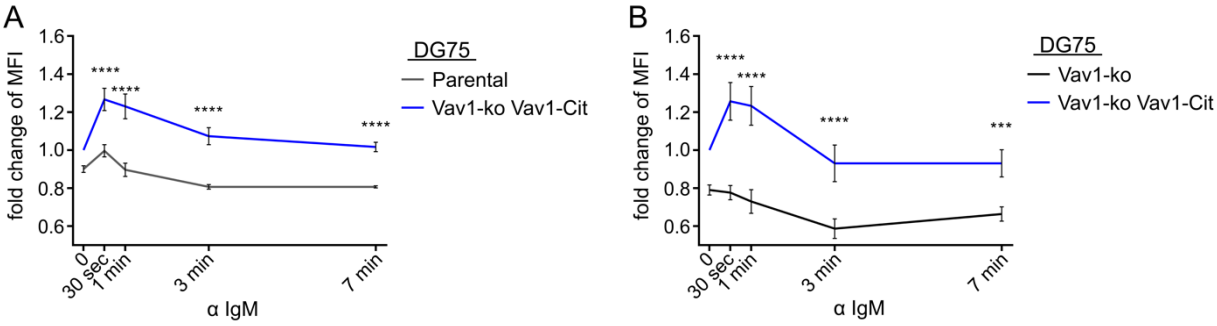

Figure 4.29 BCR-induced actin remodeling is controlled by Vav1. (A and B) Kinetics of F-actin formation in BCR-stimulated DG75 B cells, Vav1-deficient DG75 B cells and Vav1-deficient B cells reconstituted with Citrine-tagged wild-type Vav1. 20 min before stimulation, the cells were mixed in a 1:1 ratio before resting. Then, the cells were either left untreated or stimulated for 30 sec, 1 min, 3 min or 7 min with 20 µg/ml of anti-human-IgM $F(ab')_2$ fragments (α IgM). Subsequently, the cells were fixed, permeabilized and stained with Phalloidin-AlexaFluor 647. The MFI were determined by flow cytometry and the MFI of unstimulated Vav1-deficient DG75 B cells expressing Vav1-Cit was set to 1. All other MFI were normalized to this reference value. Error bars indicate standard deviation of three independently performed experiments. Significances were calculated using two-way ANOVA followed by Sidak's multiple comparison test. ****: p<0.0001, ***: p<0.001.

Both cell lines, parental DG75 cells and Vav1-deficient DG75 B cells, are negative for fluorescence detected by flow cytometry in the FITC channel. Thus, a direct comparison in the same tube of one experiment between these two cell lines is not possible. To compare both FITC-negative cell lines, Vav1-deficient DG75 B cells expressing Vav1-Cit, that are thus FITC-positive, were used as reference cells. Hence, parental DG75 B cells and Vav1-deficient DG75 B cells were mixed individually with Vav1-deficient DG75 B cells reconstituted with Vav1-Cit for this set of experiments. For analysis, all values in the following experiment were normalized to the MFI value of unstimulated DG75 Vav1-ko Vav1-Cit cells (Figure 4.29). Vav1-deficient cells reconstituted with Vav1-Cit induced actin remodeling upon stimulation of the BCR (Figure 4.29, blue lines). The highest amount of BCR-induced filamentary actin was measured 30 sec after stimulation with approx. 1.3-fold of the amount detected in unstimulated cells. The amount of filamentary actin decreased with the time of stimulation reaching the basal level 3 to 7 min after stimulation. However, parental DG75 B cells were capable of actin remodeling after stimulation of the BCR in a similar pattern as the reference cells, but to a lower extent (Figure 4.29 A, grey line). Strikingly, loss of Vav1 in DG75 B cells (Figure 4.29 B, black line) fully abolished the ability of actin remodeling in BCR-stimulated cells.

Having shown that the ability for BCR-induced actin remodeling is controlled by the presence of Vav1 in DG75 cells, the question arose whether this significant drop was due to the loss of GEF-activity mediated by Vav1.

4.5.2. Loss of GEF-activity in Vav1 and Vav3 diminishes BCR-induced actin remodeling and internalization of the BCR

Considering that BCR-induced actin remodeling was dependent on expression of Vav1 (Figure 4.29), I examined the involvement of the GEF-activity of Vav proteins in this process. For this purpose, wild-type Vav1, mVav1 and Vav3 as well as their respective mutants lacking GEF-activity were tested. Those mutant variants were Vav1 E201A, mVav1 LK334/335AA, Vav1Syk$(SH2)_2$ N371A and Vav3 E199A. For analysis of the following experiments, the MFI value of unstimulated DG75 cells lacking the expression of Vav1 was set to 1 and all other MFI values were normalized to that reference value (Figure 4.30).

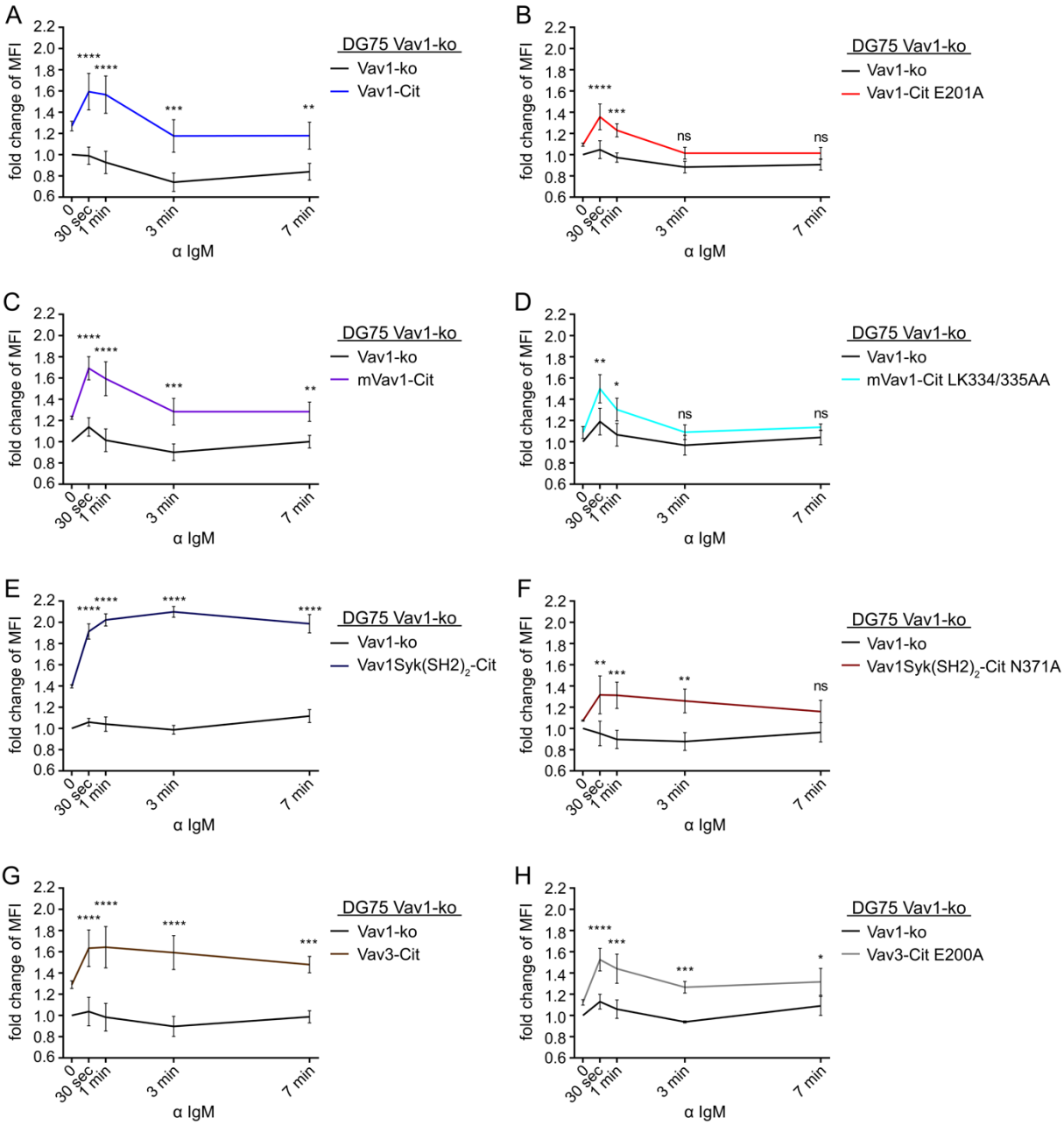

Figure 4.30 Loss of GEF-activity of Vav family members reduces the BCR-induced actin remodeling. (A to H) Kinetics of F-actin formation in BCR-stimulated Vav1-deficient DG75 B cells and Vav1-deficient B cells reconstituted with Citrine-tagged wild-type Vav1, mVav1, Vav1Syk(SH2)$_2$ or Vav3 and their respective mutants without GEF-activity towards Rac1, RhoA and Cdc42. 20 min before stimulation, the cells were mixed in a 1:1 ratio before resting. Then, the cells were either left untreated or stimulated for 30 sec, 1 min, 3 min or 7 min with 20 µg/ml of anti-human-IgM F(ab')$_2$ fragments (α IgM). Subsequently, the cells were fixed, permeabilized and stained with Phalloidin-AlexaFluor 647. The MFI were determined by flow cytometry and the MFI of unstimulated Vav1-deficient DG75 B cells was set to 1. All other MFI were normalized to this reference value. Error bars indicate standard deviation of three independently performed experiments. Significances were calculated using two-way ANOVA followed by Sidak's multiple comparison test. ****: p<0.0001, ***: p<0.001, **: p<0.01, *: p<0.05, ns: not significant.

All tested Vav family members were able to compensate for the loss of Vav1 in DG75 B cells, even though to different extents. Vav1-deficient DG75 B cells expressing wild-type (Figure 4.30 A, blue line) and mVav1 (Figure 4.30 C, purple line) were equally capable to mediate BCR-induced actin remodeling. Cells expressing either Vav1Syk(SH2)$_2$ (Figure 4.30 E, dark blue line) or wild-type Vav3 (Figure 4.30 G, brown line) showed an increased and prolonged actin remodeling phenotype. Remarkably, all Vav1-deficient DG75 B cells expressing GEF-

inactive Vav variants were significantly impaired to mediate actin remodeling upon stimulation of the BCR compared to their wild-type counterparts (Figure 4.30 B, D, F and H).

Internalization of the BCR upon stimulation is reportedly one consequence of actin remodeling and was thus monitored to determine any influence of Vav1 and its GEF-activity (for exact procedure see section 3.2.3.3.5.)[98,143].

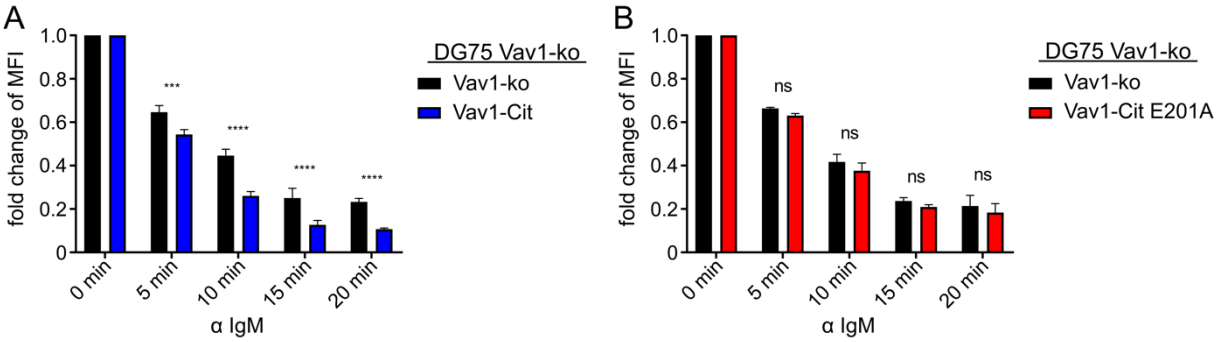

Figure 4.31 Loss of GEF-activity in Vav1 attenuates BCR-induced receptor internalization. (A and B) Kinetics of receptor internalization in BCR-stimulated Vav1-deficient DG75 B cells and Vav1-deficient B cells reconstituted with Citrine-tagged wild-type Vav1 or Vav1 E201A. 20 min before stimulation, the cells were mixed in a 1:1 ratio before resting. Then, the cells were either left untreated or stimulated for 30 sec, 1 min, 3 min or 7 min with 20 µg/ml of anti-human-IgM F(ab')$_2$ fragments (α IgM). Subsequently, the cells were fixed and stained with AlexaFluor 647-coupled antibodies to the κ light chain of the BCR. The MFI were determined by flow cytometry and the MFI of each unstimulated cell line was set to 1. All other MFI were normalized to the respective reference values. Error bars indicate standard deviation of three independently performed experiments. Significances were calculated using two-way ANOVA followed by Sidak's multiple comparison test. ****: p<0.0001, ***: p<0.001, ns: not significant.

All three tested cell lines internalized the BCR in a stimulation time-depend manner. Vav1-deficient DG75 B cells internalized up to 70% of their receptors on their surface within the first 20 min of BCR stimulation (Figure 4.31, black bars), whereas those cells reconstituted with wild-type Vav1 internalized up to 90% of their receptors on the cell surface. (Figure 4.31 A, blue bars). Notably, this significant difference in the ability of BCR-induced receptor internalization was not detected for Vav1-deficient DG75 B cells in comparison with Vav1-deficient DG75 B cells expressing Vav1 E201A (Figure 4.31 B, red bars).

These experiments suggested that the presence of Vav1 or Vav3 is critical for BCR-induced actin remodeling. Moreover, loss of GEF-activity in these isoform led to significantly attenuated actin remodeling phenotypes. Consequently, internalization of the BCR after stimulation is also diminished with the loss of GEF-activity, at least for Vav1.

4.5.3. Vav2 mediates BCR-induced actin remodeling

Wild-type Vav2 was not able to compensate for the loss of Vav1 in DG75 B cells regarding BCR-induced Ca^{2+}-mobilization (Figure 4.1). Thus, the question whether Vav2 was able to mediate BCR-induced actin remodeling was addressed. I conducted these experiments with Vav1-deficient DG75 B cells reconstituted with either wild-type Vav2, Vav2 without acidic region or the construct of Vav2 containing tyrosine to aspartate amino acid substitutions within

the acidic region, from which the last two supported BCR-induced Ca^{2+}-mobilization in Vav1-deficient DG75 B cells (Figure 4.32).

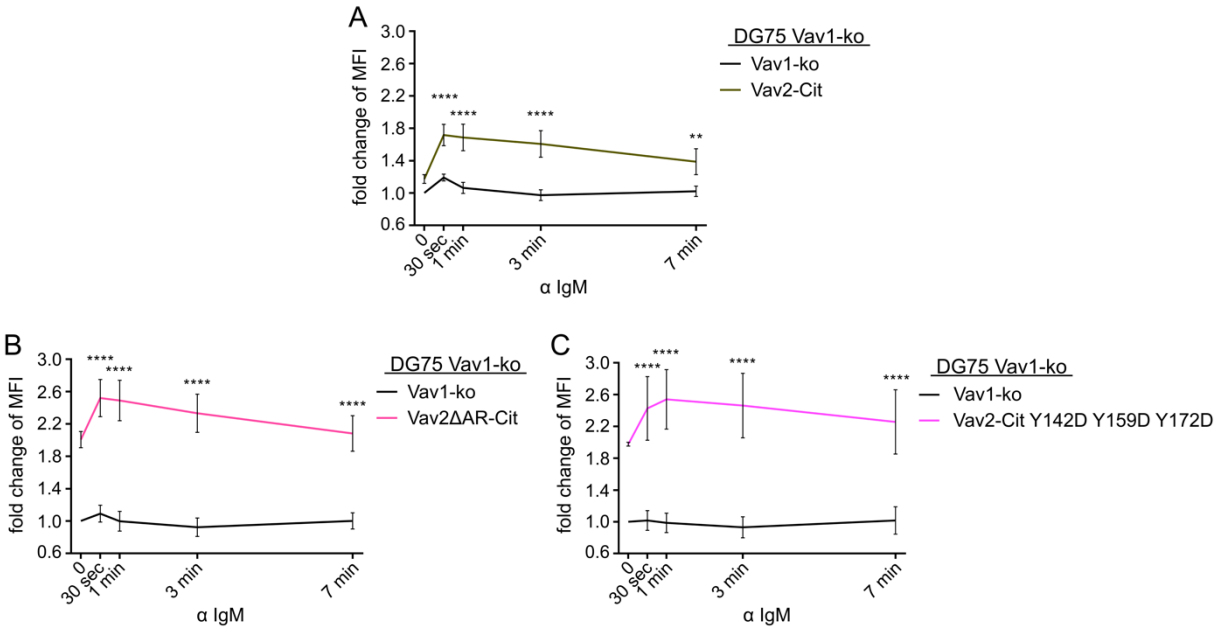

Figure 4.32 Vav2 supports the BCR-induced actin remodeling. (A to C) Kinetics of F-actin formation in BCR-stimulated DG75 B cells, Vav1-deficient DG75 B cells and Vav1-deficient B cells reconstituted with Citrine-tagged wild-type Vav2, Vav2ΔAR or Vav2 Y142D Y159D Y172D. 20 min before stimulation, the cells were mixed in a 1:1 ratio before resting. Then, the cells were either left untreated or stimulated for 30 sec, 1 min, 3 min or 7 min with 20 µg/ml of anti-human-IgM F(ab')$_2$ fragments (α IgM). Subsequently, the cells were fixed, permeabilized and stained with Phalloidin-AlexaFluor 647. The MFI were determined by flow cytometry and the MFI of unstimulated Vav1-deficient DG75 B cells was set to 1. All other MFI were normalized to this reference value. Error bars indicate standard deviation of three independently performed experiments. Significances were calculated using two-way ANOVA followed by Sidak's multiple comparison test. ****: $p<0.0001$, **: $p<0.01$.

Surprisingly, wild-type Vav2 was fully capable of inducing actin remodeling upon stimulation of the BCR (Figure 4.32 A, olive-green line) to an extent comparable to Vav1 and Vav3 (Figure 4.30 A, C and G). This ability of mediating BCR-induced actin remodeling was further increased by deletion of the acidic region (Figure 4.32 B, pink line) or imitation of the phosphorylated state for the acidic region of Vav2 (Figure 4.32 C, magenta line), even though these proteins were expressed less efficiently (Figure 4.15 B and Figure 4.16 B). Furthermore, compared to Vav1-deficient DG75 B cells, a 1.9-fold increase in the amount of filamentary actin was already present in unstimulated cells. This amount of filamentary actin was further increased by BCR activation and was approx. 2.5-fold higher at its maximum compared to the unstimulated Vav1-deficient reference cells.

In summary, the previous experiments demonstrated that in DG75 B cells the presence of Vav family members is required for BCR-induced actin remodeling and at least Vav1 for optimal BCR-induced receptor internalization.

4.5.4. Vav1 contributes to BCR-induced activation of MAPK like p38 and Erk

Vav family members reportedly play a role in the activation of MAPK like p38, JNK and Erk[72]. To test whether Vav family members are involved in the activation of Erk, intracellular staining of phosphorylated Erk with a fluorescently labeled phospho-specific antibody was used. Moreover, western blot analysis was used to verify the results acquired by flow cytometry and additionally to analyze BCR-induced activation of p38 (Figure 4.33 and Figure 4.34).

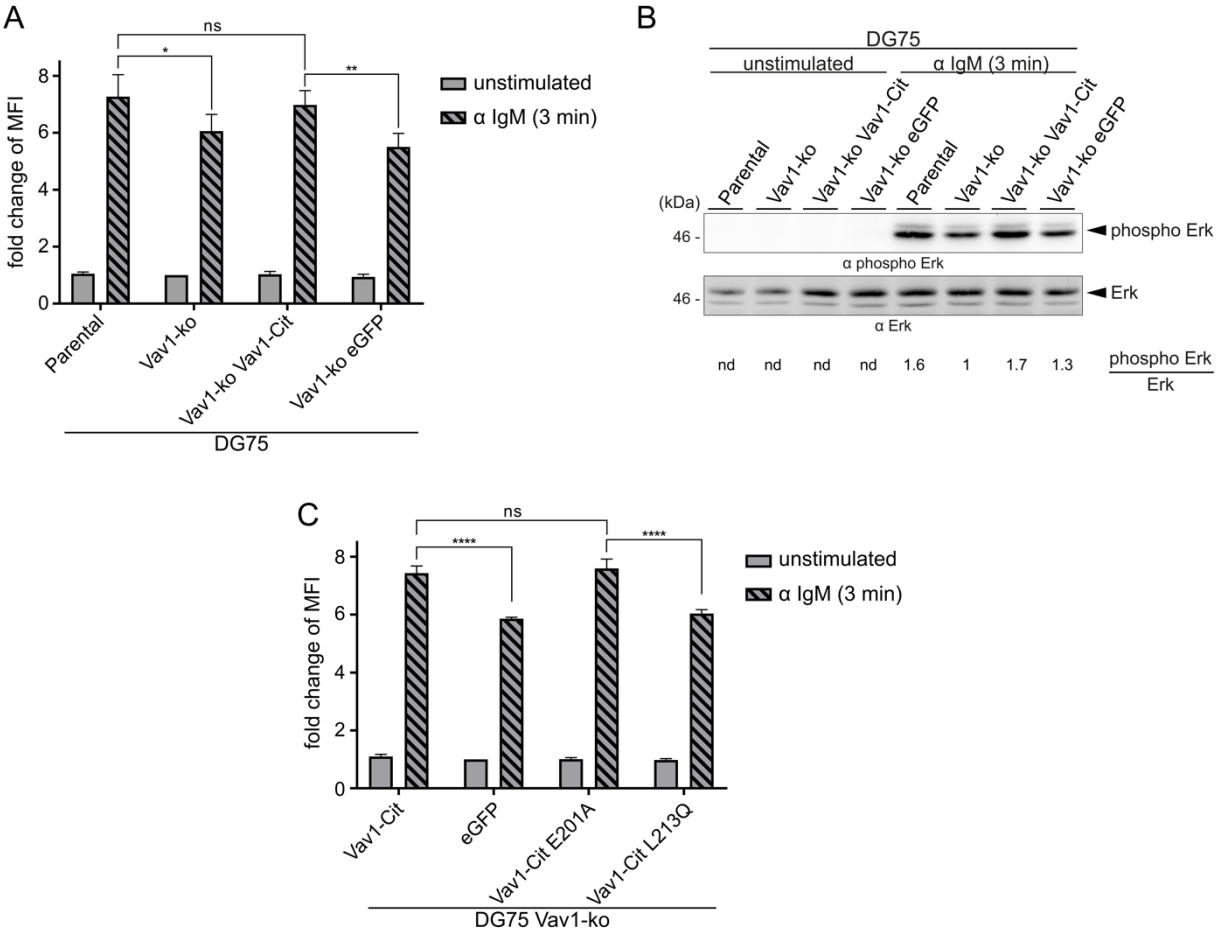

Figure 4.33 Vav1 contributes to the BCR-induced phosphorylation of Erk. (A to C) Analysis of Erk1/2 phosphorylation on positions 202 (threonine) and 204 (tyrosine) in DG75 B cells, Vav1-deficient DG75 B cells and Vav1-deficient DG75 B cells expressing either Vav1-Cit, Vav1-Cit E201A, Vav1-Cit L213Q or eGFP. The cells were either left untreated or stimulated for 3 min with 20 µg/ml of anti-human-IgM F(ab')$_2$ fragments (α IgM). (A and C) Subsequently, the cells were fixed, permeabilized and stained with pErk-AlexaFluor 647. The MFI were determined by flow cytometry and the MFI of unstimulated Vav1-deficient DG75 B cells (A) or of Vav1-deficient DG75 B cells expressing eGFP (C) were set to 1. All other MFI were normalized to the respective reference value. Error bars indicate standard deviation of three independently performed experiments. Significances were calculated using two-way ANOVA followed by Tukey's multiple comparison test. ****: $p<0.0001$, **: $p<0.01$, *: $p<0.05$, ns: not significant. (B) Immunoblot analysis of cleared cellular lysates of unstimulated or stimulated (α IgM) cells used in (A). Proteins were separated by SDS-PAGE and analyzed by western blot using antibodies specific for phospho Erk and Erk. The molecular weight of marker proteins is indicated on the left in kDa. Band intensities were determined with the LabImage 1D software (Intas). The signal intensity ratio for phospho Erk divided by Erk of stimulated Vav1-deficient B cells was set to 1.

Statistically significant differences were measured between BCR-stimulated Vav1-proficient and -deficient DG75 B cells (Figure 4.33). The latter cells were reduced in their ability to activate Erk upon stimulation of the BCR (Figure 4.33 A). Western Blot analysis of the same

cells using antibodies against phosphorylated Erk verified the data acquired by flow cytometry (Figure 4.33 B). Vav1-deficient DG75 B cells expressing Vav1-Cit E201A showed similar BCR-induced phosphorylation of Erk to Vav1-deficient cells expressing wild-type Citrine-tagged Vav1. Additionally, those cells that were reconstituted with Vav1-Cit L213Q barely showed a BCR-induced increase in the phosphorylation of Erk compared to cells expressing eGFP (Figure 4.33 C). Since the L213Q variant of Vav1 was expressed ten-fold less efficiently compared to the E201A variant or the wild-type isoform of Vav1 (Figure 4.3), activation of Erk seemed to be dependent on Vav1 expression rather than on its GEF-activity. Next, I examined the BCR-induced phosphorylation of p38 (Figure 4.34)

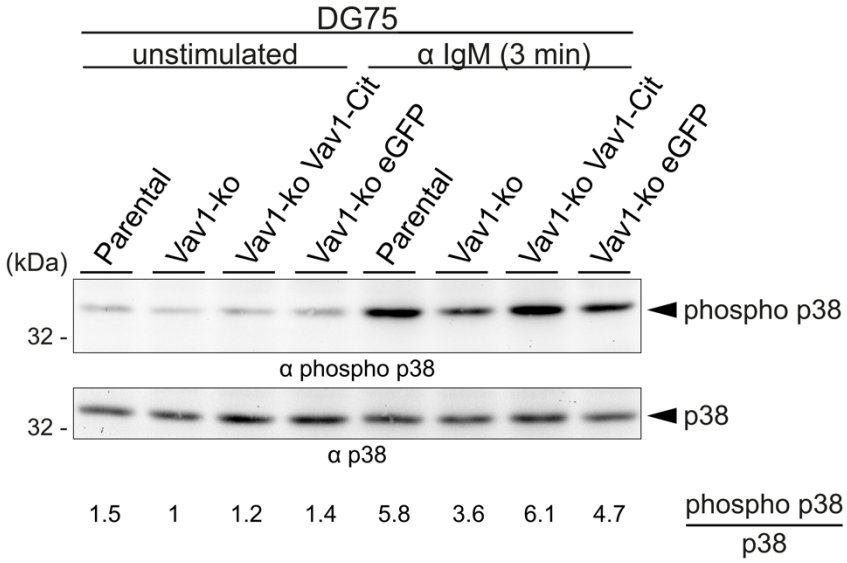

Figure 4.34 Vav1 enhances BCR-induced phosphorylation of p38. Immunoblot analysis of cleared cellular lysates of unstimulated or stimulated (α IgM) DG75 B cells, Vav1-deficient DG75 B cells and Vav1-deficient B cells expressing either Vav1-Cit or eGFP. Proteins were separated by SDS-PAGE and analyzed by western blot using antibodies specific for phospho p38 and p38. The molecular weight of marker proteins is indicated on the left in kDa. Band intensities were determined with the LabImage 1D software (Intas). The signal intensity ratio for phospho p38 divided by p38 of unstimulated Vav1-deficient B cells was set to 1.

The amount of basally phosphorylated p38 was detectable for unstimulated cells (Figure 4.34, lanes 1 to 4). A ratio between phosphorylated p38 and p38 was calculated and was set to 1 for Vav1-deficient DG75 B cells (Figure 4.34, lane 2). In comparison, BCR-stimulated DG75 and Vav1-deficient cells reconstituted with Vav1-Cit exhibited a 5.8- and 6.1-fold increase in phosphorylation of p38 (Figure 4.34, lanes 5 and 7). In contrast, for cells that were deficient for expression of Vav1 expression, the relative change of phosphorylated p38 was lower (3.6-fold for Vav1-deficient DG75 B cells and 4.7-fold for Vav1-deficient DG75 B cells expressing eGFP, Figure 4.34, lane 6 and 8).

These data implied that the activation of the MAPK Erk and p38 is supported by the presence of Vav1. While activation of Erk seemed not to be dependent on the catalytic GEF-activity of Vav1, the involvement of the enzymatic activation of Rho GTPases by Vav1 remains to be elucidated for the phosphorylation of p38.

4.5.5. Vav family members enhance BCR-induced activation of Akt

Results from a previous study using the chicken B cell line DT40 implicated that Vav3 regulates PI3K activity, however, Vav proteins seem to be dispensable in that context in primary murine B cells[140,144]. To shed light on the question, whether BCR-induced activation of Akt depends on Vav family members, I checked the phosphorylation of the serine/threonine kinase Akt on serine 473 using our established cellular model system.

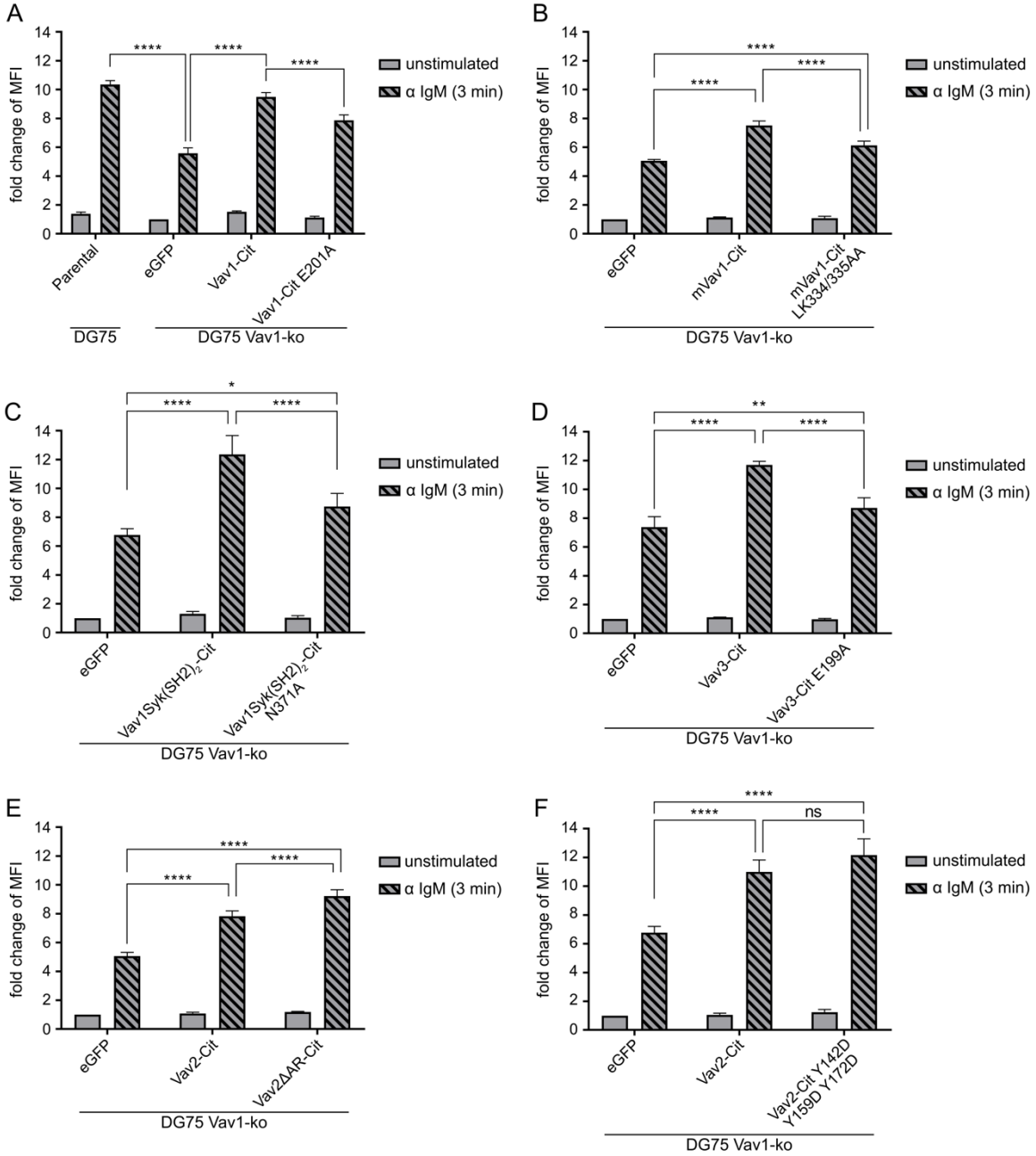

Figure 4.35 Vav family members enhance the BCR-induced phosphorylation of Akt. (A to F) Analysis of Akt phosphorylation on position 473 (serine) in DG75 B cells and Vav1-deficient DG75 B cells expressing different Vav family members and their variants. The cells were either left untreated or stimulated for 3 min with 20 µg/ml of anti-human-IgM F(ab')$_2$ fragments (α IgM). Subsequently, the cells were fixed, permeabilized and stained with pAkt-AlexaFluor 647. The MFI were determined by flow cytometry and the MFI of unstimulated Vav1-deficient DG75 B cells expressing eGFP was set to 1. All other MFI were normalized to this reference value. Error bars indicate standard deviation of three independently performed experiments. Significances were calculated using two-way ANOVA followed by Tukey's multiple comparison test. ****: p<0.0001, **: p<0.01, *: p<0.05, ns: not significant.

Indeed, the BCR-induced phosphorylation of Akt was enhanced in cells that expressed Vav1 (Figure 4.35 A). The relative BCR-induced phosphorylation of Akt in parental DG75 B cells or in Vav1-deficient DG75 B cells expressing wild-type Vav1-Cit was approx. ten-fold higher compared to unstimulated Vav1-deficient DG75 B cells expressing eGFP. As already seen for BCR-induced actin remodeling (Figure 4.30 and Figure 4.32), also wild-type Vav2 (Figure 4.35 E and F) and Vav3 (Figure 4.35 D) as well as mVav1 (Figure 4.35 B) were able to compensate for the loss of Vav1 in DG75 B cells regarding BCR-induced activation of Akt, even though to different extents. Strikingly, reduced BCR-induced Akt phosphorylation was detected in Vav1-deficient DG75 B cells expressing variants of Vav which lacked GEF-activity compared to their respective wild-type counterpart (Figure 4.35 A to D). Furthermore, in cells expressing Vav2 variants with elevated Ca^{2+}-mobilization profiles (Figure 4.15 and Figure 4.16) and enhanced actin remodeling kinetics (Figure 4.32), phosphorylation of Akt was enhanced as well (Figure 4.35 E and F). These experiments indicated that the BCR-induced activation is enhanced by the presence of Vav isoforms. Furthermore, the loss of GEF-activity in Vav1, mVav1 and Vav3 led to diminished BCR-induced activation of Akt. Since the activation profiles of BCR-induced actin remodeling and activation of Akt for Vav family member strongly correlated, both processes are possibly regulated by the same mechanism.

4.5.6. Ca^{2+}-influx, actin remodeling and activation of Akt within the BCR signaling are independent from each other

So far, I demonstrated that activation of different axes within the BCR signaling cascade were either controlled or enhanced by the presence of Vav family members. BCR-induced actin remodeling and phosphorylation of Akt was supported by each isoform of the Vav proteins. However, by contrast, proper BCR-induced Ca^{2+}-mobilization required expression of either Vav1 or Vav3. These differences in the support of the signaling axes within BCR signaling raised the question, as to whether these signaling axes depend on each other.

To answer the question, whether BCR-induced Ca^{2+}-mobilization is dependent on actin remodeling as proposed by an earlier report, the actin polymerization inhibitor LatrunculinA (LatA) was used[141]. This inhibitor binds to monomeric G-actin, thereby preventing its polymerization to F-actin. It was reported that application of LatA per se induces Ca^{2+}-influx into the cytosol of primary B cells[142]. To determine the minimal effective concentration of LatA in DG75 B cells, I generated a dose response curve using the established actin polymerization assay. To this end, Vav1-expressing DG75 B cells were treated for 5 min before stimulation with different concentrations of the inhibitor LatA or DMSO as a vehicle control (Figure 4.36). Subsequently, the cells were stimulated for 30 sec as this had been determined as the optimal stimulation time for the highest effect in BCR-induced actin remodeling (Figure 4.30 A).

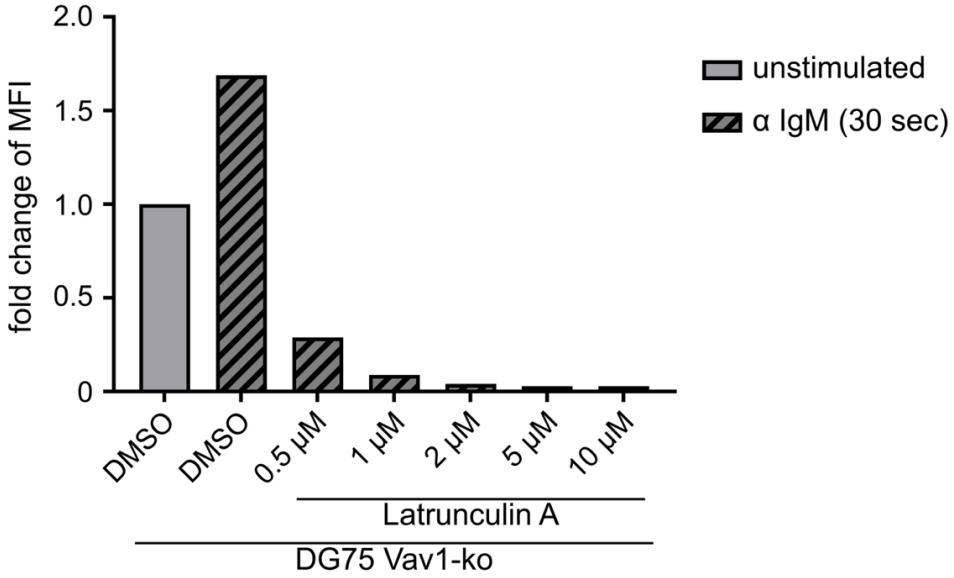

Figure 4.36 LatrunculinA inhibits the BCR-induced actin remodeling. Dose response curve of F-actin formation in BCR-stimulated Vav1-deficient DG75 B cells reconstituted with Vav1-Cit. Pre-incubation with either DMSO or the indicated concentrations of LatA for 5 min before stimulation. The cells were either left untreated or stimulated for 30 sec with 20 µg/ml of anti-human-IgM F(ab')$_2$ fragments (α IgM). Subsequently, the cells were fixed, permeabilized and stained with Phalloidin-AlexaFluor 647. The MFI were determined by flow cytometry and the MFI of unstimulated cells was set to 1. All other MFI were normalized to this reference value. N = 1 for this experiment.

LatA concentrations higher than 0.5 µM specifically impeded BCR-induced actin remodeling (Figure 4.36). The following experiments were hereafter conducted with LatA concentrations of 0.5 µM and 1 µM. The same concentrations have already been used in previous studies[141,142,145]. Pharmacological inhibition of actin polymerization with LatA was subsequently used to investigate the dependencies between BCR-induced Ca^{2+}-mobilization and actin remodeling. For this purpose, the change of intracellular Ca^{2+} was monitored for 5 min after addition of DMSO or LatA, followed by stimulation of the BCR (Figure 4.37).

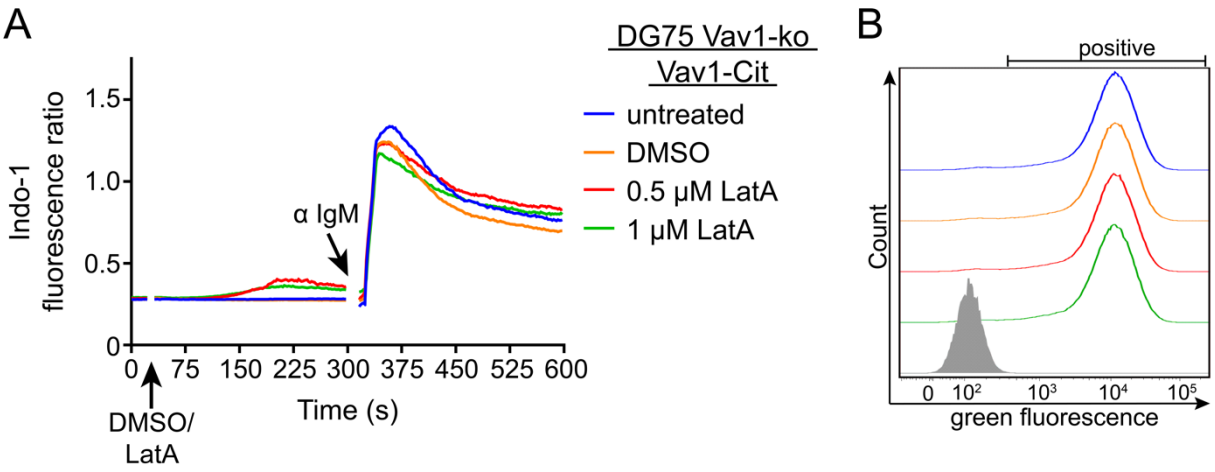

Figure 4.37 Application of LatrunculinA barely affects BCR-induced Ca^{2+}-mobilization. (A) Analysis of intracellular BCR-induced Ca^{2+}-mobilization for Vav1-deficient DG75 B cells expressing Vav1-Cit. Cells were loaded with the Ca^{2+}-sensitive fluorophore Indo-1 AM. After recording of basal Ca^{2+}-levels for 25 sec, cells were either left untreated or DMSO or LatA was added in the indicated concentrations. 270 sec later, cells were stimulated with 20 µg/ml of anti-human-IgM F(ab')$_2$ fragments (α IgM) and the fluorescence was monitored for a total time of 10 min. The graphs are representative for 1 of 3 independent experiments. (B) Green fluorescence of cells analyzed in (A). The grey filled peak represents cells negative for green fluorescence.

A minor influx of Ca^{2+} into the cytosol was detected upon addition of LatA in both concentrations. However, no substantial differences were observed for the IgM-dependent activation of the BCR and induction of Ca^{2+}-mobilization. Hence, treatment with LatA of Vav1-expressing DG75 B cells barely influenced BCR-induced Ca^{2+}-mobilization. The solvent DMSO did not have detectable effects on the experiment (Figure 4.37, blue and orange lines).

To gain further insights in processes that might depend on actin remodeling, I analyzed the potential of Vav1-proficient DG75 B cells to mediate BCR-induced phosphorylation of Akt in the presence of LatA. In detail, Vav1-deficient DG75 B cells reconstituted with Vav1-Cit were used and DMSO or LatA was added in the previously acquired concentrations 5 min before stimulation to the cells (Figure 4.38).

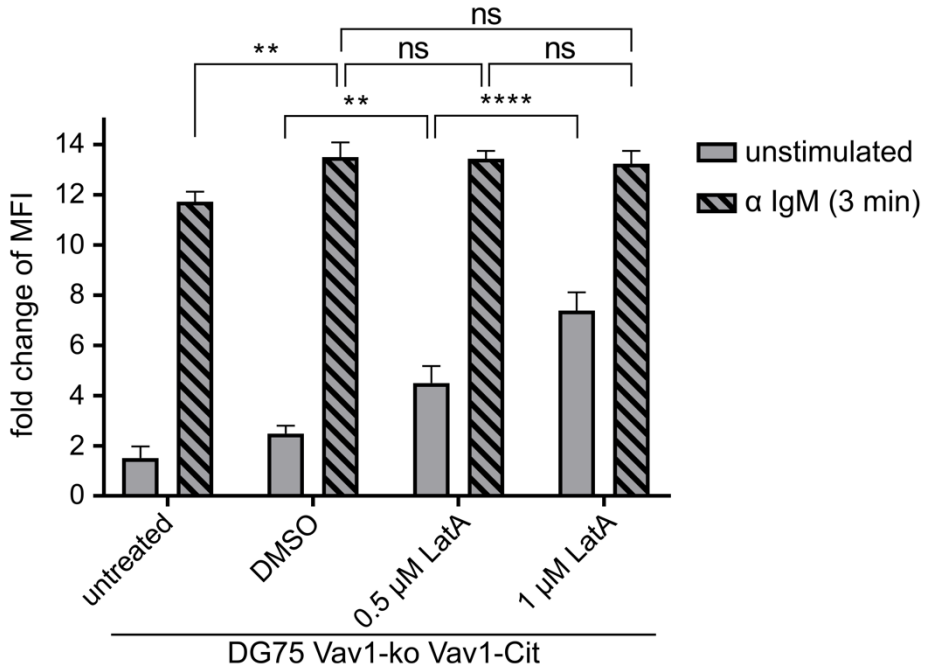

Figure 4.38 BCR-induced phosphorylation of Akt is not dependent on actin remodeling. Analysis of Akt phosphorylation on position 473 (serine) in Vav1-deficient DG75 B cells expressing Vav1-Cit. The cells were either left untreated, incubated for 5 min with DMSO or the indicated concentrations of LatA. Subsequently, the cells were either left untreated or stimulated for 3 min with 20 µg/ml of anti-human-IgM $F(ab')_2$ fragments (α IgM). Afterwards, the cells were fixed, permeabilized and stained with pAkt-AlexaFluor 647. The MFI were determined by flow cytometry and the MFI of unstimulated Vav1-deficient DG75 B cells was set to 1. All other MFI were normalized to this reference value. Error bars indicate standard deviation of three independently performed experiments. Significances were calculated using two-way ANOVA followed by Tukey's multiple comparison test. **: $p<0.01$, ns: not significant.

Unexpectedly, pre-incubation with DMSO led to an increased phosphorylation of Akt already in unstimulated DG75 B cells. Even though application of LatA in both concentrations did not affect BCR-induced phosphorylation of Akt, LatA significantly increased phosphorylation of Akt in unstimulated cells in a dose-dependent manner (Figure 4.38). Thus, for BCR-induced phosphorylation of Akt the ability to mediate actin remodeling is negligible, but inhibition of the actin cytoskeleton in resting DG75 B cells led to a strong and significant phosphorylation of Akt.

So far, the results of this chapter demonstrated that BCR-induced Ca^{2+}-mobilization was neither induced by nor dependent on actin remodeling (Figure 4.37). Vice versa, BCR-induced actin remodeling was independent from Ca^{2+}-mobilization since Vav1-deficient DG75 B cells expressing Vav2 were able to mediate actin remodeling but failed to support Ca^{2+}-mobilization (Figure 4.1 and Figure 4.32). Moreover, the results suggested that BCR-induced phosphorylation of Akt did not rely on actin remodeling, whereas inhibition of the actin cytoskeleton with LatA in resting DG75 B cells resulted in strong activation of Akt. However, lastly the dependencies between BCR-induced Ca^{2+}-mobilization and phosphorylation of Akt were elucidated.

To investigate whether BCR-induced Akt phosphorylation requires Ca^{2+}-mobilization, I used a cellular knockout model system based on PLCγ1 and PLCγ2 double-deficient DG75 B cells that are incapable of BCR-induced Ca^{2+}-mobilization[58]. Hence, these cells were compared with parental DG75 B cells and Vav1-deficient B cells regarding their ability to mediate BCR-induced phosphorylation of Akt (Figure 4.39).

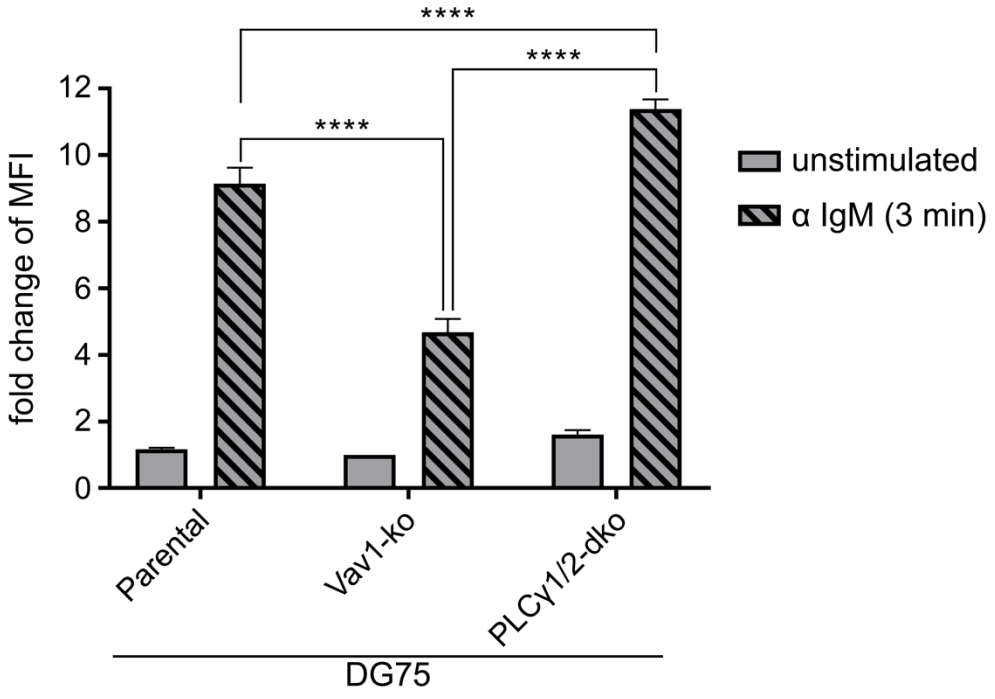

Figure 4.39 BCR-induced phosphorylation of Akt does not rely on Ca^{2+}-mobilization. Analysis of Akt phosphorylation on position 473 (serine) in DG75 B cells, Vav1-deficient DG75 B cells and PLCγ1/2 double-deficient DG75 B cells. The cells were either left untreated or stimulated for 3 min with 20 µg/ml of anti-human-IgM $F(ab')_2$ fragments (α IgM). Subsequently, the cells were fixed, permeabilized and stained with pAkt-AlexaFluor 647. The MFI were determined by flow cytometry and the MFI of unstimulated Vav1-deficient DG75 B cells was set to 1. All other MFI were normalized to this reference value. Error bars indicate standard deviation of three independently performed experiments. Significances were calculated using two-way ANOVA followed by Tukey's multiple comparison test. ****: $p<0.0001$

BCR-induced phosphorylation of Akt was possible in PLCγ1/2 double-deficient (PLCγ1/2-dko) DG75 B cells and was significantly higher compared to parental DG75 B cells (Figure 4.39).

These results indicated that in DG75 B cells BCR-induced phosphorylation of Akt was independent of the second messenger Ca^{2+}.

Finally, I addressed the question whether BCR-induced Ca^{2+}-mobilization and actin remodeling depend on phosphorylation of Akt. To investigate these dependencies however no inhibitor for Akt was used since experiments to determine the optimal time of stimulation for BCR-induced phosphorylation of Akt revealed that Akt was phosphorylated most efficiently between the first and the third minute of stimulation (Figure 4.40). While BCR-induced Ca^{2+}-mobilization and actin remodeling already peaked approx. 30 sec after stimulation, a dependency on activation of Akt for these signaling pathways seemed to be rather unlikely.

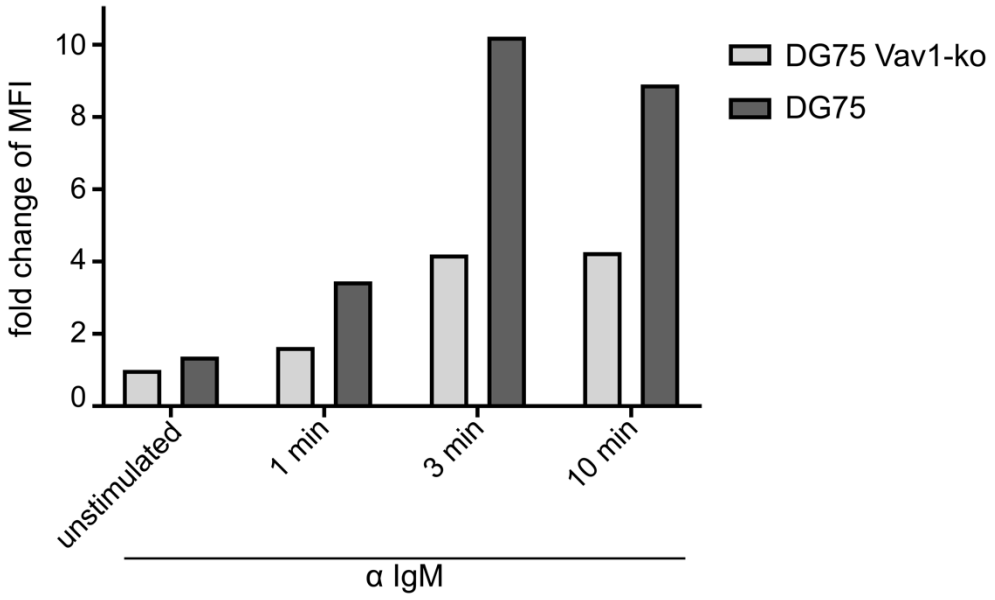

Figure 4.40 Stimulation kinetic of BCR-induced phosphorylation of Akt. Analysis of Akt phosphorylation on position 473 (serine) in Vav1-deficient DG75 B cells and parental DG75 B cells. The cells were either left untreated or stimulated for 1, 3 or 10 min with 20 µg/ml of anti-human-IgM $F(ab')_2$ fragments (α IgM). Afterwards, the cells were fixed, permeabilized and stained with pAkt-AlexaFluor 647. The MFI were determined by flow cytometry and the MFI of unstimulated Vav1-deficient DG75 B cells was set to 1. All other MFI were normalized to this reference value. N = 1 for this experiment.

Taken together, the recent results demonstrated that different signaling axes within the BCR signaling were controlled by Vav family members or were at least enhanced when Vav family members are present. Furthermore, those affected signaling axes were functionally independent from one another and Vav family members were thereby identified as a branching point within the BCR signaling cascade.

5. Discussion

Even though the signaling reactions initiated by BCR stimulation have been studied in considerable detail in the past, the exact mechanism(s) by which Vav family proteins are involved in BCR-proximal signal initiations remain unclear[21,47,149,49,58,68,69,76,146–148]. However, results regarding the capacity of BCR-induced Ca^{2+}-mobilization of primary B cells isolated from Vav1 and Vav2 double-deficient mice were inconsistent and did not provide an explanation by which mechanism(s) Vav family members support Ca^{2+} signaling[69,76,142]. Using a cellular model system based on human Vav1-deficient DG75 B cells, our working group recently validated a crucial role for Vav family members in BCR-induced Ca^{2+}-signaling. These cells do not express Vav1, barely express Vav3 and show only low expression of Vav2, thus they constitute a suitable model system to study Vav isoforms regarding their function in BCR signaling. While Vav1 and Vav3 supported BCR-induced Ca^{2+}-mobilization upon reconstitution, Vav2 failed to promote this process[47]. However, the underlying mechanism(s) by which Vav isoforms contribute to this signaling axis remained partly unknown. This work demonstrated that BCR-induced Ca^{2+}-mobilization involves the catalytic GEF-activity of Vav family members. Furthermore, additional signaling pathways downstream of the BCR, such as actin remodeling and activation of the PI3K/Akt-pathway, require the presence and the enzymatic activity of Vav proteins.

5.1. The enzymatic GEF-activity of Vav family members is required for BCR-induced Ca^{2+}-mobilization

One possible mechanism explaining the different properties of Vav family members in supporting BCR-inducible Ca^{2+}-mobilization would be a differential GEF-activity of Vav1, Vav2 and Vav3 towards different small G proteins of the Rho family. In B cells, little is known about the role of the GEF-activity of Vav proteins. Most of the published studies focused on the presence of Vav proteins in mice or in B cell lines rather than on the GEF-activity itself[47,68,69,76]. While Vav1-deficient mice barely show any differences to their wild-type counterparts regarding lymphocyte development and BCR-induced Ca^{2+}-mobilization, both processes are greatly impaired in Vav1 and Vav2 double-deficient mice[69,76]. This effect is even more pronounced in mice deficient for all three Vav proteins[68]. However, the underlying mechanism by which Vav proteins contribute to B cell development and signaling remained unknown[68,69,76]. In contrast, another group showed that isolated primary B cells from the same Vav1 and Vav2 double-deficient mice essentially exhibited comparable BCR-induced Ca^{2+}-mobilization kinetics to primary B cells isolated from wild-type mice[142]. To date, no clear connection between the GEF-activity of Vav family members and B cell development or BCR induced signaling has been drawn. On the other hand, mice deficient for Rac2 showed reduced B and

plasma cell numbers and isolated primary B cells were less able to mobilize Ca^{2+} upon BCR stimulation[106]. Rac1 and Rac2 double-deficient mice exhibited blockade in early B cell development while Rac1 deficient mice were barely affected in these processes[107,108,150].

This work demonstrated that amino acid residues in Vav1, mVav1 and Vav3 that are involved in binding of Rac1 are essential for full BCR-induced Ca^{2+}-mobilization. While amino acid substitutions at positions leucine 334 and lysine 335 in mVav1 considerably reduced the ability to promote BCR-induced Ca^{2+}-mobilization in Vav1-deficient DG75 B cells, this negative effect was not observed in the corresponding variant of human Vav1[47]. Thus, there appear to be species-specific differences of Vav proteins regarding BCR-induced Ca^{2+}-mobilization. For all variants of Vav1, mVav1 and Vav3 that exhibited diminished BCR-induced Ca^{2+}-kinetics, this reduction was manifested approx. by half. Since the expression of the Vav1 L213Q-mutant was significantly lower compared to wild-type Vav1, this variant does not represent a reliable "tool" to investigate loss-of-GEF-activity effects in Vav1, at least not in DG75 B cells.

To date, little is known about substrate specificities of Vav family members toward small GTPases. Vav1 is reported to mediate the highest GEF-activity towards Rac1, intermediate GEF-activity towards RhoA and the lowest activity towards Cdc42, while Vav2 shows the highest activity towards Rac1 and Cdc42 and lower activity towards RhoA[86–88]. So far, preferences for Vav3 remain to be elucidated. Mutations in Rac1 interaction interfaces fully disrupted any GEF-activity mediated by Vav1 or Vav3. Based on these results I concluded that the GEF-activity of Vav family members is required for full BCR-induced Ca^{2+}-mobilization. Furthermore, since wild-type human Vav1, murine Vav1 and Vav3 supported BCR-induced Ca^{2+}-mobilization in DG75 B cells and shared GEF-activity towards RhoA, this small G proteins is most likely involved in Ca^{2+}-mobilization upon stimulation of the BCR. This notion is supported by the data from the murine B cell line A20 expressing a dominant negative variant of RhoA leading to reduced BCR-induced Ca^{2+}-profiles[151]. In this context, the functions of RhoA and Rac2, which is almost exclusively expressed in the hematopoietic lineage, are most likely redundant since mice deficient for Rac2 show similarly reduced BCR-induced Ca^{2+}-mobilization[105,106,152]. Interestingly, Rac2 is described to be involved in proper activation of PLCγ2 by protein-protein interactions[153,154]. A PLCγ2 variant which is unable to interact with Rac2 led to reduced BCR-induced Ca^{2+}-kinetics in DG75 B cells (Christoffer Hitzig, unpublished data). Hence, the additional activation besides phosphorylation of PLCγ2 appears to be important for BCR-induced Ca^{2+}-mobilization. Conclusively, I hypothesized that the GEF-activity of Vav isoforms towards RhoA - and most likely Rac2 - leads to full activation of PLCγ2 and thereby the complete potential of BCR-induced Ca^{2+}-mobilization is exploited. This hypothesis would also explain why T cells were reportedly not affected in TCR-induced Ca^{2+}-mobilization by the expression of a GEF-inactive variant of Vav1[96]. In contrast to B cells, T

cells express PLCγ1 but no PLCγ2 and the requirement of optimal activation by Rho GTPases applies to PLCγ2 but not PLCγ1[96,155]. More recently, Cdc42 has been described to play an important role for B cell differentiation and BCR-signaling[156]. However, since Vav1 and Vav3 did not strongly activate this Rho GTPase, the effects on B cell differentiation and BCR signaling likely rather depend on the Cdc42-specific GEF DOCK8[157].

Consistently, loss of GEF-activity in Vav1 led to a reduction of BCR-induced Ca^{2+}-mobilization approx. by half in comparison with Vav1-deficient DG75 B cells and those cells reconstituted with the respective wild-type Vav isoform. Therefore, the GEF-activity is not the only mechanism by which Vav proteins support BCR-induced Ca^{2+}-signaling. Loss of the N-terminal CH domain in Vav1 reportedly leads to reduced Ca^{2+}-kinetics in antigen receptor-stimulated B and T cells[47,94]. By contrast, loss of the CH domain leads to enhanced GEF-activity and results in oncogenic potential of Vav for the cells[78,93]. To date, the mechanism by which the CH domain supports BCR-induced Ca^{2+}-mobilization remains unclear. Since the intramolecular localization at either termini of the protein showed normal BCR-induced Ca^{2+}-kinetics in DG75 B cells, a protein-protein interaction based mechanism becomes likely[47]. However, the C-terminus is described to loop back to the active center of Vav thereby forming an additional inhibitory loop[158]. Hence, a putative regulatory function of the CH domain cannot be excluded. Based on the data presented in this thesis and on findings from the literature, I speculate that the CH domain and the GEF-activity of Vav1 cooperate to achieve the full activation of the BCR-induced signaling cascade. To analyze whether the loss of GEF-activity was compensated by enhanced and prolonged recruitment of Vav1 to the Igα/Igβ complex, a construct was used in which the SH2 domain of Vav1 was replaced with the tandem SH2 domains of Syk[47]. The resulting protein (Vav1Syk$(SH2)_2$) is reported to be specifically recruited to the Igα and Igβ heterodimer[47]. Vav1-deficient DG75 B cells expressing Vav1Syk$(SH2)_2$ exhibited an enhanced and sustained BCR-induced Ca^{2+}-kinetic[47]. The loss of GEF-activity was partly recovered by the Vav1Syk$(SH2)_2$ construct after prolonged times of stimulation. Hence, the GEF-activity seemed to be critical especially for the Ca^{2+} signal immediately after stimulation of the BCR, but the loss of GEF-activity is compensated by prolonged recruitment in later stages of the stimulation process, one to four minutes after BCR activation. This compensation is most likely mediated by so far unknown function(s) of the CH domain.

To further elucidate the involvement of Rho GTPases for proper BCR-induced Ca^{2+}-signaling, putatively involved Rho family small G proteins were either genetically inactivated by our group or I pharmacologically inhibited these proteins[47]. DG75 B cells deficient for either Rac1 or Rac2 showed a slight reduction in BCR-induced Ca^{2+}-mobilization[47]. Unfortunately, Rac1 and Rac2 double-deficient DG75 B cells and DG75 B cells deficient for RhoA could not be obtained[47]. However, pharmacological inhibition of Rac1 or RhoA in DG75 B cells with either E-Hop or

Rhosin resulted in reduced BCR-induced Ca^{2+}-profiles comparable to the Ca^{2+}-kinetics of Vav1-deficient DG75 B cells[135–137]. Treatment of Vav1-deficient DG75 B cells with E-Hop or Rhosin showed similar reductions but to lower extents. These reducing effects in Vav1-deficient DG75 B cells might be caused by inhibition of small G proteins that are activated independently from Vav family members by other GEFs for Rho GTPases such as Tiam1, LARG or Dbl[101]. Furthermore, both inhibitors might also act on other Rho GTPases beyond the reported ones, Rac1 and Rac3 for E-Hop and RhoA and RhoC for Rhosin[135–137]. The specificity of E-Hop e.g. was determined in cells deficient for expression of Rac2, but the molecule also inhibited the close homolog Cdc42 at higher concentrations[135]. Rac2 in contrast is structurally closer related to Rac1 and Rac3 than Cdc42[105]. Hence, Rac2 might be inhibited by E-Hop as well, even at lower concentrations, which yet remains to be evaluated. One way to specifically determine which small G proteins are involved in the Ca^{2+}-influx after BCR-stimulation would be to perform further GEF-activity assays with all Rho GTPases. Nevertheless, the presented results support the hypothesis that the GEF-activity of Vav proteins - most likely towards RhoA and Rac2 - is critical for full BCR-induced Ca^{2+}-mobilization.

5.2. The role of the acidic region of Vav2

Vav2 did not support Ca^{2+}-mobilization after BCR stimulation in Vav1-defcient DG75 B cells and Jurkat T cell[47,77]. This inability was not due to a general loss-of-function in Vav2 since the protein efficiently supported BCR-induced actin remodeling and activation of Akt upon reconstitution in Vav1-deficient DG75 B cells. In mice, a double-deficiency for either Vav1 and Vav2 or Vav1 and Vav3 was required to measure defects in B and T cell development and antigen receptor-induced signaling[68,69]. Not surprisingly, these negative effects were more pronounced upon deficiency for all three Vav isoforms in mice[68]. Additionally, murine Vav2 was shown to efficiently support BCR-induced Ca^{2+}-mobilization in a murine B cell line[159]. This discrepancy between the model systems in mice and human cell line models might originate from species related differences or might be due to the respective cellular system[47,68,69,77]. Potentially, phosphorylation of Vav2 is not possible in DG75 B and Jurkat T cells because they might lack the kinase responsible for this process. In resting cells, the enzymatic GEF-activity of Vav proteins is inhibited by formation of an inhibitory loop of the acidic region[78]. Mediated by interactions between the DH domain, the adjacent PH domain and the C-SH3 domain, a “closed” conformation further supports this inhibition[72,91]. Since Vav2 did not promote BCR-induced Ca^{2+}-signaling in DG75 B cells, the molecule appeared to be an interesting Vav family member for investigations on the proposed inhibitory function of the acidic region. Consequently, the acidic region of Vav2 was deleted in one approach and the critical tyrosine residues at positions 142, 159 and 172 were each substituted with aspartate in another approach. Both resulting constructs enhanced BCR-induced Ca^{2+}-mobilization in DG75 B cells

in a sustained manner, albeit to different extents. Interestingly, this effect was observed even though both proteins were expressed approx. ten times and five times less efficiently compared to wild-type Vav2. This low expression levels could result from a putative hyperactivity of this variant. It is tempting to speculate that a constitutively activated protein might be harmful to the cells and thus, only cells with low expression of the artificial Vav2 constructs might have survived the transduction procedure.

Unfortunately, despite many optimization steps of the expression and purification procedures, none of the generated constructs of Vav2 could be purified in amounts sufficient for GEF-activity measurements. However, GEF-activity measurements were performed with a commercially available recombinant DH domain of Vav2. Although it is reported that the whole DH-PH-ZF core unit of Vav proteins is required *in vivo* to mediate GEF-activity, using the purified DH domain for GEF-activity measurements gave at least some insights into substrate preferences of Vav2 *in vitro*[72,160]. The commercially available, recombinant DH domain consisted of amino acids 189 to 374 of Vav2. Of note, the obtained results in the following have to be interpreted carefully, since three essential domains - acidic region, PH domain and ZF domain - for GEF-activity mediated by Vav proteins were missing. In contrast to a previous report which claimed that Vav2 is an activator of Rac1, RhoA and Cdc42, the recombinant DH domain of Vav2 exhibited moderate GEF-activity towards Rac1 and Cdc42, but almost no detectable GEF-activity towards RhoA[88]. Intriguingly, the fact that the isolated DH domain of Vav2 was not able to mediate GEF-activity towards RhoA further supported my assumption that RhoA - and most likely its close relatives RhoB and RhoC as well as Rac2 - have a critical role in BCR-induced Ca^{2+}-mobilization. In this work I demonstrated that the loss of GEF-activity towards Rho family members in mutant variants of Vav1 and Vav3 led to attenuated BCR-induced Ca^{2+}-mobilizations. Since the reduction of this signaling pathway for mutant variants was manifested by half, there has to be another mechanism by which Vav proteins support Ca^{2+}-influx upon stimulation of the BCR. Loss of the CH-domain in Vav1 had even more severe effects for BCR and TCR-induced Ca^{2+}-mobilization compared to the loss of GEF-activity[47,94]. Together, this allows the hypothesis that the GEF-activity and the CH domain of Vav proteins individually support Ca^{2+}-mobilization upon stimulation of the BCR while both have to act in concert for full BCR-induced signaling. For Vav1, I demonstrated that enhanced and prolonged recruitment to the BCR seemed to compensate for the loss of GEF-activity towards Rho family members, which is most likely mediated by so far unknown functions of the CH domain. The generated artificial variants of Vav2 might possibly support BCR-induced Ca^{2+}-signaling in a similar way, since no detectable GEF-activity towards RhoA of the isolated DH domain of Vav2 was measured, but Vav2 was recruited more efficiently to the BCR compared to Vav1. In addition, experiments with variants of Vav2 might have revealed a newly identified regulatory role of the acidic region of Vav proteins[78,95]. The structural relief upon phosphorylation of

several domains within Vav family members does not only enhance the GEF-activity of the proteins but might also allow the unknown functions mediated by the CH domain. Furthermore, acquisition of BCR stimulation-dependent recruitment kinetics revealed that Vav family members do not need to be recruited to specific phosphorylated docking sites but rather interact with phosphorylated tyrosine residues dependent on their availability.

5.3. The PIP5Ks as potential downstream molecules of activated Rho GTPases

So far, the results of this work strongly imply that proper BCR-induced Ca^{2+}-mobilization depend on the GEF-activity towards RhoA. Thus, I investigated which components downstream of RhoA might be activated and involved in BCR-induced Ca^{2+}-mobilization. Among other proteins, PIP5Ks are reportedly recruited to the activated BCR, eventually providing locally increased levels of the substrate PIP_2 for PLCγ2 and PI3K at the plasma membrane[122,123]. Furthermore, PIP5Ks are described to be activated by small G proteins of the Rho family[117,118,151]. This activation of PIP5Ks is further enhanced through phosphorylation by Src family kinases[119]. In addition, two reports describe a role of PIP5Ks in activation and the formation of the immunological synapse, at least in T cells[120,121].

Either PIP5Kα or PIP5Kγ were able to partially re-establish the BCR-induced Ca^{2+}-influx into the cytosol in DG75 B cells deficient for Vav1 after prolonged stimulation periods. Expression of PIP5Kβ did not affect the BCR-induced Ca^{2+}-mobilization in Vav1-deficient DG75 B cells. However, the generated DG75 B cells deficient for all three PIP5K family members showed inconsistent BCR-induced Ca^{2+}-phenotypes. These results challenge the previous postulated hypothesis that PIP5Ks provide locally increased levels of PIP_2 upon BCR stimulation[122,123,151]. Perhaps, PIP4Ks compensate for the loss of PIP5Ks in the triple-deficient DG75 sub-clones, but since the cellular amount of PI5P is ten times lower than the quantity of PI4P, this compensation seemed to be rather unlikely. Additionally, this unlikely compensation would not explain the inconsistent Ca^{2+}-phenotypes of DG75 B cells lacking either isoform of PIP5Ks. Possibly, the amounts of PIP_2 in the plasma membrane are sufficient for BCR-induced signaling and PIP5Ks are recruited to restore the amount of PIP_2. Parental DG75 B cells constitute a heterogenous cell line since they never have been sub-cloned. Thus, this cell line contains single B cells with either higher or lower capacity to mobilize Ca^{2+} upon stimulation of the BCR. The mean of hundreds of B cells is depicted as one data point for Ca^{2+}-graphs. Possibly, differences in BCR-induced Ca^{2+}-mobilization derive from the ability to mobilize Ca^{2+} after BCR stimulation of the respective single cell clones. Nevertheless, these experiments exclude involvement of PIP5Ks in Ca^{2+}-mobilization upon stimulation of the BCR in DG75 B cells and thereby support the hypothesis that the GEF-activity towards RhoA and possibly

Rac2 of Vav family members enhances the activity of PLCγ2, which further promotes the BCR-induced Ca^{2+}-mobilization[151,153,154,161].

5.4. Vav family members constitute branching points for distinct BCR signaling pathways

In this thesis I identified a critical role of Vav family members and their GEF-activity in DG75 B cells regarding BCR-induced Ca^{2+}-mobilization. As a consequence, further signaling pathways of the BCR signaling cascade, such as antigen receptor-induced actin remodeling, were tested. The loss of GEF-activity towards Rho GTPases significantly diminished actin remodeling after BCR stimulation. The observed reduction in BCR-induced actin remodeling most likely depends on the reported link between activated Rac1 and cytoskeletal rearrangements[139]. Moreover, the reduction was comparable to the observed Ca^{2+}-phenotypes and in line with the hypothesis that Vav family act at least in two manners upon recruitment to the stimulated BCR and its signaling molecules since the loss of GEF-activity did not fully abolish BCR-induced actin remodeling to the level of Vav1-deficient cells. Here, the differences between the Vav3 constructs were the least pronounced. Since Vav3 barely exhibited any GEF-activity towards Rac1, Vav3 most likely acts in this axis rather through its CH domain than through its GEF-activity. Vav2 and its enhanced variants were able to mediate BCR-induced actin remodeling, even though to a different extent. The capacity of Vav2 to support this process most likely originates from its GEF-activity towards Rac1[139]. Both gain-of-function variants of Vav2 showed enhanced abilities in BCR-induced actin remodeling. These positive effects might result from an enhanced GEF-activity towards Rac1 and enhanced CH domain-mediated functions. BCR internalization upon its stimulation, a process that requires actin remodeling, was also significantly reduced with the loss of GEF-activity in the Vav1 E201A variant[98]. However, as for BCR-induced Ca^{2+}-mobilization, I proposed that actin remodeling depends on the GEF-activity and CH domain mediated functions of Vav family members. Here, in contrast to BCR-induced Ca^{2+}-mobilization, the GEF-activity towards Rac1 might be of high importance.

Activation of MAPK within the BCR signaling cascade is reportedly induced by Vav proteins[66,99]. Vav1-deficient DG75 B cells showed a reduced BCR-induced phosphorylation of the MAPK Erk similar to those cells reconstituted with the barely expressed Vav1 L213Q variant while Vav1-deficient DG75 B cells that were reconstituted with Vav1 E201A showed no differences in comparison to cells reconstituted with wild-type Vav1. Hence, these data implicated that the GEF-activity is dispensable for BCR-induced activation of Erk. I proposed that phosphorylation of Erk rather depends on the interaction of Vav1 with Grb2[82]. This protein was lately identified to control activation of Erk upon stimulation of the BCR[58]. Since Vav1

L213Q was expressed ten-fold less efficiently, is probably folded incorrectly and degraded in the proteasome, this variant is likely unable to mediate any interaction with Grb2. In addition to Erk, the BCR-induced activation of p38 was tested. DG75 B cells with Vav1 deficiency showed a severely reduced capacity to BCR-dependently phosphorylate p38. Experiments to validate these data obtained by western blot analysis and for statistical analysis were conducted. Unfortunately, the phospho-specific antibodies used for detection of p38 produced a strong background staining, complicating a reliable evaluation of the acquired data by flow cytometry. The underlying mechanism whether the GEF-activity or so far unknown functions of the CH domain mediate the BCR-induced activation of p38 remain to be elucidated since these experiments were not conducted with any variant that lack GEF-activity towards Rac1, RhoA and Cdc42.

In chicken DT40 B cells, a cellular model system that was frequently used in the past to investigate BCR signaling, activation of Akt has been reported to be dependent on Vav3[140]. In contrast, other studies suggested that Vav family members are dispensable for this process in primary murine B cells[144]. To shed light on the question of BCR-induced activation of Akt, I investigated whether stimulation of the BCR in Vav1-deficient DG75 B cells resulted in phosphorylation of Akt. BCR-induced activation of Akt was significantly enhanced in Vav1-proficient DG75 B cells. Interestingly, similar to BCR-induced Ca^{2+}-mobilization and actin remodeling, all variants of Vav1 and Vav3 lacking GEF-activity towards Rac1, RhoA and Cdc42 showed once again a reduction by half in phosphorylation of Akt compared to their wild-type counterparts. Therefore, I proposed that the GEF-activity and the CH domain of Vav proteins collaborate to achieve the full potential in BCR signaling of these proteins since the loss of Vav1 had more severe effects than the loss of GEF-activity in Vav family members. Similar to BCR-induced actin remodeling, Vav2 was also able to support the BCR-induced activation of Akt, thus Rac1 potentially might be the critical Rho GTPases involved in this signaling axis. Discrepancies between avian and human model B cell lines compared to primary murine B cell possibly originate from species differences or differences between primary cells versus malignant transformed cells[140,144]. Collectively, the results of this thesis demonstrated that BCR-induced Ca^{2+}-mobilization, actin remodeling and activation of Akt and MAPK such as Erk and p38 are supported by the presence of Vav family members (Figure 5.1). Furthermore, at least BCR-induced Ca^{2+}-mobilization, actin remodeling and phosphorylation of Akt depend on the GEF-activity of Vav proteins. From the results of this thesis and with published data I concluded that BCR-induced Ca^{2+}-mobilization was regulated by the GEF-activity of Vav proteins towards RhoA and most likely Rac2. In contrast, I concluded that actin remodeling and phosphorylation of Akt might be dependent on activation of Rac1.

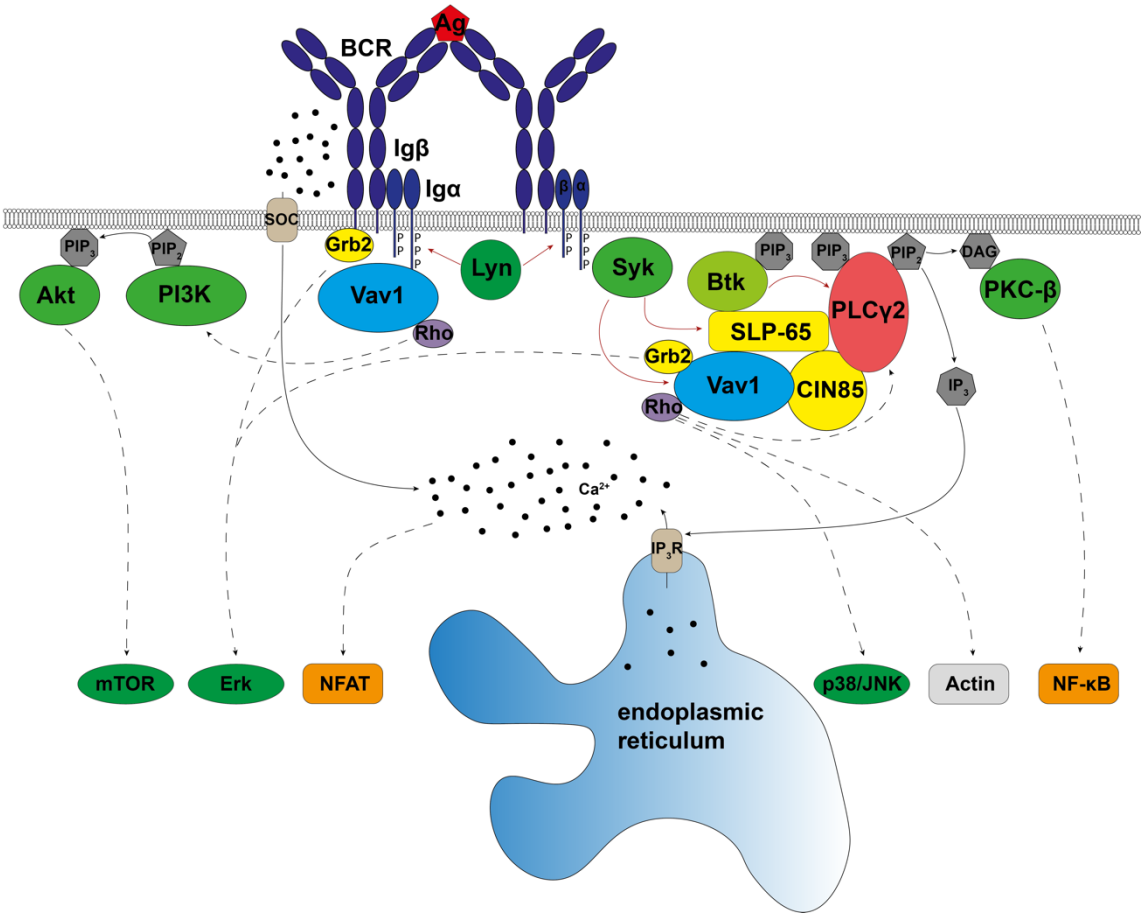

Figure 5.1 Schematic overview of the BCR-induced signaling cascade. The BCR signaling cascade is triggered by binding of the cognate antigen (Ag) to the BCR, mediating activation. Tyrosine residues inside and outside of ITAMs in Igα and Igβ are phosphorylated by Src family kinases like Lyn. Consequently, Syk and SLP-65 are recruited. Due to generation of binding sites for SH2 containing proteins by phosphorylation of SLP-65 through Syk, the Ca^{2+} initiation complex is formed consisting of Btk, PLCγ2, CIN85 and Vav1. As a result, Ca^{2+} is mobilized into the cytosol, mediating the nuclear translocation of the transcription factor NFAT. Additionally, the translocation of the transcription factor NF-κB into the nucleus is induced and MAPK like Erk, JNK and p38 are activated. Survival and proliferation are promoted via the PI3K/Akt pathway. Red arrows indicate phosphorylation processes, solid arrows indicate translocation processes and dashed arrows indicate multistep activation processes. Ca^{2+} is indicated as black dots. Kinases are colored in green, adaptor proteins in yellow, PLCγ2 in red, Vav1 in blue, Rho GTPases in purple, transcription factors in orange, Ca^{2+}-channels in light brown, phosphatidylinositols and relatives in dark grey, actin in light grey, the BCR complex with Igα and Igβ in dark blue and the antigen in dark red.

All of the before mentioned pathways that were controlled or enhanced by Vav proteins and their GEF-activity play an indispensable role in various developmental stages of a B cell. For example, proper BCR-induced Ca^{2+}-mobilization along with activation of the transcription factors NFAT and NF-κB is already critical in B cell development during testing of functionality of the BCR after somatic recombination of the heavy and the light chain[14,22]. Most likely, B and T cells in either Vav1 and Vav2 double-deficient, Vav1 and Vav3 double-deficient or Vav1, Vav2 and Vav3 triple-deficient mice are unable to develop because they are not able to pass these checkpoints and most of the cells die by apoptosis due to insufficient BCR-induced signaling[14,68,69]. Similar to B cell development, the capacity of BCR-induced signaling is pivotal for the quality of the immune response upon activation of B cells[21,49]. Furthermore, proliferation and metabolic changes have to be induced through the PI3K/Akt pathway for clonal expansion[60,61]. Rearrangement of the cytoskeleton is reportedly critical for migration and BCR

internalization[97,98,141,142]. Activation of MAPK like Erk and p38 support cell proliferation and survival, gene transcription and stability of messenger RNA (mRNA)[162]. The generated data of this thesis strongly imply involvement of Vav proteins and their GEF-activity in all of the mentioned processes thereby highlighting the central role of this protein family for B cells.

Lastly, the presented results gave rise to the question whether BCR-induced Ca^{2+}-mobilization, actin remodeling and phosphorylation of Akt are dependent or independent of each other. From the generated data, I assumed that Vav family members are central coordinators of signaling pathways downstream of the stimulated BCR. Previous reports suggest that BCR-induced Ca^{2+}-mobilization depends on actin remodeling and that treatment of B cells with the actin polymerization inhibitor Latrunculin A (LatA) induces a Ca^{2+}-influx into the cytosol without BCR stimulation[141,142]. Later it was demonstrated that this initiation of Ca^{2+}-mobilization in the absence of BCR stimulation relies on co-expression of membrane-bound IgD, the co-receptor CD19 and the chemokine receptor CXCR4[145]. Therefore, the intracellular Ca^{2+}-concentration was monitored for the 5 min of LatA treatment before BCR stimulation. In comparison to DG75 B cells treated with the vehicle control DMSO, a slight increase in the intracellular Ca^{2+}-concentration was observed during treatment with LatA. However, this did not affect the capacity for BCR-induced Ca^{2+}-mobilization. Hence, in DG75 B cells, the BCR-induced Ca^{2+}-mobilization did not depend on BCR-induced actin remodeling. An opposite dependency, that BCR-induced Ca^{2+}-mobilization is required for actin remodeling, had already been excluded with the experiments that were conducted with Vav1-deficient DG75 B cells expressing wild-type Vav2. Thus, I concluded that Ca^{2+}-mobilization and actin remodeling most likely work independently of each other in BCR stimulated DG75 B cells. Additionally, the effect of LatA treatment on BCR-induced phosphorylation of Akt was tested. While inhibition of the actin polymerization appeared to have no significant effects on BCR-induced phosphorylation of Akt compared to DMSO treated DG75 B cells, treatment of these cells with LatA induced a dose-dependent, significant phosphorylation of Akt in resting cells. To date, only the reversed process, that Akt induces cytoskeletal rearrangements promoting motility of the cells, has been described[163]. However, these results demonstrated that the BCR-induced activation of Akt takes place independently from actin remodeling. In the following, possible dependencies between BCR-induced Ca^{2+}-mobilization and activation of Akt were examined. PLCγ1 and PLCγ2 double-deficient DG75 B cells were used based on their lack of Ca^{2+}-mobilization upon stimulation of the BCR[58]. These cells were however still able to mediate BCR-induced activation of Akt, even to significantly higher extents than parental DG75 B cells. As for BCR-induced actin remodeling, experiments with Vav1-deficient cells reconstituted with wild-type Vav2 supported these findings. Therefore, I concluded that BCR-induced activation of Akt is independent from Ca^{2+}-mobilization. Both, BCR-induced Ca^{2+}-mobilization and actin remodeling were at the highest 30 sec after BCR stimulation. However, after 1 min of

stimulation barely any phosphorylation of Akt was detected in DG75 B cells. Based on those findings, I assumed that these two early events in BCR signaling do not depend on the phosphorylation of Akt since full activation of Akt was observed later in the stimulation process, 3 min after BCR stimulation.

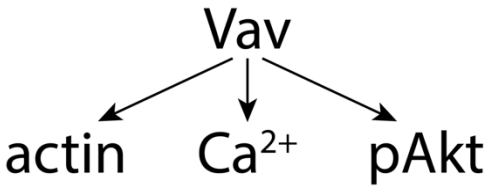

Figure 5.2 Schematic overview of processes within BCR signaling that are independently regulated by Vav family members. "actin" refers to BCR-induced actin remodeling, "Ca^{2+}" refers to BCR-induced Ca^{2+}-mobilization, "pAkt" refers to BCR-induced phosphorylation of Akt, "Vav" refers to Vav family members.

The results of this last chapter of my thesis revealed that Vav-dependent pathways within BCR signaling work independently from each other leading to the hypothesis that Vav family members constitute a central branching point in this signaling cascade (Figure 5.2).

6. Conclusion and Outlook

The results of this thesis unraveled a new concept for the possible role of Vav family members within the BCR signaling cascade. Direct recruitment to the stimulated BCR and its associated signaling components is a prerequisite for Vav proteins to exert their functions. The GEF-activity of Vav1 and Vav3 proteins towards RhoA and probably Rac2 was required for full BCR-induced Ca^{2+}-mobilization in DG75 B cells. Activated RhoA and Rac2 most likely support this signaling pathway within BCR signaling by full activation of PLCγ2. In contrast, the catalytic activity on Rac1 seems to be critical for Vav1 and Vav2 in BCR-induced actin remodeling and phosphorylation of Akt. Yet, the enzymatic GEF-activity was not the only mechanism by which Vav family members support BCR signaling. Another mechanism for full BCR signaling is possibly mediated by an unknown role of the CH domain, since the loss of this domain in Vav1 reportedly led to severely reduced antigen receptor-induced Ca^{2+}-kinetics. Furthermore, this work demonstrated that BCR-induced Ca^{2+}-mobilization, actin remodeling and phosphorylation of Akt were independent processes within BCR signaling. I hence concluded that Vav family members and their GEF-activity are central coordinators of the BCR signaling cascade. Thus, a new class of proteins with enzymatic GEF-activity, besides the already known protein classes such as kinases, adaptor molecules and lipases, should be included in the literature into the protein classes of relevance for BCR proximal signaling.

Despite intensive and successful research on Vav proteins and their detailed role in BCR-induced signaling, several questions remain to be elucidated. Most importantly, the question of the role of the CH domain of Vav family members should be addressed. Using affinity purification experiments interaction partners could be determined in comparison of stimulated and unstimulated B cells. Putatively relevant proteins should be filtered and further investigated. In addition, GEF-activity assays for Vav family members and the respective mutant variants should be performed for the other Rho GTPases that haven't been tested in this study. Here, special focus should be placed on Rac2, Rac3, RhoB and RhoC, the closest relatives of Rac1 and RhoA, respectively. Moreover, the influence of the GEF-activity of Vav family members regarding BCR-induced phosphorylation of p38 could be elucidated. Lastly, all the so far obtained results were obtained based on cancerous cells. To exclude any effects driven by malignant transformation and to confirm putative species differences between human and mice, the generation of primary human knockout B cells is considered.

7. Literature

1. Chaplin, D. D. Overview of the human immune response. *J. Allergy Clin. Immunol.* **117**, 430–435 (2006).

2. Beutler, B., Hoebe, K., Du, X. & Ulevitch, R. J. How we detect microbes and respond to them: the Toll-like receptors and their transducers. *J. Leukoc. Biol.* **74**, 479–485 (2003).

3. Flajnik, M. F. & Kasahara, M. Origin and evolution of the adaptive immune system: Genetic events and selective pressures. *Nat. Rev. Genet.* **11**, 47–59 (2010).

4. Chaplin, D. D. Overview of the Immune Response. *J. Allergy Clin. Immunol.* **125**, (2010).

5. Rao, D. S. *Overview and Compartmentalization of the Immune System*. *Hematology* (Elsevier, 2018). doi:10.1016/B978-0-323-35762-3.00019-6.

6. Medzhitov, R. & Janeway, C. A. Innate immunity: The virtues of a nonclonal system of recognition. *Cell* **91**, 295–298 (1997).

7. Janeway, C. A. & Medzhitov, R. Innate Immune Recognition. *Annu. Rev. Immunol.* **20**, 197–216 (2002).

8. Morgan, B. P., Marchbank, K. J., Longhi, M. P., Harris, C. L. & Gallimore, A. M. Complement: central to innate immunity and bridging to adaptive responses. *Immunol. Lett.* **97**, 171–179 (2005).

9. Selsted, M. E. & Ouellette, A. J. Mammalian defensins in the antimicrobial immune response. *Nat. Immunol.* **6**, 551–557 (2005).

10. Abel, A. M., Yang, C., Thakar, M. S. & Malarkannan, S. Natural killer cells: Development, maturation, and clinical utilization. *Front. Immunol.* **9**, 1–23 (2018).

11. Iwasaki, A. & Medzhitov, R. Control of adaptive immunity by the innate immune system. *Nat. Immunol.* **16**, 343–353 (2015).

12. Cooper, M. D. The early history of B cells. *Nat. Rev. Immunol.* **15**, 191–197 (2015).

13. Cooper, M. D. & Alder, M. N. The evolution of adaptive immune systems. *Cell* **124**, 815–822 (2006).

14. Pieper, K., Grimbacher, B. & Eibel, H. B-cell biology and development. *J. Allergy Clin. Immunol.* **131**, 959–971 (2013).

15. Salzberg, S. L. Open questions: How many genes do we have? *BMC Biol.* **16**, 10–12 (2018).

16. Monroe, J. G. *et al.* Positive and negative selection during B lymphocyte development. *Immunol. Res.* **27**, 427–442 (2003).

17. Starr, T. K., Jameson, S. C. & Hogquist, K. A. Positive and Negative Selection of T Cells. *Annu. Rev. Immunol.* **21**, 139–176 (2003).

18. Müller, A. M., Medvinsky, A., Strouboulis, J., Grosveld, F. & Dzierzakt, E. Development of hematopoietic stem cell activity in the mouse embryo. *Immunity* **1**, 291–301 (1994).

19. Reth, M. Antigen receptor tail clue. *Nature* **338**, 383–384 (1989).

20. Reth, M. Antigen receptors on B lymphocytes. *Annu. Rev. Immunol.* **10**, 97–121 (1992).

21. Reth, M. & Wienands, J. Initiation and Processing of Signals From the B Cell Antigen Receptor. *Annu. Rev. Immunol.* **15**, 453–479 (1997).

22. Melchers, F. The pre-B-cell receptor: Selector of fitting immunoglobulin heavy chains for the B-cell repertoire. *Nat. Rev. Immunol.* **5**, 578–584 (2005).

23. Van Zelm, M. C., Szczepański, T., Van Der Burg, M. & Van Dongen, J. J. M. Replication history of B lymphocytes reveals homeostatic proliferation and extensive antigen-induced B cell expansion. *J. Exp. Med.* **204**, 645–655 (2007).

24. Cyster, J. G. & Schwab, S. R. Sphingosine-1-Phosphate and Lymphocyte Egress from Lymphoid Organs. *Annu. Rev. Immunol.* **30**, 69–94 (2012).

25. Nutt, S. L., Hodgkin, P. D., Tarlinton, D. M. & Corcoran, L. M. The generation of antibody-secreting plasma cells. *Nat. Rev. Immunol.* **15**, 160–171 (2015).

26. Hoffman, W., Lakkis, F. G. & Chalasani, G. B cells, antibodies, and more. *Clin. J. Am. Soc. Nephrol.* **11**, 137–154 (2016).

27. Kurosaki, T., Shinohara, H. & Baba, Y. B Cell Signaling and Fate Decision. *Annu. Rev. Immunol.* **28**, 21–55 (2010).

28. Basso, K. & Dalla-Favera, R. Germinal centres and B cell lymphomagenesis. *Nat. Rev. Immunol.* **15**, 172–184 (2015).

29. Roco, J. A. *et al.* Class-Switch Recombination Occurs Infrequently in Germinal Centers. *Immunity* **51**, 337-350.e7 (2019).

30. Kurosaki, T., Kometani, K. & Ise, W. Memory B cells. *Nat. Rev. Immunol.* **15**, 149–159 (2015).

31. Schroeder, H. W. & Cavacini, L. Structure and function of immunoglobulins. *J. Allergy Clin. Immunol.* **125**, S41–S52 (2010).

32. Clem, A. S. Fundamentals of vaccine immunology. *J. Glob. Infect. Dis.* **3**, 73–78 (2011).

33. Chames, P., Van Regenmortel, M., Weiss, E. & Baty, D. Therapeutic antibodies: successes, limitations and hopes for the future. *Br. J. Pharmacol.* **157**, 220–233 (2009).

34. Ansell, S. M. *et al.* PD-1 Blockade with Nivolumab in Relapsed or Refractory Hodgkin's Lymphoma. *N. Engl. J. Med.* **372**, 311–319 (2014).

35. Liu, W., Sohn, H. W., Tolar, P. & Pierce, S. K. It's All About Change: The Antigen-driven Initiation of B-Cell Receptor Signaling. *Cold Spring Harb. Perspect. Biol.* **2**, (2010).

36. Treanor, B. B-cell receptor: From resting state to activate. *Immunology* **136**, 21–27 (2012).

37. Schamel, W. W. A. & Reth, M. Monomeric and Oligomeric Complexes of the B Cell Antigen Receptor. *Immunity* **13**, 5–14 (2000).

38. Gomes de Castro, M. A. *et al.* Differential organization of tonic and chronic B cell antigen receptors in the plasma membrane. *Nat. Commun.* **10**, 1–11 (2019).

39. Campbell, M. A. & Sefton, B. M. Association between B-lymphocyte membrane immunoglobulin and multiple members of the Src family of protein tyrosine kinases. *Mol. Cell. Biol.* **12**, 2315–2321 (1992).

40. Kurosaki, T. *et al.* Role of the syk autophosphorylation site and SH2 domains in B cell antigen receptor signaling. *J. Exp. Med.* **182**, 1815–1823 (1995).

41. Wienands, J. *et al.* SLP-65: A new signaling component in B lymphocytes which requires expression of the antigen receptor for phosphorylation. *J. Exp. Med.* **188**, 791–795 (1998).

42. Engels, N., Wollscheid, B. & Wienands, J. Association of SLP-65/BLNK with the B cell antigen receptor through a non-ITAM tyrosine of Ig-α. *Eur. J. Immunol.* **31**, 2126–2134 (2001).

43. Fu, C., Turck, C. W., Kurosaki, T. & Chan, A. C. BLNK: A central linker protein in B cell activation. *Immunity* **9**, 93–103 (1998).

44. Grabbe, A. & Wienands, J. Human SLP-65 isoforms contribute differently to activation and apoptosis of B lymphocytes. *Blood* **108**, 3761–3768 (2006).

45. Oellerich, T. *et al.* SLP-65 phosphorylation dynamics reveals a functional basis for signal integration by receptor-proximal adaptor proteins. *Mol. Cell. Proteomics* **8**, 1738–1750 (2009).

46. Jumaa, H. *et al.* Abnormal development and function of B lymphocytes in mice deficient for the signaling adaptor protein SLP-65. *Immunity* **11**, 547–554 (1999).

47. Hitzing, C. Vav guanine nucleotide exchange factors control B cell antigen receptor-induced Ca2+-signaling. (2015).

48. Oellerich, T. *et al.* The B-cell antigen receptor signals through a preformed transducer module of SLP65 and CIN85. *EMBO J.* **30**, 3620–3634 (2011).

49. Engelke, M., Engels, N., Dittmann, K., Stork, B. & Wienands, J. Ca2+ signaling in antigen receptor-activated B lymphocytes. *Immunol. Rev.* **218**, 235–246 (2007).

50. Salim, K. *et al.* Distinct specificity in the recognition of phosphoinositides by the pleckstrin homology domains of dynamin and Bruton's tyrosine kinase. *EMBO J.* **15**, 6241–6250 (1996).

51. Falasca, M. *et al.* Activation of phospholipase Cγ by PI 3-kinase-induced PH domain-mediated membrane targeting. *EMBO J.* **17**, 414–422 (1998).

52. Su, Y. W. *et al.* Interaction of SLP adaptors with the SH2 domain of Tec family kinases. *Eur. J. Immunol.* **29**, 3702–3711 (1999).

53. Hashimoto, S. *et al.* Identification of the SH2 domain binding protein of Bruton's tyrosine kinase as BLNK - Functional significance of Btk-SH2 domain in B-cell antigen receptor-coupled calcium signaling. *Blood* **94**, 2357–2364 (1999).

54. Patterson, R. L., Boehning, D. & Snyder, S. H. Inositol 1,4,5-Trisphosphate Receptors as Signal Integrators. *Annu. Rev. Biochem.* **73**, 437–465 (2004).

55. Cahalan, M. D. STIMulating store-operated Ca2+ entry. *Nat. Cell Biol.* **11**, 669–677 (2009).

56. Saijo, K. *et al.* Protein kinase C beta controls nuclear factor kappaB activation in B cells through selective regulation of the IkappaB kinase alpha. *J. Exp. Med.* **195**, 1647–1652 (2002).

57. Sen, R. Control of B Lymphocyte Apoptosis by the Transcription Factor NF-κB. *Immunity* **25**, 871–883 (2006).

58. Vanshylla, K. *et al.* Grb2 and GRAP connect the B cell antigen receptor to Erk MAP kinase activation in human B cells. *Sci. Rep.* **8**, 1–17 (2018).

59. Engels, N. *et al.* The immunoglobulin tail tyrosine motif upgrades memory-type BCRs by incorporating a Grb2-Btk signalling module. *Nat. Commun.* **5**, (2014).

60. Deane, J. A. & Fruman, D. A. Phosphoinositide 3-Kinase: Diverse Roles in Immune Cell Activation. *Annu. Rev. Immunol.* **22**, 563–598 (2004).

61. Hers, I., Vincent, E. E. & Tavaré, J. M. Akt signalling in health and disease. *Cell. Signal.* **23**, 1515–1527 (2011).

62. Manning, B. D. & Cantley, L. C. AKT/PKB signaling: navigating downstream. *Cell* **129**, 1261–1274 (2007).

63. Davis, R. E. *et al.* Chronic active B-cell-receptor signalling in diffuse large B-cell lymphoma. *Nature* **463**, 88–92 (2010).

64. Rawlings, D. J., Metzler, G., Wray-Dutra, M. & Jackson, S. W. Altered B cell signalling in autoimmunity. *Nat. Rev. Immunol.* **17**, 421–436 (2017).

65. Chapuy, B. *et al.* Molecular subtypes of diffuse large B cell lymphoma are associated with distinct pathogenic mechanisms and outcomes. *Nat. Med.* **24**, 679–690 (2018).

66. Salojin, K. V, Zhang, J. & Delovitch, T. L. TCR and CD28 are coupled via ZAP-70 to the activation of the Vav/Rac-1-/PAK-1/p38 MAPK signaling pathway. *J. Immunol.* **163**, 844–53 (1999).

67. Hehner, S. P., Hofmann, T. G., Dienz, O., Dröge, W. & Schmitz, M. L. Tyrosine-phosphorylated Vav1 as a point of integration for T-cell receptor- and CD28-mediated activation of JNK, p38, and interleukin-2 transcription. *J. Biol. Chem.* **275**, 18160–18171 (2000).

68. Fujikawa, K. *et al.* Vav1/2/3-null Mice Define an Essential Role for Vav Family Proteins in Lymphocyte Development and Activation but a Differential Requirement in MAPK Signaling in T and B Cells. *J. Exp. Med.* **198**, 1595–1608 (2003).

69. Tedford, K. *et al.* Compensation between Vav-1 and Vav-2 in B cell development and antigen receptor signaling. *Nat. Immunol.* **2**, 548–555 (2001).

70. Barreira, M., Rodríguez-Fdez, S. & Bustelo, X. R. New insights into the Vav1 activation cycle in lymphocytes. *Cell. Signal.* **45**, 132–144 (2018).

71. Bustelo, X. R. Regulatory and Signaling Properties of the Vav Family. *Mol. Cell. Biol.* **20**, 1461–1477 (2000).

72. Rodríguez-Fdez, S. & Bustelo, X. R. The Vav GEF Family: An Evolutionary and Functional Perspective. *Cells* **8**, 465 (2019).

73. Katzav, S., Martin-Zanca, D. & Barbacid, M. Vav, a Novel Human Oncogene Derived From a Locus Ubiquitously Expressed in Hematopoietic Cells. *EMBO J.* **8**, 2283–2290 (1989).

74. HENSKE, E. P. *et al.* Identification of VAV2 on 9q34 and its exclusion as the tuberous sclerosis gene TSC1. *Ann. Hum. Genet.* **59**, 25–37 (1995).

75. Movilla, N. & Bustelo, X. R. Biological and Regulatory Properties of Vav-3, a New Member of the Vav Family of Oncoproteins. *Mol. Cell. Biol.* **19**, 7870–7885 (1999).

76. Doody, G. M. *et al.* Signal transduction through Vav-2 participates in humoral immune responses and B cell maturation. *Nat. Immunol.* **2**, 542–547 (2001).

77. Fray, M. A., Charpentier, J. C., Sylvain, N. R., Seminario, M.-C. & Bunnell, S. C. Vav2 lacks calcium entry-promoting scaffolding functions unique to Vav1 and inhibits T cell activation via Cdc42. *J. Cell Sci.* jcs.238337 (2020) doi:10.1242/jcs.238337.

78. Zugaza, J. L. *et al.* Structural determinants for the biological activity of Vav proteins. *J. Biol. Chem.* **277**, 45377–45392 (2002).

79. Birge, R. B., Knudsen, B. S., Besser, D. & Hanafusa, H. SH2 and SH3-containing adaptor proteins: Redundant or independent mediators of intracellular signal transduction. *Genes to Cells* **1**, 595–613 (1996).

80. Deckert, M., Tartare-Deckert, S., Couture, C., Mustelin, T. & Altman, A. Functional and physical interactions of Syk family kinases with the Vav proto-oncogene product. *Immunity* **5**, 591–604 (1996).

81. Ksionda, O. *et al.* Mechanism and function of Vav1 localisation in TCR signalling. *J. Cell Sci.* **125**, 5302–5314 (2012).

82. Nishida, M. *et al.* Novel recognition mode between Vav and Grb2 SH3 domains. *EMBO J.* **20**, 2995–3007 (2001).

83. Hobert, O., Schilling, J., Beckerle, M., Ullrich, A. & Jallal, B. SH3 domain-dependent interaction of the proto-oncogene product Vav with the focal contact protein zyxin. *Oncogene* **12**, 1577–1581 (1996).

84. Romero, F. *et al.* p95vav associates with the nuclear protein Ku-70. *Mol. Cell. Biol.* **16**, 37–44 (1996).

85. Romero, F. *et al.* Vav binding to heterogeneous nuclear ribonucleoprotein (hnRNP) C: Evidence for Vav-hnRNP interactions in an RNA-dependent manner. *J. Biol. Chem.* **273**, 5923–5931 (1998).

86. Chrencik, J. E. *et al.* Structural Basis of Guanine Nucleotide Exchange Mediated by the T-Cell Essential Vav1. *J. Mol. Biol.* **380**, 828–843 (2008).

87. Rapley, J., Tybulewicz, V. L. J. & Rittinger, K. Crucial structural role for the PH and C1 domains of the Vav1 exchange factor. *EMBO Rep.* **9**, 655–661 (2008).

88. Abe, K. *et al.* Vav2 is an activator of Cdc42, Rac1, and RhoA. *J. Biol. Chem.* **275**, 10141–10149 (2000).

89. Lopez-Lago, M., Lee, H., Cruz, C., Movilla, N. & Bustelo, X. R. Tyrosine Phosphorylation Mediates Both Activation and Downmodulation of the Biological Activity of Vav. *Mol. Cell. Biol.* **20**, 1678–1691 (2000).

90. Blomberg, N., Baraldi, E., Nilges, M. & Saraste, M. The PH superfold: A structural scaffold for multiple functions. *Trends Biochem. Sci.* **24**, 441–445 (1999).

91. Das, B. *et al.* Control of intramolecular interactions between the pleckstrin homology and Dbl homology domains of Vav and Sos1 regulates Rac binding. *J. Biol. Chem.* **275**, 15074–15081 (2000).

92. Gimona, M., Djinovic-Carugo, K., Kranewitter, W. J. & Winder, S. J. Functional plasticity of CH domains. *FEBS Lett.* **513**, 98–106 (2002).

93. Katzav, S., Cleveland, J. L., Heslop, H. E. & Pulido, D. Loss of the amino-terminal helix-loop-helix domain of the vav proto-oncogene activates its transforming potential. *Mol. Cell. Biol.* **11**, 1912–1920 (1991).

94. Li, S. Y. *et al.* The N-terminal 20-amino acid region of guanine nucleotide exchange factor vavl plays a distinguished role in T cell receptor-mediated calcium signaling. *J. Biol. Chem.* **288**, 3777–3785 (2013).

95. Aghazadeh, B., Lowry, W. E., Huang, X. Y. & Rosen, M. K. Structural basis for relief of autoinhibition of the Dbl homology domain of proto-oncogene Vav by tyrosine phosphorylation. *Cell* **102**, 625–633 (2000).

96. Saveliev, A. *et al.* Function of the Nucleotide Exchange Activity of Vav1 in T cell Development and Activation *. *Sci. Signal.* **2**, (2009).

97. Arana, E. *et al.* Activation of the Small GTPase Rac2 via the B Cell Receptor Regulates B Cell Adhesion and Immunological-Synapse Formation. *Immunity* **28**, 88–99 (2008).

98. Malhotra, S., Kovats, S., Zhang, W. & Coggeshall, K. M. Vav and Rac activation in B cell antigen receptor endocytosis involves Vav recruitment to the adapter protein LAB. *J. Biol. Chem.* **284**, 36202–36212 (2009).

99. Crespo, P. *et al.* Rac-1 dependent stimulation of the JNK/SAPK signaling pathway by Vav. *Oncogene* **13**, 455–460 (1996).

100. Valencia, A., Chardin, P., Wittinghofer, A. & Sander, C. The ras Protein Family: Evolutionary Tree and Role of Conserved Amino Acids. *Biochemistry* **30**, (1991).

101. Hodge, R. G. & Ridley, A. J. Regulating Rho GTPases and their regulators. *Nat. Rev. Mol. Cell Biol.* **17**, 496–510 (2016).

102. Wennerberg, K. & Der, C. J. Rho-family GTPases: It's not only Rac and Rho (and i like it). *J. Cell Sci.* **117**, 1301–1312 (2004).

103. Heasman, S. J. & Ridley, A. J. Mammalian Rho GTPases: New insights into their functions from in vivo studies. *Nat. Rev. Mol. Cell Biol.* **9**, 690–701 (2008).

104. Rossman, K. L., Der, C. J. & Sondek, J. GEF means go: Turning on Rho GTPases with guanine nucleotide-exchange factors. *Nat. Rev. Mol. Cell Biol.* **6**, 167–180 (2005).

105. Bustelo, X. R., Sauzeau, V. & Berenjeno, I. M. GTP-binding proteins of the Rho/Rac family: Regulation, effectors and functions in vivo. *BioEssays* **29**, 356–370 (2007).

106. Croker, B. A. *et al.* The Rac2 Guanosine Triphosphatase Regulates B Lymphocyte Antigen Receptor Responses and Chemotaxis and Is Required for Establishment of B-1a and Marginal Zone B Lymphocytes. *J. Immunol.* **168**, 3376–3386 (2002).

107. Walmsley, M. J. *et al.* Critical Roles for Rac1 and Rac2 GTPases in B Cell Development and Signaling. *Science (80-.).* **302**, 459–462 (2003).

108. Gu, Y. *et al.* Hematopoietic Cell Regulation by Rac1 and Rac2 Guanosine Triphosphatases. *Science (80-.).* **302**, 445–449 (2003).

109. Kanaho, Y., Kobayashi-Nakano, A. & Yokozeki, T. The phosphoinositide kinase PIP5K that produces the versatile signaling phospholipid PI4,5P2. *Biol. Pharm. Bull.* **30**, 1605–1609 (2007).

110. Rameh, L. E., Tolias, K. F., Duckworth, B. C. & Cantley, L. C. A new pathway for synthesis of phosphatidylinositol-4,5-bisphosphate. *Nature* **390**, 192–196 (1997).

111. van den Bout, I. & Divecha, N. PIP5K-driven PtdIns(4,5)P2 synthesis: regulation and cellular functions. *J. Cell Sci.* **122**, 3837–3850 (2009).

112. Carpenter, C. L. & Cantley, L. C. Phosphoinositide Kinases. *Biochemistry* **29**, 11147–11156 (1990).

113. Kanaho, Y., Nakayama, K., Frohman, M. A. & Yokozeki, T. Regulation of Phosphatidylinositol 4-Phosphate 5-Kinase Activity by Partner Proteins. *Methods Enzymol.* **434**, 155–169 (2007).

114. Ishihara, H. *et al.* Cloning of cDNAs encoding two isoforms of 68-kDa type I phosphatidylinositol-4-phosphate 5-kinase. *J. Biol. Chem.* **271**, 23611–23614 (1996).

115. Loijens, J. C. & Anderson, R. A. Type I phosphatidylinositol-4-phosphate 5-kinases are distinct members of this novel lipid kinase family. *J. Biol. Chem.* **271**, 32937–32943 (1996).

116. Ishihara, H. *et al.* Type I phosphatidylinositol-4-phosphate 5-kinases. Cloning of the third isoform and deletion/substitution analysis of members of this novel lipid kinase family. *J. Biol. Chem.* **273**, 8741–8748 (1998).

117. Chong, L. D., Traynor-Kaplan, A., Bokoch, G. M. & Schwartz, M. A. The small GTP-binding protein Rho regulates a phosphatidylinositol 4-phosphate 5-kinase in mammalian cells. *Cell* **79**, 507–513 (1994).

118. Halstead, J. R. *et al.* Rac controls PIP5K localisation and PtdIns(4,5)P2 synthesis, which modulates vinculin localisation and neurite dynamics. *J. Cell Sci.* **123**, 3535–3546 (2010).

119. Ling, K. *et al.* Tyrosine phosphorylation of type Iγ phosphatidylinositol phosphate kinase by Src regulates an integrin-talin switch. *J. Cell Biol.* **163**, 1339–1349 (2003).

120. Porciello, N., Kunkl, M., Viola, A. & Tuosto, L. Phosphatidylinositol 4-phosphate 5-kinases in the regulation of T cell activation. *Front. Immunol.* **7**, 1–8 (2016).

121. Kallikourdis, M. *et al.* Phosphatidylinositol 4-Phosphate 5-Kinase β Controls Recruitment of Lipid Rafts into the Immunological Synapse. *J. Immunol.* **196**, 1955–1963 (2016).

122. O'Rourke, L. M. *et al.* CD19 as a membrane-anchored adaptor protein of B lymphocytes: Costimulation of lipid and protein kinases by recruitment of Vav. *Immunity* **8**, 635–645 (1998).

123. Saito, K. *et al.* BTK regulates PtdIns-4,5-P2synthesis: Importance for calcium signaling and PI3K activity. *Immunity* **19**, 669–678 (2003).

124. Ben-Bassat, H. *et al.* Establishment in Continuous Culture of a New Type of Lymphocyte from a "Burkitt-Like" Malignant Lymphoma (Line D.G.-75). *Int. J. Cancer* **19**, 27–33 (1977).

125. König, L. B Cell Antigen Receptor-intrinsic Costimulation of IgG and IgE Isotypes Isotype-specific Signaling Mechanisms of IgG- and IgE-B Cell Antigen Receptors. (2012).

126. Morita, S., Kojima, T. & Kitamura, T. Plat-E: An efficient and stable system for transient packaging of retroviruses. *Gene Ther.* **7**, 1063–1066 (2000).

127. Griesbeck, O., Baird, G. S., Campbell, R. E., Zacharias, D. A. & Tsien, R. Y. Reducing the Environmental Sensitivity of Yellow Fluorescent Protein: MECHANISM AND APPLICATIONS . *J. Biol. Chem.* **276**, 29188–29194 (2001).

128. Cormack, B. P., Valdivia, R. H. & Falkow, S. FACS-optimized mutants of the green fluorescent protein (GFP). *Gene* **173**, 33–38 (1996).

129. Mullis, K. *et al.* Specific Enzymatic Amplification of DNA In Vitro: The Polymerase Chain Reaction. *Cold Spring Harb. Symp. Quant. Biol.* **51**, 263–273 (1986).

130. Weber, K. & Osborn, M. The reliability of molecular weight determinations by dodecyl sulfate-polyacrylamide gel electrophoresis. *J. Biol. Chem.* **244**, 4406–4412 (1969).

131. Towbin, H., Staehelin, T. & Gordon, J. Electrophoretic transfer of proteins from polyacrylamide gels to nitrocellulose sheets: Procedure and some applications. *Proc. Natl. Acad. Sci.* **76**, 4350–4354 (1979).

132. Faulstich, H., Zobeley, S., Rinnerthaler, G. & Small, J. V. Fluorescent phallotoxins as probes for filamentous actin. *J. Muscle Res. Cell Motil.* **9**, 370–383 (1988).

133. Wieland, T. *Peptides of Poisonous Amanita Mushrooms*. (Springer, 1986). doi:https://doi.org/10.1007/978-3-642-71295-1.

134. Ran, F. A. *et al.* Genome engineering using the CRISPR-Cas9 system. *Nat. Protoc.* **8**, 2281–2308 (2013).

135. Montalvo-Ortiz, B. L. *et al.* Characterization of EHop-016, novel small molecule inhibitor of Rac GTPase. *J. Biol. Chem.* **287**, 13228–13238 (2012).

136. Shang, X. *et al.* Rational design of small molecule inhibitors targeting rhoa subfamily rho GTPases. *Chem. Biol.* **19**, 699–710 (2012).

137. Shang, X. *et al.* Small-molecule inhibitors targeting G-protein-coupled Rho guanine nucleotide exchange factors. *Proc. Natl. Acad. Sci.* **110**, 3155–3160 (2013).

138. Loijens, J. C., Boronenkov, I. V., Parker, G. J. & Anderson, R. A. The phosphatidylinositol 4-phosphate 5-kinase family. *Adv. Enzyme Regul.* **36**, 115–140 (1996).

139. Brezski, R. J. & Monroe, J. G. B Cell Antigen Receptor-Induced Rac1 Activation and Rac1-Dependent Spreading Are Impaired in Transitional Immature B Cells Due to Levels of Membrane Cholesterol. *J. Immunol.* **179**, 4464–4472 (2007).

140. Inabe, K. *et al.* Vav3 modulates B cell receptor responses by regulating phosphoinositide 3-kinase activation. *J. Exp. Med.* **195**, 189–200 (2002).

141. Treanor, B. *et al.* The Membrane Skeleton Controls Diffusion Dynamics and Signaling through the B Cell Receptor. *Immunity* **32**, 187–199 (2010).

142. Mattila, P. K. *et al.* The Actin and Tetraspanin Networks Organize Receptor Nanoclusters to Regulate B Cell Receptor-Mediated Signaling. *Immunity* **38**, 461–474 (2013).

143. Stoddart, A., Jackson, A. P. & Brodsky, F. M. Plasticity of B Cell Receptor Internalization upon Conditional Depletion of Clathrin. *Mol. Biol. Cell* **16**, 5356–5372 (2005).

144. Vigorito, E., Clayton, E. & Turner, M. BCR activation of PI3K is Vav-independent in murine B cells. *Biochem. Soc. Trans.* **32**, 781–4 (2004).

145. Becker, M., Hobeika, E., Jumaa, H., Reth, M. & Maity, P. C. CXCR4 signaling and function require the expression of the IgD-class B-cell antigen receptor. *Proc. Natl. Acad. Sci. U. S. A.* **114**, 5231–5236 (2017).

146. Kühn, J. *et al.* The adaptor protein CIN85 assembles intracellular signaling clusters for B cell activation. *Sci. Signal.* **9**, 1–15 (2016).

147. Bartsch, C. Revisiting Erk signaling following B cell antigen receptor activation by different stimulatory agents. (University of Göttingen, Medical Faculty, 2017).

148. Kruse, V. Identification of therapeutic targets in the Burkitt's lymphoma specific B cell antigen receptor signaling network. (University of Göttingen, 2018).

149. Kurosaki, T. & Wienands, J. *B Cell Receptor Signaling*. *Cell Signaling* (Springer, 2008). doi:10.1074/jbc.R400012200.

150. Cancelas, J. A. *et al.* Rac GTPases differentially integrate signals regulating hematopoietic stem cell localization. *Nat. Med.* **11**, 886–891 (2005).

151. Saci, A. & Carpenter, C. L. RhoA GTPase Regulates B Cell Receptor Signaling. *Mol. Cell* **17**, 205–214 (2005).

152. Didsbury, J., Weber, R. F., Bokoch, G. M., Evans, T. & Snyderman, R. Rac, a Novel Ras-Related Family of Proteins That Are Botulinum Toxin Substrates. *J. Biol. Chem.* **264**, 16378–16382 (1989).

153. Walliser, C. *et al.* Rac regulates its effector phospholipase Cγ2 through interaction with a split pleckstrin homology domain. *J. Biol. Chem.* **283**, 30351–30362 (2008).

154. Walliser, C. *et al.* Rac-mediated stimulation of phospholipase Cγ2 amplifies B cell receptor-induced calcium signaling. *J. Biol. Chem.* **290**, 17056–17072 (2015).

155. Piechulek, T. *et al.* Isozyme-specific Stimulation of Phospholipase C-γ2 by Rac GTPases. *J. Biol. Chem.* **280**, 38923–38931 (2005).

156. Burbage, M. *et al.* Cdc42 is a key regulator of B cell differentiation and is required for antiviral humoral immunity. *J. Exp. Med.* **212**, 53–72 (2014).

157. Randall, K. L. *et al.* Dock8 mutations cripple B cell immunological synapses, germinal centers and long-lived antibody production. *Nat. Immunol.* **10**, 1283–1291 (2009).

158. Barreira, M. *et al.* The C-Terminal SH3 Domain Contributes to the Intramolecular Inhibition of Vav Family Proteins. *Sci. Signal.* **7**, ra35 LP-ra35 (2014).

159. Doody, G. M. *et al.* Vav-2 controls NFAT-dependent transcription in B- but not T-lymphocytes. *EMBO J.* **19**, 6173–6184 (2000).

160. Lemmon, M. a. Pleckstrin Homology (PH) domains and phosphoinositides. *Biochem. Soc. Symp.* **74**, 81–93 (2007).

161. Reynolds, L. F. *et al.* Vav1 transduces T cell receptor signals to the activation of phospholipase C-γ1 via phosphoinositide 3-kinase-dependent and -independent pathways. *J. Exp. Med.* **195**, 1103–1114 (2002).

162. Cargnello, M. & Roux, P. P. Activation and function of the MAPKs and their substrates, the MAPK-activated protein kinases. *Microbiol. Mol. Biol. Rev.* **75**, 50–83 (2011).

163. Xue, G. & Hemmings, B. A. PKB/Akt–Dependent Regulation of Cell Motility. *JNCI J. Natl. Cancer Inst.* **105**, 393–404 (2013).

8. Appendix

8.1. Abbreviations

α	anti
aa	amino acid
Ag	antigen
approx.	approximately
AR	acidic region
BCR	B cell antigen receptor
BLNK	B cell linker protein
bp	base pair
BSA	bovine serum albumin
Btk	Bruton's tyrosine kinase
° C	degree Celsius
Cas9	CRISPR associated protein 9
Cbl	Casitas B-lineage lymphoma
CCL	cleared cellular lysate
CD	Cluster of Differentiation
Cdc42	Cell division control protein 42
cDNA	complementary DNA
CH	Calponin-homology
CIN85	Cbl-interacting protein of 85 kDa
CIP	calf intestine phosphatase
Cit	Citrine
CRISPR	Cluster Regulatory Interspaced Short Palindromic Repeats
C-terminal	carboxy-terminal
DAG	diacylglycerol
dATPs	deoxyribose adenine triphosphate
DH	Dbl-homology
DMSO	dimethylsulfoxide
DNA	deoxyribonucleic acid
DSMZ	Deutsche Sammlung für Mikroorganismen und Zellkulturen
EB	EcoBlast (Ecotropic receptor, Blasticidine as selection marker)
ECL	enhanced chemiluminescence
E. coli	*Escherichia coli*
e.g.	exempli gratia
eGFP	enhanced green fluorescent protein
env	envelope, gene encoding glycoprotein 160
ER	endoplasmic reticulum
Erk	extracellular regulated kinase
$F(ab')_2$	bivalent antigen binding fragment
FACS	fluorescent activated cell sorter
Fc region	fragment crystallizable region
FCS	fetal calf serum
g	gram
gag	group specific antigen, gene encoding p55 (core protein)
GC	germinal center

GDI	guanine-nucleotide dissociation inhibitor
GDP	guanosine diphosphate
GEF	guanine-nucleotide exchange factor
Grb2	growth factor receptor-bound protein 2
GTP	guanosine triphosphate
h	hours
HEK	human embryonic kidney
HEPES	N-2-Hydroxyethyl piperazine-N'-2-ethane sulphonic acid
HRPO	horseradish peroxidase
i.e.	id est
Ig	immunoglobulin
Indo-1 AM	1H-Indole-6-carboxylic acid, 2-[4-[bis[2-[(acetyloxy)methoxy]-2-oxoethyl]amino]-3-[2-[2-[bis[2-[(acetyloxy)methoxy]-2-oxoethyl]amino]-5-methylphenoxy]ethoxy]phenyl]-, (acetyloxy)methyl ester
IP_3	inositol-1,4,5-trisphosphate
IP_3R	IP_3 receptor
IPTG	Isopropyl-β-D-thiogalacto-pyranoside
IRES	internal ribosome entry site
ITAM	immunoreceptor tyrosine-based activation motif
JNK	c-Jun N-terminal kinase
l	liter
LB	Lysogeny broth
Lyn	Lck/yes-related protein kinase
kDa	kilo Dalton
M	mole
mA	milliampere
MAPK	mitogen activated protein kinases
µg	microgram
mg	milligram
MHC	major histocompatibility complex
min	minutes
µl	microliter
ml	milliliter
µM	micromole
mM	millimole
MMLV	Moloney murine leukemia virus
mRNA	messenger RNA
NFAT	nuclear factor of activated T cell
NF-κB	nuclear factor ‘kappa-light-chain-enhancer’ of activated B cells
nM	nanomole
NP-40	Nonidet P40
N-terminal	amino-terminal
OD	optical density
ORF	open reading frame
PAGE	polyacrylamide gel electrophoresis
PBS	phosphate buffered saline
PCR	polymerase chain reaction
PH	Pleckstrin-homology
PI3K	Phosphoinositide 3’-kinase

PI4P	phosphatidylinositol-4-phosphate
PI5P	phosphatidylinositol-5-phosphate
PIP_2	phosphatidyl-inositol-4,5-bisphosphate
PIP_3	phosphatidyl-inositol-3,4,5-trisphosphate
PIP5K	phosphatidyl-inositol-4-phosphate 5-kinase
PKB	protein kinase B
PKC	protein kinase C
PlatE	Platinum E
PR	proline rich
PRR	pattern recognition receptors
Rac	Ras-related C3 botulinum toxin substrate
Ras	Rat sarcoma
Rho	Ras homolog
RNA	ribonucleic acid
RPMI	Roswell Park Memorial Institute medium
RT	room temperature
s	seconds
S1P	sphingosine-1-phosphate
SDS	sodium dodecyl sulfate
SH2	Src-homology 2 domain
SH3	Src-homology 3 domain
SLP-65	SH2-domain-containing leukocyte adaptor protein of 65 kDa
SOC	Store-operated Ca^{2+}-channels
Src	sarcoma
STED	stimulated emission depletion
STIM	Stromal interaction molecule
Syk	Spleen tyrosine kinase
TAE buffer	Tris Acetate EDTA buffer
TALEN	Transcription activator-like effector nuclease
TB	terrific broth
TBS	Tris buffered saline
TCR	T cell antigen receptor
Tris	Tris-(hydroxymethyl)-amino methane
Triton-X-100	4-(1,1,3,3-Tetramethylbutyl)phenyl-polyethylene glycol ether
UV	ultraviolet
V	volt
v/v	volume/volume
w/v	weight/volume
X-Gal	5-Bromo-4-chloro-3-indolyl β-D-galactopyranoside
ZF	zinc finger

8.2. List of tables

8.3. List of figures

8.4. Curriculum vitae